

AD 663834

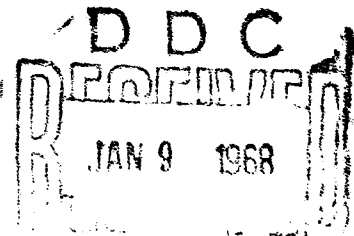
A COMPUTER PROGRAM FOR THE DYNAMIC BLAST RESPONSE
OF BOX-TYPE STRUCTURES

Final Report

Contract OCD-PS-64-201
OCD Work Unit 1157B

December 1967

This document has been approved
for public release and sale;
its distribution is unlimited



T. Y. LIN AND ASSOCIATES
Consulting Engineers

LOS ANGELES • DALLAS • CHICAGO • NEW YORK

A COMPUTER PROGRAM FOR THE DYNAMIC BLAST RESPONSE
OF BOX-TYPE STRUCTURES

Final Report

December 1956

Contract OCD-PS-64-201
OCD Work Unit 1157B

by

Ian R. Stubbs
K. L. Benuska

for

Office of Civil Defense
Office of the Secretary of the Army
Washington, D. C. 20310

OCD Review Notice

This report has been reviewed in the Office of Civil Defense and approved for publication. Approval does not signify that the contents necessarily reflect the views and policies of the Office of Civil Defense.

Distribution of this document is unlimited

T. Y. LIN AND ASSOCIATES
Consulting Engineers

Los Angeles

Dallas

Chicago

New York

**A COMPUTER PROGRAM FOR THE DYNAMIC BLAST RESPONSE
OF BOX-TYPE STRUCTURES**

**Summary of
Final Report**

December 1966

**Contract OCD-PS-64-201
OCD Work Unit 1157B**

by

**Ian R. Stubbs
K. L. Benuska**

for

**Office of Civil Defense
Office of the Secretary of the Army
Washington, D. C. 20310**

**T. Y. LIN AND ASSOCIATES
Consulting Engineers**

Los Angeles

Dallas

Chicago

New York

SUMMARY

This report describes two computer programs developed to analyze the response of multi-cell rectangular box-structures to external dynamic loads. The first of the two programs considers the dynamic response of the box-structure with its material properties remaining linear. The output consists of displacements, moments and stresses. Also, response spectra may be generated at equipment attachment points within the structure. The second program calculates the dynamic response with the added provision that when moments in any plate exceed a predetermined yield value, that plate will not accept any increase in loads normal to its plane.

The report applies to shallow buried, reinforced concrete protective structures. The walls, floors, roof and partitions of these structures are assumed to be mutually connected at right angles. The structure can have more than one room in the width, depth and height. The loading is that caused by an above ground nuclear detonation some distance from the location of the structure.

The method of analyzing the structure is by considering it as a system of finite elements, each plate being divided into four rectangular elements. The finite element method is a means of approximating the equations of equilibrium of the elastic continuum with a set of algebraic equilibrium equations. The continuum is considered as being an assemblage of discrete structural elements inter-connected at a finite number of nodal points. The analysis involves the evaluation of the element elastic properties which are represented by the stiffness matrix expressing the relationship between element nodal forces and displacements. The nodal points are taken as the four corners of the element.

The basic operation in the definition of an element stiffness matrix is the choice of deformation characteristics which are to be allowed. The most important criterion to be considered is the compatibility of deformations of adjacent elements. The element stiffness matrix has twenty-four degrees of freedom, six per nodal point, and consists of a 12x12 bending stiffness matrix

and a 12x12 inplane stiffness matrix. The bending stiffness is calculated from a twelve term polynomial for the displacement. The inplane stiffness consists of an 8x8 linear force-displacement matrix and a 4x4 moment-rotation matrix. For the purpose of this work these were assumed to be uncoupled. At any nodal point it is possible to have elements intersecting in three mutually perpendicular planes. This makes it necessary to convert the local coordinates for each element into a global coordinate system for the whole structure.

At any instant of time, the applied distributed load on the structure can be specified. This is converted into a nodal point loading equivalent to the distributed load such that the nodal deformations and the total work done are the same in each system. By using a process similar to that used in determining the stiffness matrix for the complete structure, the load matrix for the complete structure can be obtained by taking the load matrices for each individual plate and expanding them into a global coordinate system.

Through the finite element method, the structure is replaced by lumped parameters at discrete nodal points, therefore, the mass which is distributed throughout the structure is assumed to be concentrated at those nodal points. In order to get the response of the structure for a time-dependent load, the equilibrium of the discrete mass system at time t is expressed by the matrix equation

$$[M]\{\ddot{x}\}_t + [C]\{\dot{x}\}_t + [K]\{x\}_t = \{P\}_t$$

where

- $[M]$ = mass matrix
- $[C]$ = damping matrix
- $[K]$ = stiffness matrix
- $\{x\}_t$ = displacement of the system
- $\{P\}_t$ = force acting on the system

The equations are solved by means of a step by step procedure. The accelerations of the masses are assumed to be linear in each time increment. A diagonal mass matrix is used. Since the determination of mode shapes and frequencies is not a part of the step by step method of solution, modal damping cannot be used directly. The damping matrix is assumed to be a linear function of the mass matrix and the stiffness matrix. The solution of the equations makes use of the Gaussian elimination technique.

An example of a dynamic analysis is given.

A synoptic review of selected literature pertaining to the failure modes and failure loadings of two-way slabs is presented at the end of the report.

PREFACE

During the year of 1963, the Office of Civil Defense, Protective Structures Division, initiated the development of a series of computer programs directed toward providing a complete engineering analysis of buildings considering the multiple effects of nuclear weapons. These computer codes are the backbone of the *Computer Analysis For Protective Structures (CAPS)* system.

The CAPS-1 program, entitled *Analysis of Structures for Resistance to Nuclear Blast*, began with the development of a code for determining the blast resistance of multi-story buildings. T.Y. Lin and Associates completed the computer program under Contract No. OCD-OS-63-44. Subsequently, the programming effort to provide a code for analysing box-structures was begun under Contract No. OCD-PS-65-7, Subtask 1157A. The responsibility for continuation of the program passed to Stanford Research Institute under the provisions of Contract No. OCD-PS-64-201 between OCD and SRI. T. Y. Lin and Associates has performed the work contained in this report under Subcontract No. B-81869(4949A-46)-US with SRI.

ACKNOWLEDGEMENTS

The indebtedness of the authors to Dr. R.W. Clough and Dr. E. L. Wilson for their contributions to the art of finite element analysis will be readily understood by others engaged in this area of study. Appreciation is expressed to Drs. Clough and Wilson for their invaluable consultation.

TABLE OF CONTENTS

	Page
Preface	i
Acknowledgements	ii
Table of Contents	iii
List of Symbols	v
Section 1	
INTRODUCTION	
1-1 Background	1-1
1-2 Scope of the Report	1-2
Section 2	
DEFINITION OF THE STRUCTURE	
2-1 General	2-1
2-2 The Stiffness Matrix	2-3
Section 3	
NODAL POINT LOADS	
	3-1
Section 4	
DYNAMIC RESPONSE ANALYSIS	
4-1 Equation of Equilibrium	4-1
4-2 Mass Matrix	4-1
4-3 Damping Matrix	4-4
4-4 Response Calculations	4-7
4-5 Solution of the Equilibrium Equation	4-11
4-5.1 Gaussian Elimination	4-11
4-5.2 Simplification for Band Matrices	4-13
4-5.3 Stresses	4-14

4-6	Response Spectra For Sheltered Equipment	4-18
	4-6.1 General	4-18
	4-6.2 Definition of the Response Spectrum	4-19
4-7	Sample Dynamic Analysis	4-21
	4-7.1 Orientation of the Structure and Loading	4-21
	4-7.2 Numbering Sequence	4-21
	4-7.3 Listing of the Data on the Input Forms	4-23
	4-7.4 Sample Analysis	4-25

Section 5

DYNAMIC NON-LINEAR PROGRAM

5-1	General Procedure	5-1
5-2	Failure Criterion	5-1
	5-2.1 Method of Failure	5-1
	5-2.2 Failure Assumption	5-2
	5-2.3 Failure Condition	5-4
5-3	Sample Non-linear Analysis	5-4

Section 6

SYNOPTIC REVIEW OF SELECTED LITERATURE PERTAINING TO THE FAILURE MODES AND FAILURE LOADINGS OF TWO-WAY SLABS

6-1	Introduction	6-1
6-2	Synoptic Review of Selected Literature	6-1
6-3	Selected References with Abstracts of More Pertinent Publications	6-6

Section 7

7-1	References	7-1
-----	------------	-----

Appendix A

	COMPUTER SUBROUTINE FOR CALCULATING LOADS ON AN UNDERGROUND BOX	A-1
--	-----------------------------------------------------------------	-----

SYMBOLS

a	Length of Finite Element in x Direction in Local Coordinates
a_n	Term Used to Define Damping Matrix
a_θ	Transformation Matrix Rotation to Strain
a_u	Transformation Matrix Displacement to Strain
A	Pseudo Acceleration
b	Length of Finite Element in y Direction in Local Coordinates
c	Damping Due to a Dash Pot; Ground Shock Velocity
C	Damping Matrix
c_n	Coefficient Used to Define Displacement in Plate
d	Distance from Origin of Global System to Point of Interest
D_p^+	Positive Duration Time
$D(t)$	Outrunning Ground Motion Displacement Waveform
E	Modulus of Elasticity
f	Natural Frequency of Vibration
g	Acceleration Due to Gravity
H	Depth of Structure
k	Stiffness of a Weightless Spring
K	Stiffness
K_0	Coefficient of Earth Pressure at Rest
L	Length of Structure
m	Mass of a Single Degree of Freedom System
M	Moment; Mass

p	Stress in the Soil
P	Externally Applied Force
Q	Shear Force Per Unit Length
R_s	Shock Radius
S_b	Bending Stiffness
S_i	Inplane Stiffness
S	Insitu Specific Gravity
S_L	Inplane Linear Stiffness Matrix
S_r	Inplane Rotational Stiffness Matrix
t	Time; Thickness of Plate
t_2	The Period of the First Three Half Waves of the Type II Vertical Ground Motion Waveform
t_s	Thickness of soil; Arrival Time of Shock Front
u	Nodal Displacements in Global System
$u(x,y)$	Inplane Displacement of Plate in x Direction
U	Velocity of Airblast; Maximum Spring Deformation
$U(t)$	Outrunning Ground Motion Horizontal Waveform
$v(x,y)$	Inplane Displacement of Plate in y Direction
V	Pseudo Velocity
$V(t)$	Outrunning Ground Motion Vertical Waveform
w	Displacement at any Point in a Plate Due to Bending
\ddot{w}	Actual Acceleration of Mass of the Single Degree of Freedom System
W	Yield in Megatons; Width of Structure

x	Distance from Origin to a Point in the Plate in the x Direction; Deformation of the Weightless Spring in the Single Degree of Freedom System
\ddot{x}	Relative Acceleration of Mass of the Single Degree of Freedom System
x_t	Displacement of the System
\dot{x}_t	Velocity of the System
\ddot{x}_t	Acceleration of the System
y	Distance from Origin to a Point in the Plate in the y Direction; Displacement of the Origin of the Point of Origin in the Single Degree of Freedom System
\ddot{y}	Acceleration of the Attachment point of the Single Degree of Freedom System
a_n	Coefficient used to Define Displacement in a Plate due to Bending;
a	Depth Attenuation Factor
γ	Shear Strain
ΔP	Overpressure
ϵ	Axial Strain
θ	Nodal Rotations in Local System
λ_d	Modal Damping Ratio
ν	Poissons Ratio
ρ	Density of Plate
ρ_s	Density of Soil
σ	Axial Stress

- τ Shear Stress; Time After Shock Arrival
Measured in Units of Positive Phase
Duration
- ω Circular Frequency of Vibration
- ϕ_i Rotation About i Axis

Section 1

INTRODUCTION

1-1 Background

This report describes the initial development of a computer program designed to analyze the dynamic response of box-type structures to nuclear blast. A box-type structure generally carries external loads by slabs spanning between bearing walls or shear walls. When used as shelters, these structures may be aboveground, located in the basement of a larger building, or buried.

A previous report, by T. Y. Lin and Associates^{1*} under Contract No. OCD-PS-65-7, drew together pertinent conclusions of a large number of research papers and design manuals in order to bring them to bear on the development of this computer program. Airblast loadings and ground motions were reviewed. Also, the equations for the dynamic response of lumped mass systems were presented in detail.

Many other publications have presented design-analysis methods applicable to boxes^{2,3,4,5}. In general, an element-by-element approach is used. That is, the loads are applied to the primary resisting element, the response is determined from a single-degree-of-freedom idealization, and the reactions subsequently applied as loads to the supporting members.

For purposes of this computer program, the box has been thought of as a multi-degree-of-freedom system consisting of plates, rigidly connected to each other at right angles along each edge. The response analysis is a finite element technique, utilizing rectangular plate elements.

Other publications have described airblast loads on an aboveground box^{2,3}. Loads on an underground box are not well defined. The fundamental phenomena of the soil-structure interaction process are not completely understood. However, the relative compressibility of the soil and structure probably controls the load experienced by the buried structure.¹⁴

*Superscripts refer to references found in Section 7.

The computer program models the compressibility of a box. An adequate model of the soil is still needed before an analysis of a soil-structure system can be undertaken with any degree of confidence.

1-2 Scope of the Report

The program development is divided into four major phases.

- Phase I Development of a static analysis for box-type structures utilizing rectangular finite elements
- Phase II Extension of the static analysis to elastic dynamic response analysis using a step-by-step integration procedure
- Phase III Incorporate a procedure for determining the response spectrum at each nodal point of the elastic system
- Phase IV Incorporate non-linear definition of plate bending property into Phase II

This report covers the complete mathematical formulation of each phase. An example of an elastic multi-cell box analysis for dynamic loads is given. An example of a non-linear single cell box analysis for dynamic loads is also given, in which plates fail successively as they exceed a given yield capacity.

The dynamic loads are assumed to act on the exterior surfaces of the multi-cell box. Time did not permit the programming of a comprehensive load routine. However, a simple formulation of loads on a shallow buried box was added to the main program in order to carry out an example analysis of a box responding to a time-dependent load. The load subroutine is described in Appendix A.

Section 2

DEFINITION OF THE STRUCTURE

2-1 General

Many underground protective structures are built of heavy concrete walls, with a concrete floor and a thick concrete roof. The structures may have more than one level in which case the intermediate floors are concrete also. Thus, the whole structure can be considered as a set of interconnecting plates mutually at right angles; i.e., a box-type structure.

The analysis of plates at right angles presents two major problems. The first is that two systems of coordinates have to be used, i.e., a local system for the individual plates and a global system for the whole structure. Extreme care must be taken when changing from one to the other.

The second major problem is the large number of mutually dependent coordinates. In the case of three dimensional frame analyses the numbering of dependent coordinates may be arranged in such a manner that the stiffness matrix can be formulated with a narrow band width; thus, core space in the computer is conserved. In the case of plates mutually connecting at right angles, the band width can become very large, thereby creating a storage problem.

An accurate method of analyzing box-type structures and the method adopted in this work, is to define the box as a system of finite elements. Each plate can be considered as an element or further subdivided into a number of elements. The essential feature of the finite element method is the means by which the differential equations of equilibrium of the elastic continuum are approximated by a set of algebraic equilibrium equations. This procedure is generally looked upon as the substitution for the actual continuum of an assemblage of discrete structural elements, interconnected at a finite number of nodal points. In effect, the continuum may be visualized as being physically cut up into the finite element system, the material properties of the original material being retained in the elements. The analysis involves the evaluation of the element elastic properties, which are represented by the stiffness matrix expressing the relationship between element nodal forces

and displacements. The nodal points are taken as the four corners of the element.

With this system, it is possible to define each panel as an element, determine the equivalent nodal point stiffness and load and solve for displacements. From the displacements, the moments and shears at the nodal points can be determined. In order to determine the distribution of the moments and shears throughout the panels, it is necessary to subdivide each panel into smaller elements. The smallest number of subdivisions to obtain the moments and shears at the center of each panel is four elements. As the least complicated box, i.e., a cube, has six sides, it is apparent that the stiffness matrix can soon get impossibly large. For this work it was decided that a four-element panel was the least that could be used to get results for moments and shears in the middle of the panels and that larger subdivisions would be unworkable.

It was realized that the development of the stiffness matrix for the structure in the global coordinate system would require some difficult programming, so the preliminary work was done on a cube. A symmetrical static load was applied about one major plane so that symmetrical displacements would constitute one check on the accuracy of the stiffness matrix.

When the stiffness matrix was considered correct, steps were taken to convert the program to a system of plates divided into four elements. The correctness of this change was determined by comparing the analysis of a one-box structure using the four-element-per-panel system with the same structure modelled as an eight-box structure using the one-element-per-panel system. In the latter case, the stiffness of the interior elements was set to zero.

The method of determining the nodal point loading for a time dependent blast force was solved in the early stages of the work. By considering this load at any given time as a statically applied load, it was possible to get representative moments and shears in the structure. The procedure adopted resulted in a method of complete checking as every stage was completed and provided for a logical flow of work from a system of single-element panels under static loads to a system of four-element panels under dynamic loads.

2-2 The Stiffness Matrix

The box-type structure is considered as a set of interconnecting plates in three mutually perpendicular planes. In order to determine the stiffness matrix for the complete box, it is necessary to determine the stiffness of each plate in its own local coordinate system and then convert this to the global system. The definition of these systems is shown in Figure 2-1.

The development of the system for considering four elements per panel is essentially the same as that for the system with one element per panel with the one difference that there will be restraining panels at right angles on only two of the edges. For simplicity of presentation, the stiffness matrix of the structure will be developed as if each panel consists of only one element.

Since the method used is to consider each plate as a finite element in the box, by assuming Kirchoff plate bending theory, the stiffness is determined in terms of the 24-corner displacements of each plate. The intersection of the corners of the plates are the nodal points of the complete system.

The basic operation in the definition of an element stiffness matrix is the choice of the deformation characteristics which are to be allowed. The most important criterion to be considered in this selection is the compatibility of deformations of adjacent elements. It can be shown that if deformation patterns are specified which provide internal compatibility within the elements, and at the same time achieve full compatibility of displacements along the element boundaries, then the strain energy in the idealization will represent a lower bound to the strain energy of the actual continuum.

The relationship between the externally applied forces and the resulting displacement on a plate in its own local coordinate system can be expressed in the form

$$(P) = \begin{bmatrix} S_b & \\ & S_L \end{bmatrix} (u)$$

Direction of the Airblast

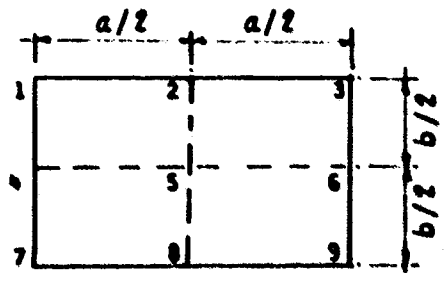
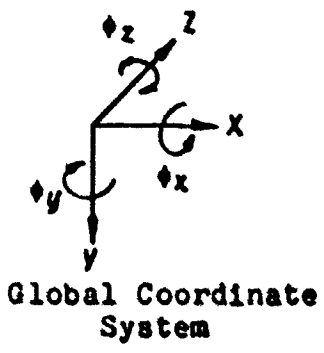
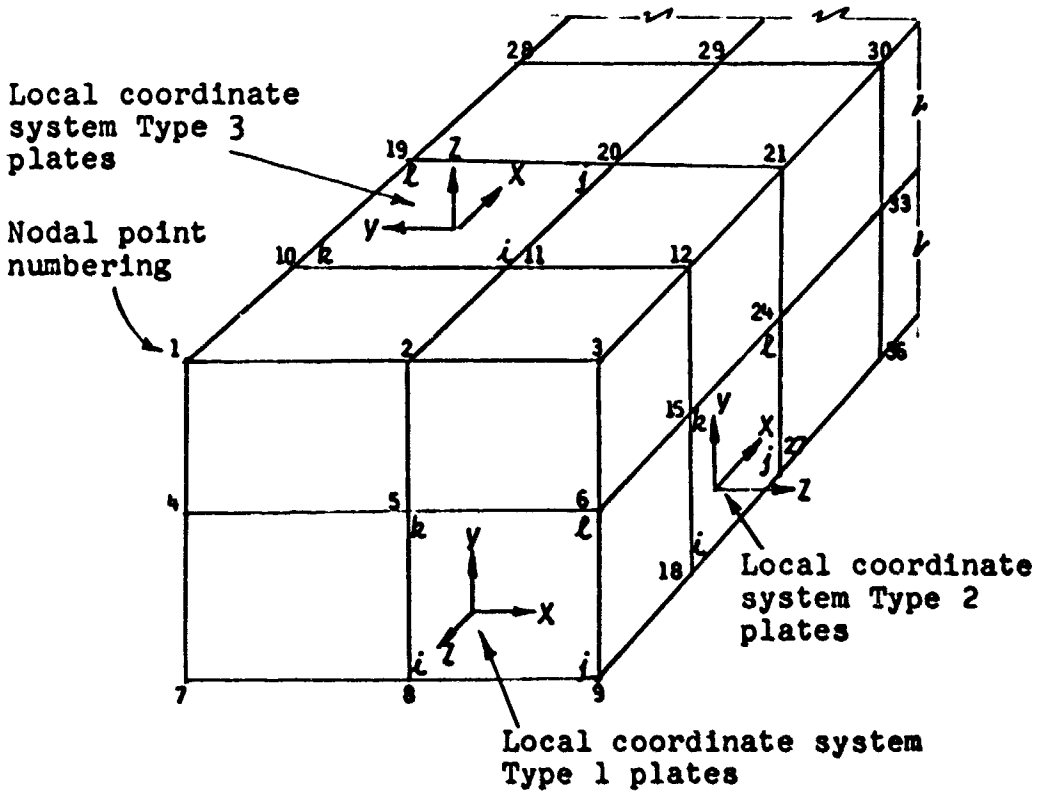


Figure 2-1
DEFINITION OF THE STRUCTURE

where S_b is the 12x12 bending stiffness matrix
 S_i is the 12x12 inplane stiffness matrix.
 There is no coupling between these two matrices.

The simplest expression which has been used in defining the rectangular element bending stiffness S_b is the 12-term polynomial in x and y ; ¹³

$$w = a_1 + a_2x + a_3y + a_4x^2 + a_5xy + a_6y^2 + a_7x^3 + a_8x^2y + a_9xy^2 + a_{10}y^3 + a_{11}x^3y + a_{12}xy^3 \quad (2-1)$$

The two fourth degree terms which are included to provide the required number of displacement patterns were selected to maintain symmetry and also to satisfy the bi-harmonic equilibrium equation. A complete 12 by 12 stiffness matrix which represents the nodal force deflection relationships is shown in Figure 2-2. This 12 by 12 matrix may be constructed from the 12 by 3 matrices associated with each joint. For any given joint i , the stiffness matrix can be represented as the sum of four 12 by 3 matrices K_a , K_b , K_c and K_d , i.e., $K_i = K_a + K_b + K_c + K_d$. These represent the energy contributions from the $(w_{xx})^2$, $(w_{yy})^2$, $(v_{xx} \cdot w_{yy})$ and $(u_{xy})^2$ curvature terms, respectively. The coefficients of these four stiffness component matrices as developed by Adini⁷ are shown in Figure 2-3.

The 12 x 12 inplane stiffness matrix can be considered as an 8 x 8 linear force-displacement matrix S_ℓ and a 4 x 4 moment-rotation matrix S_r together with the corresponding coupling terms $S_{\ell r}$ and $S_{r\ell}$

$$[S_i] = \begin{bmatrix} S_\ell & S_{\ell r} \\ S_{r\ell} & S_r \end{bmatrix}$$

In order to determine the $S_{\ell r}$ and $S_{r\ell}$ terms a rigorous solution is required, according to the theory of elasticity. The authors have assumed the accuracy requirements do not warrant this, and expressions for the linear and rotational displacements were developed as if uncoupled.

For the 8 x 8 linear stiffness matrix S_ℓ the displacement pattern is as shown in Figure 2-4. The sides remain straight after deformation.

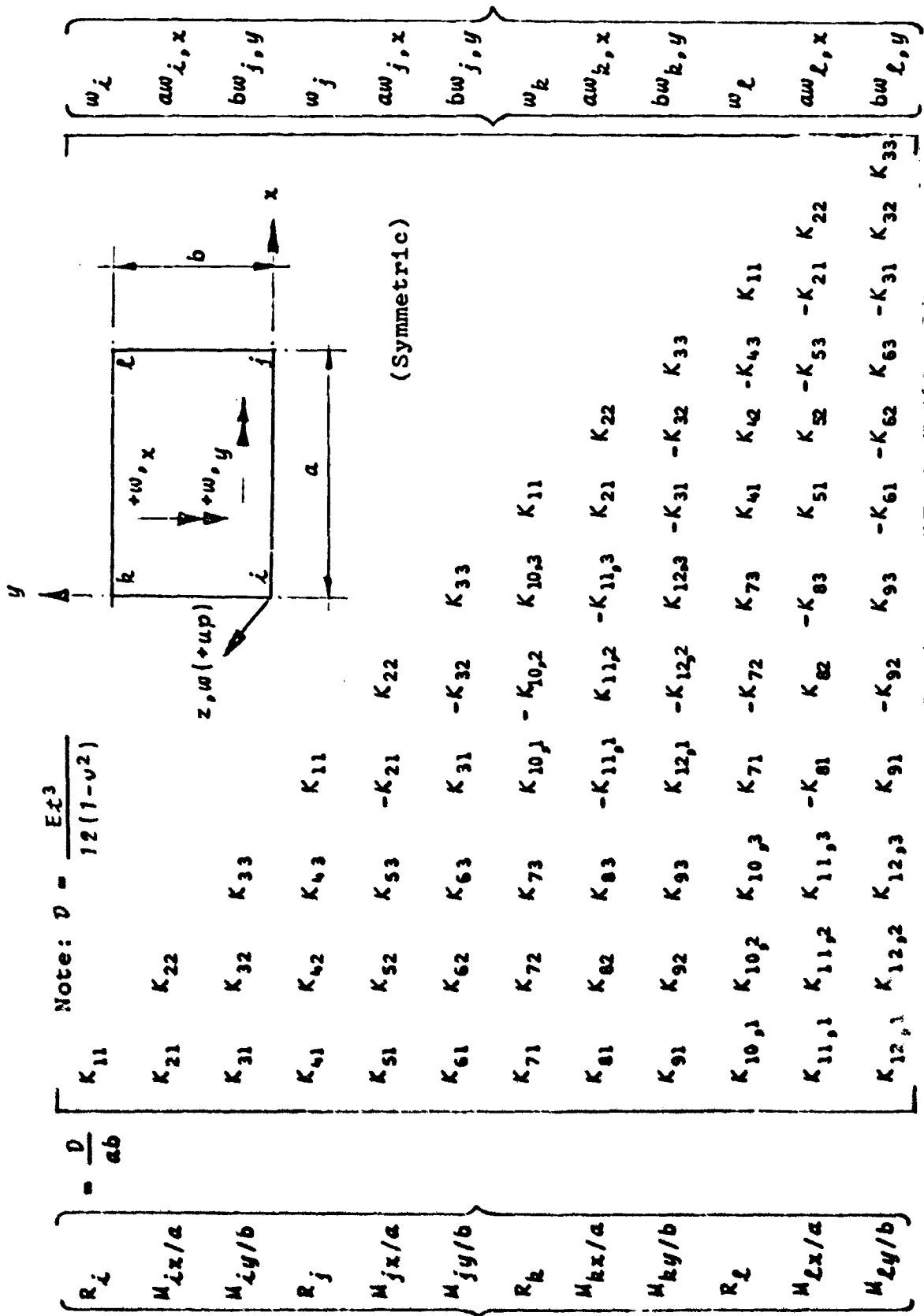


Figure 2-2 ARRANGEMENT OF BENDING STIFFNESS MATRIX
 (Reference 13 - Note: All minus signs omitted in reference)

$$K_a = \frac{1}{3} \left(\frac{b}{a} \right)^2 \begin{bmatrix} 12 & 6 & 0 \\ 6 & 4 & 0 \\ 0 & 0 & 0 \\ -12 & -6 & 0 \\ 6 & 2 & 0 \\ 0 & 0 & 0 \\ 6 & 3 & 0 \\ 3 & 2 & 0 \\ 0 & 0 & 0 \\ -6 & -3 & 0 \\ 3 & 1 & 0 \\ 0 & 0 & 0 \end{bmatrix}$$

$$K_b = \frac{1}{3} \left(\frac{a}{b} \right)^2 \begin{bmatrix} 12 & 0 & 6 \\ 0 & 0 & 0 \\ 6 & 0 & 4 \\ 6 & 0 & 3 \\ 0 & 0 & 0 \\ 3 & 0 & 2 \\ -12 & 0 & -6 \\ 0 & 0 & 0 \\ 6 & 0 & 2 \\ -6 & 0 & -3 \\ 0 & 0 & 0 \\ 3 & 0 & 1 \end{bmatrix}$$

$$K_c = \nu \begin{bmatrix} 2 & 1 & 1 \\ 1 & 0 & 1 \\ 1 & 1 & 0 \\ -2 & 0 & -1 \\ 0 & 0 & 0 \\ -1 & 0 & 0 \\ -2 & -1 & 0 \\ -1 & 0 & 0 \\ 0 & 0 & 0 \\ 2 & 0 & 0 \\ 0 & 0 & 0 \\ 0 & 0 & 0 \end{bmatrix}$$

$$K_d = \frac{1-\nu}{15} \begin{bmatrix} 42 & 3 & 3 \\ 3 & 4 & 0 \\ 3 & 0 & 4 \\ -42 & -3 & -3 \\ 3 & -1 & 0 \\ -3 & 0 & -4 \\ -42 & -3 & -3 \\ -3 & -4 & 0 \\ 3 & 0 & -1 \\ 42 & 3 & 3 \\ -3 & 1 & 0 \\ -3 & 0 & 1 \end{bmatrix}$$

Figure 2-3 ADINI COEFFICIENTS (Reference 7)

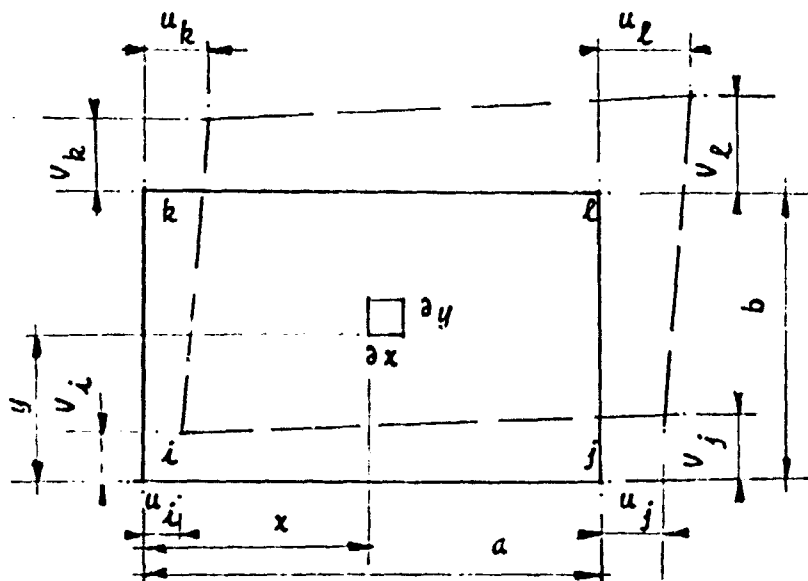


Figure 2-4
INPLANE LINEAR STRAIN OF AN ELEMENT

The geometrical compatibility condition is satisfied by the following equations:

$$u(x, y) = C_1 + C_2 x + C_3 y + C_4 xy \quad (2-2)$$

$$v(x, y) = C_5 + C_6 x + C_7 y + C_8 xy \quad (2-3)$$

If Equation 2-1 is evaluated at the four corners, i , j , k , and l ,

$$u_i = C_1$$

$$u_j = C_1 + C_2 a$$

$$u_k = C_1 + C_3 b$$

$$u_l = C_1 + C_2 a + C_3 b + C_4 ab$$

Solving the above equations for C_1 , C_2 , C_3 , and C_4 ,

$$\begin{aligned}
C_1 &= u_i \\
C_2 &= \frac{1}{a}(u_j - u_i) \\
C_3 &= \frac{1}{b}(u_k - u_i) \\
C_4 &= \frac{1}{ab}(u_i - u_j - u_k + u_l)
\end{aligned}$$

or in matrix form,

$$\begin{bmatrix} C_1 \\ C_2 \\ C_3 \\ C_4 \end{bmatrix} = \frac{1}{ab} \begin{bmatrix} ab & 0 & 0 & 0 \\ -b & b & 0 & 0 \\ -a & 0 & a & 0 \\ 1 & -1 & -1 & 1 \end{bmatrix} \begin{bmatrix} u_i \\ u_j \\ u_k \\ u_l \end{bmatrix} \quad (2-4)$$

Following the same procedure for the v displacements yields the same result, i.e.,

$$\begin{bmatrix} C_5 \\ C_6 \\ C_7 \\ C_8 \end{bmatrix} = \frac{1}{ab} \begin{bmatrix} ab & 0 & 0 & 0 \\ -b & b & 0 & 0 \\ -a & 0 & a & 0 \\ 1 & -1 & -1 & 1 \end{bmatrix} \begin{bmatrix} v_i \\ v_j \\ v_k \\ v_l \end{bmatrix} \quad (2-5)$$

From the definition of strain;

$$\begin{aligned}
\epsilon_x &= \frac{\delta u}{\delta x} \\
\epsilon_y &= \frac{\delta v}{\delta y} \\
\gamma &= \frac{\delta u}{\delta y} + \frac{\delta v}{\delta x}
\end{aligned}$$

Hence, the relationship between the displacements and the strains can be expressed in the form

$$\begin{bmatrix} \epsilon_x \\ \epsilon_y \\ \gamma \end{bmatrix} = \frac{1}{ab} \begin{bmatrix} -b+y & b-y & -y & y & 0 & 0 & 0 & 0 \\ 0 & 0 & 0 & 0 & -a+x & -x & a-x & x \\ -a+x & -x & a-x & x & -b+y & b-y & -y & y \end{bmatrix} \begin{bmatrix} u_i \\ u_j \\ u_k \\ u_l \\ v_i \\ v_j \\ v_k \\ v_l \end{bmatrix}$$

or symbolically

$$[\epsilon] = [a_u][u]$$

The stress-strain relationship for an isotropic elastic material in a state of plain stress is

$$\begin{Bmatrix} \sigma_x \\ \sigma_y \\ \tau_{xy} \end{Bmatrix} = \begin{bmatrix} \alpha & \beta & 0 \\ \beta & \alpha & 0 \\ 0 & 0 & G \end{bmatrix} \begin{Bmatrix} \epsilon_x \\ \epsilon_y \\ \gamma_{xy} \end{Bmatrix}$$

or $[\sigma] = [K][\epsilon]$ (2-6)

where

$$\alpha = \frac{E}{(1-\nu^2)}$$

$$\beta = \frac{\nu E}{(1-\nu^2)}$$

$$G = \frac{E}{2(1+\nu)}$$

K = the stiffness of an infinitesimal element of area dA .

The stiffness of a system of infinitesimal elements is given by

$$[S_\ell] = \iint_{\text{area}} [a_u]^T [K] [a_u] d_x d_y$$

which results in an 8 x 8 symmetrical matrix.

The rotational stiffness matrix is difficult to define. Because of this fact, the procedure in plate and shell theory has been to ignore it. For the box type structure this is not possible so displacement functions were decided on which would represent the rotation of the corners in turn.

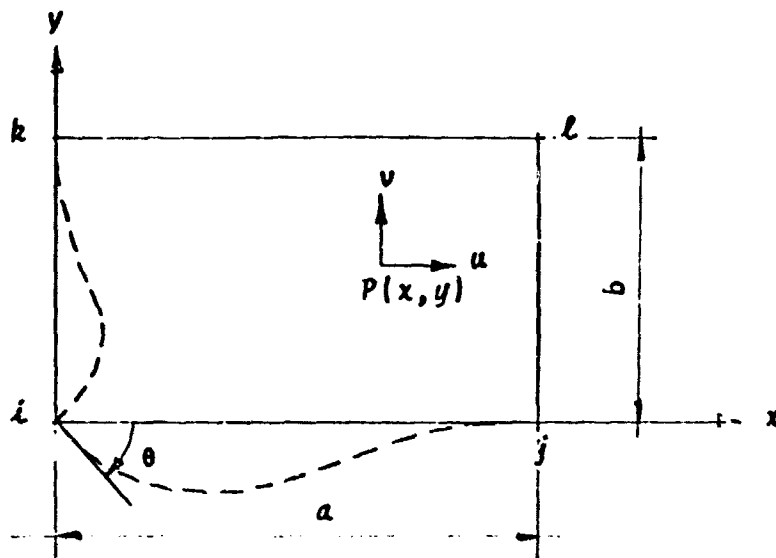


Figure 2-5

INPLANE ROTATIONAL STRAIN OF AN ELEMENT

The displacement pattern is shown in Figure 2-5 where

$$u(x,y) = \frac{y\theta}{ab^2} (y-b)^2(a-x) = F_1(x,y)\theta \quad (2-7)$$

$$v(x,y) = \frac{-x\theta}{a^2b} (x-a)^2(b-y) = F_2(x,y)\theta \quad (2-8)$$

Since the assumed displacement functions have a linear θ dependence, superposition can be used.

Hence

$$u(x,y) = u(i) + u(j) + u(k) + u(l)$$

$$v(x,y) = v(i) + v(j) + v(k) + v(l)$$

or in matrix form as shown in Figure 2-6.

The relationship between the displacements and the strains can be expressed in the form

$$\begin{Bmatrix} \epsilon_x \\ \epsilon_y \\ \gamma_z \end{Bmatrix} = [a_\theta] \begin{Bmatrix} \theta_i \\ \theta_j \\ \theta_k \\ \theta_l \end{Bmatrix}$$

or

$$[\epsilon] = [a_\theta](\theta) \quad (2-9)$$

where $[a_\theta]$ is given in Figure 2-7.

Due to the displacement field (u,v) for the set of angle changes (θ) there is a field of external self equilibrating moments $[M]$.

The equilibrium condition is satisfied if the set of external moments, $[M]$, acting on the external angle changes, (θ) produces the same work as the set of internal stresses, (σ) , acting on the internal strains, (ϵ) .

$$\text{Hence } \int_{vol} (\theta)^T [M] = \int_{vol} (\epsilon)^T (\sigma) d(vol) \quad (2-10)$$

Using equations 2-6 and 2-9

$$(\theta)^T [M] = \int_{00}^{ab} (\theta)^T [a_\theta]^T [K] [a_\theta] (\theta) dx dy \quad (2-11)$$

Since (θ) is independent of "x" and "y",

$$[M] = \left[\int_{00}^{ab} [a_\theta]^T [K] [a_\theta] dx dy \right] (\theta) \quad (2-12)$$

$$\begin{Bmatrix} u(x,y) \\ v(x,y) \end{Bmatrix} = \begin{bmatrix} F_1(x,y)F_1(a-x,y) - F_1(x,b-y) - F_1(a-x,b-y) \\ F_2(x,y)F_2(a-x,y) - F_2(x,b-y) - F_2(a-x,b-y) \end{bmatrix} \begin{Bmatrix} \theta_i \\ \theta_j \\ \theta_k \\ \theta_l \end{Bmatrix}$$

Figure 2-6 ASSUMED DISPLACEMENT FUNCTION

$$[a_\theta] = \begin{bmatrix} F_1(x,y)_{,x} & F_1(a-x,y)_{,x} & -F_1(x,b-y)_{,x} & -F_1(a-x,b-y)_{,x} \\ -F_2(x,y)_{,y} & F_2(a-x,y)_{,y} & -F_2(x,b-y)_{,y} & F_2(a-x,b-y)_{,y} \\ a_{31} & a_{32} & a_{33} & a_{34} \end{bmatrix}$$

where

$$a_{31} = F_1(x,y)_{,y} - F_2(x,y)_{,x}$$

$$a_{32} = F_1(a-x,y)_{,y} + F_2(a-x,y)_{,x}$$

$$a_{33} = -F_1(x,b-y)_{,y} - F_2(x,b-y)_{,x}$$

$$a_{34} = -F_1(a-x,b-y)_{,y} + F_2(a-x,b-y)_{,x}$$

Figure 2-7 DISPLACEMENT STRAIN RELATIONSHIP

So that,

$$[S_r] = \int_0^a \int_0^b [a_\theta]^T [K] [a_\theta] dx dy \quad (2-13)$$

The expansion of the integral in equation 2-13 for the first row of the matrix $[S_r]$ is shown in Figure 2-8.

It can be seen that there is a lack of equilibrium, therefore the matrix was brought into equilibrium by arbitrarily subtracting $\frac{G\delta b}{4}$ from each element. This is numerically small compared with the other terms and has little effect on the results.

The first row of the matrix $[S_r]$ is expanded into a consistent matrix as shown in Figure 2-9.

As plates in different planes are joined together, the elements of the stiffness matrices cannot be added directly. It is necessary to convert the coordinates from a local to a global system. This can be done by using the coordinate transformation matrix for stiffness as shown in Table 2-1. Once in the global system the stiffness matrices can be combined into a single stiffness matrix $[K]$ for the complete box by keeping track of the nodal points of the four corners of the individual elements.

$$S_{r1,1} = \frac{ab^3}{105a} + \frac{aa^3}{105b} - \frac{8ab}{72} + \frac{3Gab}{40}$$

$$S_{r1,2} = \frac{-ab^3}{105a} - \frac{aa^3}{140b} - \frac{8ab}{36} + \frac{Gab}{40}$$

$$S_{r1,3} = \frac{-ab^3}{140a} - \frac{aa^3}{105b} - \frac{8ab}{36} + \frac{Gab}{40}$$

$$S_{r1,4} = \frac{ab^3}{140a} + \frac{aa^3}{140b} + \frac{58ab}{72} - \frac{Gab}{40}$$

Figure 2-8
ELEMENTS OF FIRST ROW OF $[S_r]$

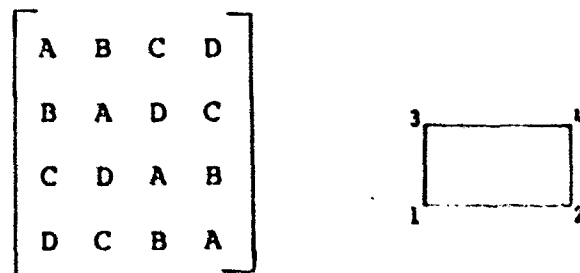


Figure 2-9
CONSISTENT MATRIX $[s_p]$

TABLE 2-1

Coordinate Transformation
for
Stiffness Coefficients

LOCAL I	GLOBAL		
	Type 1	Type 2	Type 3
1	1	3	3
2	7	9	9
3	13	15	15
4	19	21	21
5	-2	-2	-1
6	-8	-8	-7
7	-14	-14	-13
8	-20	-20	-19
9	-3	1	-2
10	5	5	4
11	4	6	6
12	-9	7	-8
13	11	11	10
14	10	12	12
15	-15	13	-14
16	17	17	16
17	16	18	18
18	-21	19	-20
19	23	23	22
20	22	24	24
21	-6	4	-5
22	-12	10	-11
23	-18	16	-17
24	-24	22	-23

Section 3

NODAL POINT LOADS

At any instant of time, the applied distributed load on the structure can be specified. This must be converted into a nodal point loading equivalent to the distributed load such that the nodal deformations and the total work are the same in each system.

$$\begin{array}{l} \text{External Energy} \\ \text{due to actual} \\ \text{distributed load} \end{array} = \frac{1}{2} \int_A q(x,y) w(x,y) dA \quad (3-1)$$

$$\begin{array}{l} \text{External Energy} \\ \text{due to equivalent} \\ \text{nodal point loads} \end{array} = \frac{1}{2} (L)^T \{\phi\} \quad (3-2)$$

where q is the load on the area dA and w is its displacement. For one plate, (L) is a 12 x 1 column matrix consisting of a force and two moments at each corner of the plate, and $\{\phi\}$ is the associated displacement.

From Equations 3-1 and 3-2,

$$(L)^T \{\phi\} = \int_A q(x,y) w(x,y) dA \quad (3-3)$$

Substituting the 12-term polynomial for w in Equation 2-1,

$$(L)^T \{\phi\} = \int_A q(x,y) [d](a) dA$$

where $[d]$ is a 1 x 12 matrix of the terms of the polynomial and (a) is a 12 x 1 matrix of the coefficients.

Substituting for $(a) = [N](\phi)$

$$(L)^T = \int_A q(x,y) [d][N] dA$$

or

$$(L) = [N]^T \int_A q(x,y) [d]^T dA \quad (3-4)$$

The matrix $[N]$ which has been introduced can be evaluated through the polynomial in w with this expression and by differentiating it with respect to x and y , the values of w can be related for each displacement at each corner for the twelve coefficients α . The development of the inverse matrix $[N]^{-1}$ is given in Figure 3-1.

The $q(x, y)$ function can be expressed as:

$$q(x, y) = C_1 + C_2x + C_3y + C_4xy$$

where the coefficients $C_1, C_2, C_3,$ and C_4 are evaluated from the load conditions at the nodal points.

The integral $\int_A q(x, y) [d]^T dA$ can be written as:

$$(I) = \int_A (C_1 + C_2x + C_3y + C_4xy) [d]^T dA$$

or

$$(I) = [F(a, b)] \begin{Bmatrix} C_1 \\ C_2 \\ C_3 \\ C_4 \end{Bmatrix}$$

and

$$\begin{Bmatrix} q_i \\ q_j \\ q_k \\ q_l \end{Bmatrix} = [Q]^{-1} \begin{Bmatrix} C_1 \\ C_2 \\ C_3 \\ C_4 \end{Bmatrix}$$

so that $(L) = [N]^T [F(a, b)] [Q] (q)$ (3-5)

where

$$[Q]^{-1} = \begin{bmatrix} 1 & 0 & 0 & 0 \\ 1 & a & 0 & 0 \\ 1 & 0 & b & 0 \\ 1 & a & b & ab \end{bmatrix}$$

and $F(a, b)$ is shown in Figure 3-2.

$$w = \alpha_1 + \alpha_2 x + \alpha_3 y + \alpha_4 x^2 + \alpha_5 xy + \alpha_6 y^2 + \alpha_7 x^3 + \alpha_8 x^2 y + \alpha_9 xy^2 + \alpha_{10} y^3 + \alpha_{11} x^3 y + \alpha_{12} xy^3$$

$$w, x = \alpha_2 + 2\alpha_4 x + \alpha_5 y + 3\alpha_7 x^2 + 2\alpha_8 xy + \alpha_9 y^2 + 3\alpha_{11} x^2 y + \alpha_{12} y^3$$

$$w, y = \alpha_3 + \alpha_5 x + 2\alpha_6 y + \alpha_8 x^2 + 2\alpha_9 xy + 3\alpha_{10} y^2 + \alpha_{11} x^3 + 3\alpha_{12} xy^2$$

$$\text{At joint } i \quad x = 0 \quad y = 0$$

$$j \quad x = a \quad y = 0$$

$$k \quad x = 0 \quad y = b$$

$$l \quad x = a \quad y = b$$

$$\phi = [N]^{-1} \{a\}$$

$$(\phi) = \begin{Bmatrix} w^i \\ w^i, x \\ w^i, y \\ w^j \\ w^j, x \\ w^j, y \\ w^k \\ w^k, x \\ w^k, y \\ w^l \\ w^l, x \\ w^l, y \end{Bmatrix} = \begin{bmatrix} 1 & 0 & 0 & 0 & 0 & 0 & 0 & 0 & 0 & 0 & 0 & 0 \\ 0 & 1 & 0 & 0 & 0 & 0 & 0 & 0 & 0 & 0 & 0 & 0 \\ 0 & 0 & 1 & 0 & 0 & 0 & 0 & 0 & 0 & 0 & 0 & 0 \\ 1 & a & 0 & a^2 & 0 & 0 & a^3 & 0 & 0 & 0 & 0 & 0 \\ 0 & 1 & 0 & 2a & 0 & 0 & 3a^2 & 0 & 0 & 0 & 0 & 0 \\ 0 & 0 & 1 & 0 & a & 0 & 0 & a^2 & 0 & 0 & a^3 & 0 \\ 1 & 0 & b & 0 & 0 & b^2 & 0 & 0 & 0 & b^3 & 0 & 0 \\ 0 & 1 & 0 & 0 & b & 0 & 0 & 0 & b^2 & 0 & 0 & b^3 \\ 0 & 0 & 1 & 0 & 0 & 2b & 0 & 0 & 0 & 3b^2 & 0 & 0 \\ i & a & b & a^2 & ab & b^2 & a^3 & a^2 b & ab^2 & b^3 & a^3 b & ab^3 \\ 0 & 1 & 0 & 2a & b & 0 & 3a^2 & 2ab & b^2 & 0 & 3a^2 b & b^3 \\ 0 & 0 & 1 & 0 & a & 2b & 0 & a^2 & 2ab & 3b^2 & a^3 & 3ab^2 \end{bmatrix} \begin{Bmatrix} \alpha_1 \\ \alpha_2 \\ \alpha_3 \\ \alpha_4 \\ \alpha_5 \\ \alpha_6 \\ \alpha_7 \\ \alpha_8 \\ \alpha_9 \\ \alpha_{10} \\ \alpha_{11} \\ \alpha_{12} \end{Bmatrix}$$

$$[N]^{-1}$$

Figure 3-1 DEVELOPMENT OF MATRIX [N]

ab	$\frac{1}{2}a^2b$	$\frac{1}{2}ab^2$	$\frac{1}{4}a^2b^2$
$\frac{1}{2}a^2b$	$\frac{1}{3}a^3b$	$\frac{1}{4}a^2b^2$	$\frac{1}{6}a^3b^2$
$\frac{1}{2}ab^2$	$\frac{1}{4}a^2b^2$	$\frac{1}{3}ab^3$	$\frac{1}{6}a^2b^3$
$\frac{1}{3}a^3b$	$\frac{1}{4}a^4b$	$\frac{1}{6}a^3b^2$	$\frac{1}{8}a^4b^2$
$\frac{1}{4}a^2b^2$	$\frac{1}{6}a^3b^2$	$\frac{1}{6}a^2b^3$	$\frac{1}{9}a^3b^3$
$\frac{1}{3}ab^3$	$\frac{1}{6}a^2b^3$	$\frac{1}{4}ab^4$	$\frac{1}{8}a^2b^4$
$\frac{1}{4}a^4b$	$\frac{1}{5}a^5b$	$\frac{1}{8}a^4b^2$	$\frac{1}{10}a^5b^2$
$\frac{1}{6}a^3b^2$	$\frac{1}{8}a^4b^2$	$\frac{1}{9}a^3b^3$	$\frac{1}{12}a^4b^3$
$\frac{1}{6}a^2b^3$	$\frac{1}{9}a^3b^3$	$\frac{1}{8}a^2b^4$	$\frac{1}{12}a^3b^4$
$\frac{1}{4}ab^4$	$\frac{1}{8}a^2b^4$	$\frac{1}{5}ab^5$	$\frac{1}{10}a^2b^5$
$\frac{1}{8}a^4b^2$	$\frac{1}{10}a^5b^2$	$\frac{1}{12}a^4b^3$	$\frac{1}{15}a^5b^3$
$\frac{1}{8}a^2b^4$	$\frac{1}{12}a^3b^4$	$\frac{1}{10}a^2b^5$	$\frac{1}{15}a^3b^5$

Figure 3-2
 MATRIX F(a, b)

By using a procedure similar to that used in determining the stiffness matrix for the complete structure, the load matrix for the complete structure can be obtained by taking the load matrices for each individual plate and expanding them into a global coordinate system by using a coordinate transformation matrix and inserting the elements of the submatrices in the large matrix at the desired location. The load coordinate transformation matrix is shown in Table 3-1.

TABLE 3-1

Coordinate Transformation for Nodal Loads

LOCAL	GLOBAL		
	Type 1	Type 2	Type 3
1	-3	1	-2
2	5	5	4
3	4	6	6
4	-9	7	-8
5	11	11	10
6	10	12	12
7	-15	13	-14
8	17	17	16
9	16	18	18
10	-21	19	-20
11	23	23	22
12	22	24	24

Section 4

DYNAMIC RESPONSE ANALYSIS - ELASTIC

4-1 Equation of Equilibrium

Through the finite element method, the box structure is replaced by lumped parameters at discrete nodal points. The mass, which is distributed throughout the structure, is assumed to be concentrated at the nodal points. The deformation-resistance characteristics of the box are defined for relative displacement of the mass coordinates by the stiffness matrix described in Section 2.

The equilibrium of the discrete mass system at time t is expressed by the following matrix equation:

$$[M] \{\ddot{X}\}_t + [C] \{\dot{X}\}_t + [K] \{X\}_t = \{P\}_t \quad (4-1)$$

where $\{\ddot{X}\}_t$ = acceleration of the system

$\{\dot{X}\}_t$ = velocity of the system

$\{X\}_t$ = displacement of the system

$\{P\}_t$ = force acting on the system

$[M]$ = the diagonal mass matrix

$[C]$ = the damping matrix

$[K]$ = the stiffness matrix

4-2 Mass Matrix

A lumped mass approach is used to calculate the dynamic response, with the displacement of each mass directly represented by a single coordinate. The advantage of this simple mass idealization is that it eliminates any mass coupling. Thus, a diagonal mass matrix is used in equation 4-1.

The mass at each nodal point of the structure contains a contribution from each plate element attached to the node. Referring to Figure 4-1, this typical mass contribution at a node from a single element is expressed as,

$$\begin{Bmatrix} M_x \\ M_y \\ M_z \\ M_{\theta x} \\ M_{\theta y} \\ M_{\theta z} \end{Bmatrix} = \frac{\rho abt}{840g} \begin{Bmatrix} 210 \\ 210 \\ 210 \\ a^2 \\ b^2 \\ a^2+b^2 \end{Bmatrix} + \rho_s t_s \frac{ab}{4g} \begin{Bmatrix} 0 \\ 0 \\ 1 \\ 0 \\ 0 \\ 0 \end{Bmatrix} \quad (4-2)$$

where ρ and t are, respectively, the density and thickness of the plate element. Similarly, ρ_s and t_s are, respectively, the density and thickness of soil layer assumed acting with the plate element.

In equation 4-2, the distributed mass of each plate element is assumed lumped at its corners, one-fourth of the total mass to each. Figure 4-1 illustrates this physical lumping of mass. The mass at each corner, or nodal point, can be put into motion in the local x , y and z directions. Mass quantities associated with these movements are expressed by the first term of the right-hand side of the equation. This mass matrix in its diagonalized form is an extension of the work by Archer on consistent mass matrices for distributed mass systems.¹²

Since the structure is in contact with soil, many exterior plate motions will be coupled with the movement of a certain mass of soil. The second term of Equation 4-2 assigns a mass quantity to the local z direction of element displacement only. In other words, soil inertia forces are considered only for motions perpendicular to each element's plane. The thickness of soil, t_s , is an arbitrary quantity. For the roof of a shallow buried box, t_s equals the depth of soil cover.

Figure 4-1

MASS CONCENTRATION AT A TYPICAL NODE

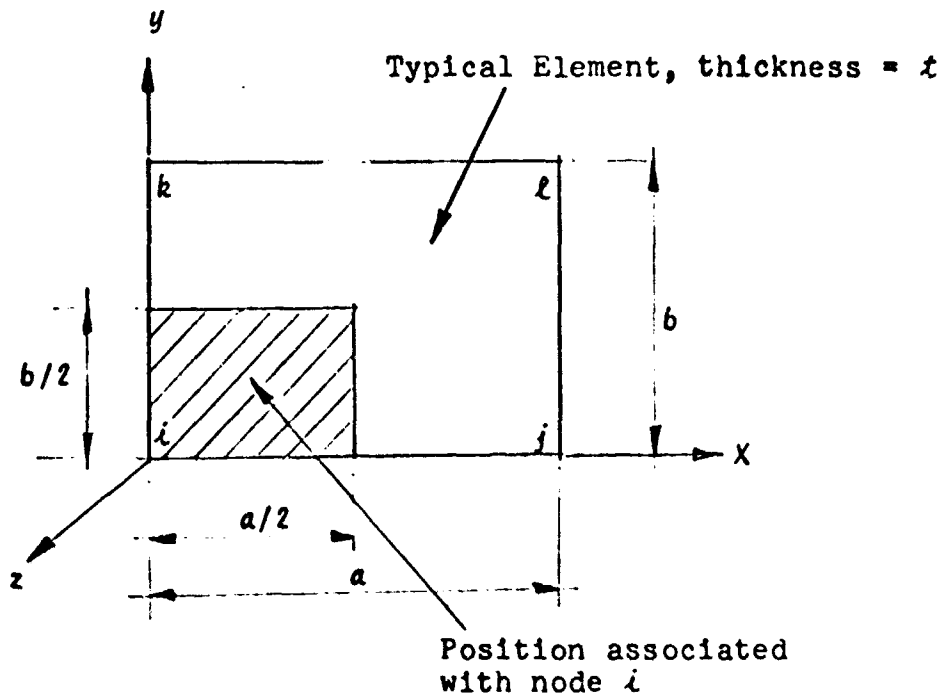


TABLE 4-1

GLOBAL	LOCAL		
	Type 1	Type 2	Type 3
1	1	3	3
2	2	2	1
3	3	1	2
4	4	6	6
5	5	5	4
6	6	4	5

COORDINATE TRANSFORMATION FOR MASSES

The mass matrix for the whole structure is obtained by expanding the mass matrix for each individual element into the global coordinate system by means of a coordinate transformation, and superposing the expansions.

A generalized mass approach, based on assumed displacement functions, could be used. However, this would lead to coupled (i.e., off-diagonal) mass matrix terms which complicate the storage problems in the computer. Furthermore, assumed shape functions will not necessarily lead to improved accuracy in the results. The most severe approximation is the number of degrees of freedom allowed. It is believed that the physical lumping of mass is a satisfactory approximation for this particular system.

4-3 Damping Matrix

The exact form of the damping matrix is unknown for box-structures, as is the case for most structural systems. However, in most instances, its effect on the mode of vibration will be small. Therefore, it is reasonable to replace the [C] matrix by the following matrix relationship:¹

$$[C] = a_0 [M] + a_1 [K] \quad (4-3)$$

By assuming the damping matrix to be a linear combination of the mass matrix and the stiffness matrix, computations are simplified and computer storage requirements are minimized.

The significant test experience in determining energy losses due to structural damping has related these losses to the frequencies and mode shapes of particular systems. Since the determination of frequencies and mode shapes is not a part of the step-by-step method of solution, modal damping cannot be used directly. However, a_0 and a_1 may be interpreted in terms of equivalent modal damping¹ if the significant frequency range of response is known or can be estimated.

The modal damping ratio λ_i for the i^{th} mode is given in terms of a_0 and a_1 by,

$$\lambda_i = \frac{a_0}{2\omega_i} + \frac{a_1 \omega_i}{2} \quad (4-4)$$

where ω_i is the circular frequency of the i^{th} mode.

The frequency $\bar{\omega}$, which yields a minimum value of the damping ratio $\bar{\lambda}$, is given by

$$\bar{\omega} = \sqrt{\frac{a_0}{a_1}} \quad (4-5)$$

If the minimum damping ratio $\bar{\lambda}$ and its associated frequency $\bar{\omega}$ are given, the damping coefficients a_0 and a_1 are calculated from the following equations:

$$a_0 = \bar{\lambda} \bar{\omega} \quad (4-6a)$$

$$a_1 = \bar{\lambda} / \bar{\omega} \quad (4-6b)$$

Equation 4-4 can now be rewritten:

$$\lambda_i = \left(\frac{\bar{\omega}}{\omega_i} + \frac{\omega_i}{\bar{\omega}} \right) \frac{\bar{\lambda}}{2} \quad (4-7)$$

Usually, the numerical value of the minimum damping ratio will be established from judgement regarding past structural tests. It may vary through a range of 2 percent to 30 percent of critical ($.02 < \bar{\lambda} < .30$). Having estimated a minimum damping, however, does not fully define the coefficients a_0 and a_1 . The associated frequency $\bar{\omega}$ must be established.

If the significant frequency range of response is between the values ω_1 and ω_n , such that;

$$\omega_1 < \bar{\omega} < \omega_n \quad (4-8)$$

it is convenient to select the frequency $\bar{\omega}$ as a multiple of the lowest frequency ω_1 and, in turn, such that the highest frequency ω_n is the same multiple of $\bar{\omega}$.

That is;

$$\bar{\omega} = m \omega_1 \quad (4-9a)$$

$$\omega_n = m \bar{\omega} = m^2 \omega_1 \quad (4-9b)$$

where m is any positive constant. Now, the frequency $\bar{\omega}$ can be calculated simply from the established frequency range, as follows:

$$\bar{\omega} = \sqrt{\omega_1 \omega_n} \quad (4-10)$$

The values of a_0 and a_1 are, as given previously;

$$a_0 = \bar{\lambda} \bar{\omega} \quad (4-6a)$$

$$a_1 = \bar{\lambda} / \bar{\omega} \quad (4-6b)$$

The damping ratio for the first mode, λ_1 , and the highest mode of interest, λ_n , becomes (rewriting equation 4-7);

$$\lambda_1 = \lambda_n = \left(\frac{\omega_1 + \omega_n}{\sqrt{\omega_1 \omega_n}} \right) \frac{\bar{\lambda}}{2} \quad (4-11)$$

As an example calculation, assume the minimum damping ratio to be 5 percent of critical. Further, assume that the fundamental period of vibration is associated with the flexural response of thick slabs and is $\omega_1 = 31.6$ rad/sec. Also, assume that the highest frequency of interest is that due to inplane response of the slab elements and is equal to 316 rad/sec:

$$\bar{\omega} = \sqrt{31.6 \times 316} = 100 \text{ rad/sec}$$

$$\bar{\lambda} = .05$$

$$\lambda_1 = \lambda_n = \frac{(31.6 + 316)}{100} \frac{.05}{2} = .087$$

$$a_0 = .05 \times 100 = 5.0$$

$$a_1 = .05 + 100 = 0.0005$$

4-4 Response Calculations

It is assumed that the acceleration of each discrete mass varies linearly within a time interval Δt . This assumption, which is illustrated in Figure 4-2, leads to a parabolic variation of velocity and a cubic variation of displacement within the time interval.

A direct integration over the interval gives the following equations for acceleration and velocity at the end of the time interval:

$$\ddot{x}_t = \frac{6}{\Delta t^2} x_t - A_t \quad (4-12a)$$

$$\dot{x}_t = \frac{3}{\Delta t} x_t - B_t \quad (4-12b)$$

where
$$A_t = \frac{6}{\Delta t^2} x_{t-\Delta t} + \frac{6}{\Delta t} \dot{x}_{t-\Delta t} + 2\ddot{x}_{t-\Delta t} \quad (4-12c)$$

$$B_t = \frac{3}{\Delta t} x_{t-\Delta t} + 2\dot{x}_{t-\Delta t} + \frac{\Delta t}{2} \ddot{x}_{t-\Delta t} \quad (4-12d)$$

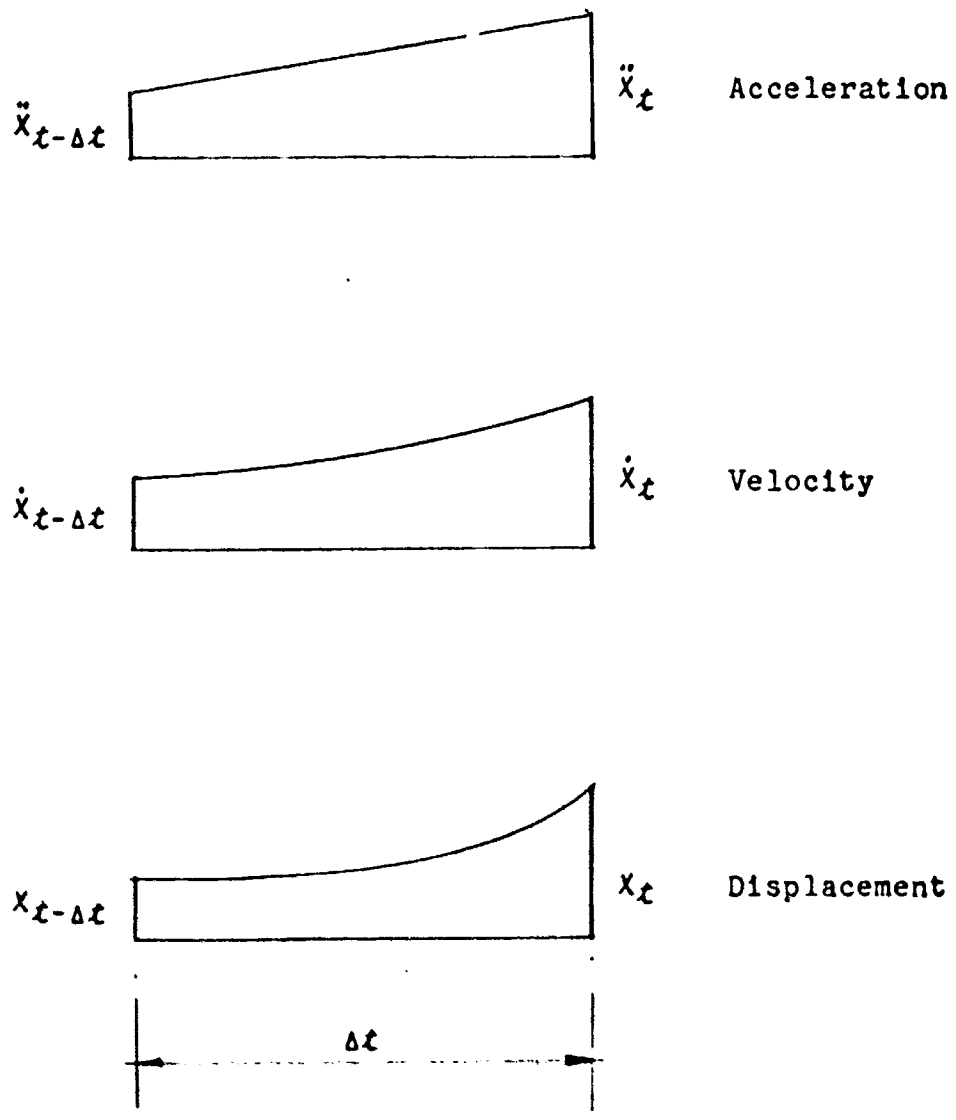


Figure 4-2

ASSUMED BEHAVIOR OF TYPICAL DISPLACEMENT COMPONENT

Substituting Equations 4-3, 4-12a and 4-12b into the dynamic equilibrium relation 4-1 yields the following set of linear equations in terms of some unknown "effective" displacement.

$$[\bar{K}] [\bar{X}]_t = [\bar{P}]_t \quad (4-13)$$

where

$$[\bar{K}] = [K] + C_2 [M] \quad (4-14a)$$

$$[\bar{P}]_t = [P]_t + [M] \left[[A]_t + C_4 [B]_t \right] \quad (4-14b)$$

$$[\bar{X}]_t = \frac{1}{C_1} [\bar{X}]_t - \frac{C_3}{C_2} [B]_t \quad (4-14c)$$

in which

$$C_0 = \frac{6}{\Delta t^2} + \frac{3a_0}{\Delta t} \quad (4-15a)$$

$$C_1 = \frac{1}{1 + \frac{3a_1}{\Delta t}} \quad (4-15b)$$

$$C_2 = C_0 C_1 \quad (4-15c)$$

$$C_3 = C_2 a_1 \quad (4-15d)$$

$$C_4 = a_0 - C_3 \quad (4-15e)$$

The dynamic response of the structure is obtained from the above relationships by using the following step by step procedure.

1. Initialization

a. Form stiffness matrix $[K]$ and mass matrix $[M]$

b. Form "effective" stiffness matrix

$$[\bar{K}] = [K] + C_2 [M]$$

c. Triangularize $[K]$

2. For Each Time Increment

a. Form $[A]_t$ and $[B]_t$

$$[A]_t = \frac{6}{\Delta t^2} [X]_{t-\Delta t} + \frac{6}{\Delta t} [\dot{X}]_{t-\Delta t} + 2[\ddot{X}]_{t-\Delta t}$$

$$[B]_t = \frac{3}{\Delta t} [X]_{t-\Delta t} + \frac{3}{2} [\dot{X}]_{t-\Delta t} + \frac{\Delta t}{2} [\ddot{X}]_{t-\Delta t}$$

b. Form "effective" load

$$[\bar{P}]_t = [P]_t + [M] \left[[A]_t + c_4 [B]_t \right]$$

c. Solve for "effective" displacements

$$[\bar{X}]_t = [K]^{-1} [\bar{P}]_t$$

d. Calculate Displacements, Velocities and Accelerations at time t .

$$[X]_t = c_1 [\bar{X}]_t + c_1 a_1 [B]_t$$

$$[\dot{X}]_t = \frac{3}{\Delta t} [X]_t - [B]_t$$

$$[\ddot{X}]_t = \frac{6}{\Delta t^2} [X]_t - [A]_t$$

e. Repeat for next time increment

It is important to note that for elastic structures, the matrix $[K]$ need only be formed once since it is independent of time.

4-5 Solution of the Equilibrium Equation

Equation 4-13 expresses the dynamic equilibrium of the system in an equation of the form, $[A][X] = [B]$.

The method used for the solution of these equations is the Gaussian Elimination method.

4-5.1 Gaussian Elimination

The equilibrium equations for a system of finite elements may be written in the following form:

$$A_{11}X_1 + A_{12}X_2 + A_{13}X_3 \dots\dots\dots + A_{1N}X_N = B_1 \quad (4-16a)$$

$$A_{21}X_1 + A_{22}X_2 + A_{23}X_3 \dots\dots\dots + A_{2N}X_N = B_2 \quad (4-16b)$$

$$A_{31}X_1 + A_{32}X_2 + A_{33}X_3 \dots\dots\dots + A_{3N}X_N = B_3 \quad (4-16c)$$

⋮
⋮
⋮
⋮

$$A_{N1}X_1 + A_{N2}X_2 + A_{N3}X_3 \dots\dots\dots + A_{NN}X_N = B_N$$

The first step in the solution of the above set of equations is to solve equation 4-16a for X_1 , or

$$X_1 = B_1/A_{11} - (A_{12}/A_{11})X_2 - (A_{13}/A_{11})X_3 \dots\dots (A_{1N}/A_{11})X_N \quad (4-17)$$

If equation 4-17 is substituted into equations (4-16a, 4-16b, ..., N) a modified set of $N-1$ equations is determined.

$$A_{22}^1X_2 + A_{23}^1X_3 \dots\dots\dots + A_{2N}^1X_N = B_2^1 \quad (4-18a)$$

$$\begin{aligned}
 A_{32}^1 X_2 + A_{33}^1 X_3 \dots\dots\dots + A_{3N}^1 X_N &= B_2^1 & (4-18b) \\
 \vdots & \\
 \vdots & \\
 \vdots & \\
 A_{N2}^1 X_2 + A_{N3}^1 X_3 \dots\dots\dots + A_{NN}^1 X_N &= B_N^1
 \end{aligned}$$

where

$$A_{ij}^1 = A_{ij} - A_{i1}A_{1j}/A_{11} \quad i, j = 2, \dots, N \quad (4-19a)$$

$$B_i^1 = B_i - A_{i1}B_1/A_{11} \quad i = 2, \dots, N \quad (4-19b)$$

A similar procedure is used to eliminate X_2 from equation 4-18a, etc.

A general algorithm for the elimination of X_n may be written as

$$X_n = (B_n^{n-1}/A_{nn}^{n-1}) - \sum (A_{nj}^{n-1}/A_{nn}^{n-1})X_j \quad j = n+1, \dots, N \quad (4-20)$$

$$A_{ij}^n = A_{ij}^{n-1} - A_{in}^{n-1}(A_{nj}^{n-1}/A_{nn}^{n-1}) \quad i, j = n+1, \dots, N \quad (4-21)$$

$$B_i^n = B_i^{n-1} - A_{in}^{n-1}(B_n^{n-1}/A_{nn}^{n-1}) \quad i = n+1, \dots, N \quad (4-22)$$

Equations 4-20, 4-21, and 4-22 may be rewritten in compact form:

$$X_n = D_n - \sum C_{nj}X_j \quad j = n+1, \dots, N \quad (4-23)$$

$$A_{ij}^n = A_{ij}^{n-1} - A_{in}^{n-1}C_{nj} \quad i, j = n+1, \dots, N \quad (4-24a)$$

$$B_i^n = B_i^{n-1} - A_{in}^{n-1}D_n \quad i = n+1, \dots, N \quad (4-24b)$$

where

$$D_n = B_n^{n-1} / A_{nn}^{n-1} \quad (4-25a)$$

$$C_{nj} = A_{nj}^{n-1} / A_{nn}^{n-1} \quad (4-25b)$$

After the above procedure is applied $N-1$ times the original set of equations is reduced to the following single equation

$$A_{NN}^{N-1} X_N = B_N^{N-1}$$

which is solved directly for X_N

$$X_N = B_N^{N-1} / A_{NN}^{N-1}$$

In terms of the previous notation, this is

$$X_N = D_N \quad (4-26)$$

The remaining unknowns are determined in reverse order by the repeated application of equation 4-23.

4-5.2 Simplification for Band Matrices

The stiffness matrix was placed in a "band" form which resulted in the concentration of the elements of the stiffness matrix along the main diagonal. Therefore, the following simplifications in the general algorithm (equations 4-23, 4-24a, and 4-24b) were possible:

$$X_n = D_n - \sum C_{nj} X_j \quad j = n + 1, \dots, n + M - 1 \quad (4-27)$$

$$A_{ij}^n = A_{ij}^{n-1} - A_{in}^{n-1} C_{nj} \quad i, j = n + 1, \dots, n + M - 1 \quad (4-28)$$

$$B_i^n = B_i^{n-1} - A_{in}^{n-1} D_n \quad i = n + 1, \dots, n + M - 1 \quad (4-29)$$

where M is the band width of the matrix.

The number of numerical operations can further be reduced by recognizing that the reduced matrix at any stage of procedure is symmetric. Accordingly, equation 4-28 may be replaced by the following equation:

$$A_{ij}^n = A_{ij}^{n-1} - A_{in}^{n-1} C_{nj} \quad \begin{array}{l} i = n + 1, \dots, n + M - 1 \\ j = i, \dots, n + M - 1 \end{array} \quad (4-30)$$

since

$$A_{ji}^n = A_{ij}^n$$

The number of numerical operations required for the solution of a band matrix is proportional to NM^2 as compared to N^3 which is required for the solution of a full matrix. Also, the computer storage required by the band matrix procedure is NM as compared to N^2 required by a set of N arbitrary equations.

4-5.3 Stresses

Once the nodal displacements are known, it is possible to determine the stresses at these points. For design purposes the following forces are required:

M_x = Moment per unit length in the x direction

M_y = Moment per unit length in the y direction

M_{xy} = Twisting moment at the point

Q_x = Shear force per unit length in the x direction

Q_y = Shear force per unit length in the y direction

σ_x = Inplane stress in the x direction

σ_y = Inplane stress in the y direction

τ_{xy} = Inplane shear stress at the point

The moments are obtained from Equation 4-31

$$\begin{Bmatrix} M_x \\ M_y \\ M_{xy} \end{Bmatrix} = \begin{bmatrix} -D & -\nu D & 0 \\ -\nu D & -D & 0 \\ 0 & 0 & (1-\nu)D \end{bmatrix} \begin{Bmatrix} w_{,xx} \\ w_{,yy} \\ 2w_{,xy} \end{Bmatrix} \quad (4-31)$$

$$\text{where } D = \frac{Et^3}{12(1-\nu^2)}$$

The shear forces are obtained from Equation 4-32.

$$\begin{Bmatrix} Q_x \\ Q_y \end{Bmatrix} = -D \begin{Bmatrix} \frac{\partial}{\partial x}(\nabla^2 w) \\ \frac{\partial}{\partial y}(\nabla^2 w) \end{Bmatrix} \quad (4-32)$$

Since the displacement w at any point is represented by the 12-term polynomial (Equation 2-1), we can say

$$w(x,y) = [1|x|y|x^2|xy|y^2|x^3|x^2y|xy^2|x^3|x^3y|xy^3|][N](\phi)$$

$$\text{or } (w) = [d][N](\phi) \quad (4-33)$$

The matrix $[N]^{-1}$ is as shown in Figure 3-5.

From Equation 4-31, 4-32 and 4-33, we get

$$\begin{Bmatrix} M_x \\ M_y \\ M_{xy} \\ Q_x \\ Q_y \end{Bmatrix} = -D \begin{bmatrix} 1 & \nu & 0 & 0 & 0 \\ \nu & 1 & 0 & 0 & 0 \\ 0 & 0 & \nu-1 & 0 & 0 \\ 0 & 0 & 0 & 1 & 0 \\ 0 & 0 & 0 & 0 & 1 \end{bmatrix} \begin{Bmatrix} d_{,xx} \\ d_{,yy} \\ 2d_{,xy} \\ \partial/\partial x \nabla^2 d \\ \partial/\partial y \nabla^2 d \end{Bmatrix} [N](\phi) \quad (4-34)$$

Multiplying the derivatives of the second matrix by the first and assuming $\nu = 0.2$, we get

$$\begin{Bmatrix} M_x \\ M_y \\ M_{xy} \\ Q_x \\ Q_y \end{Bmatrix} = \begin{bmatrix} 0 & 0 & 0 & 2. & 0 & .4 & 3x & 2y & .4x & 1.2y & 6xy & 1.2xy \\ 0 & 0 & 0 & .4 & 0 & 2 & 1.2x & .4y & 2x & 6y & 1.2xy & 6xy \\ 0 & 0 & 0 & 0 & -1.6 & 0 & 0 & -3.2x-3.2y & 0 & -4.8x^2-4.8y^2 & 0 & 0 \\ 0 & 0 & 0 & 0 & 0 & 0 & 6 & 0 & 2 & 0 & 6y & 6y \\ 0 & 0 & 0 & 0 & 0 & 0 & 0 & 2 & 0 & 6 & 6x & 6x \end{bmatrix}.$$

$$[N]\{\phi\}\left(-\frac{Ex^3}{11.52}\right)$$

For the normal and shearing stresses, we have

$$\begin{Bmatrix} \sigma_x \\ \sigma_y \\ \tau_{xy} \end{Bmatrix} = \begin{bmatrix} a & b & 0 \\ b & a & c \\ 0 & 0 & G \end{bmatrix} \begin{Bmatrix} \epsilon_x \\ \epsilon_y \\ \gamma_{xy} \end{Bmatrix}$$

$$\text{or } [L]\sigma = [K](\epsilon) \quad (4-35)$$

$$\text{where } a = \frac{E}{(1-\nu^2)}; \quad b = \frac{\nu E}{(1-\nu^2)}; \quad G = \frac{E}{2(1+\nu)};$$

$$\text{but } \begin{Bmatrix} \epsilon_x \\ \epsilon_y \\ \gamma_{xy} \end{Bmatrix} = \begin{bmatrix} (-b+y) & (b-y) & -y & y & 0 & 0 & 0 & 0 \\ 0 & 0 & 0 & 0 & (-a+x) & -x & (a-x) & x \\ (-a+x) & -x & (a-x) & x & (-b+y) & (b-y) & -y & y \end{bmatrix} \begin{Bmatrix} u_i \\ u_j \\ u_k \\ u_L \\ v_i \\ v_j \\ v_k \\ v_L \end{Bmatrix} \cdot \frac{1}{ab}$$

$$\text{or } (\epsilon) = [f](u) \quad (4-36)$$

From Equations 4-35 and 4-36, we get

$$\{\sigma\} = [K][f](u) \quad (4-37)$$

These moments, shears and stresses are in the global system. Therefore, for proper identification, it is necessary to convert them to the local coordinates of the plates. The coordinate transformation matrix is shown in Table 4-2.

GLOBAL I	LOCAL SYSTEM		
	Type 1	Type 2	Type 3
1	1	9	5
2	-5	-5	-9
3	-9	1	1
4	11	0	10
5	10	10	0
6	0*	11	11
7	2	12	-6
8	-6	-6	-12
9	-12	2	2
10	14	0	13
11	13	13	0
12	0	14	14
13	3	15	-7
14	-7	-7	-15
15	-15	3	3
16	17	0	16
17	16	16	0
18	0	17	17
19	4	18	-8
20	-8	-8	-18
21	-18	4	4
22	20	0	19
23	19	19	0
24	0	20	20

*This and all zeros appearing here are computer controls just to avoid the ϕ_7 local coordinate transformation.

Table 4-2

COORDINATE TRANSFORMATION COEFFICIENTS

4-6 Response Spectra For Sheltered Equipment

4-6.1 General

Equipment sheltered within the structure will be subjected to both vertical and horizontal movement at its point of attachment. If these movements cause serious damage to the equipment, it may matter little that the structure successfully withstood the blast loading.

Equipment and utilities may be attached to the structure by means of a flexible support system (Figure 4-3).

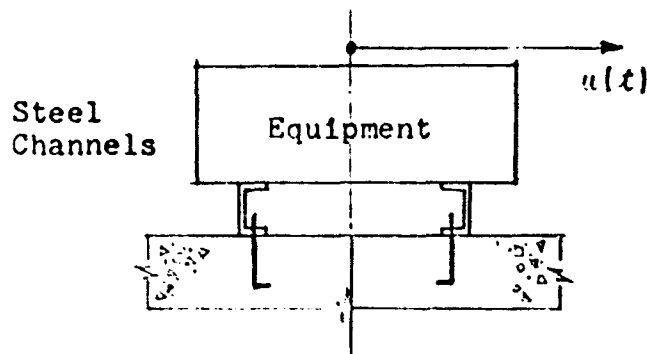


Figure 4-3 EXAMPLE OF A FLEXIBLE HORIZONTAL MOUNTING

Often, this is done in order to isolate the item from large accelerations or may result simply from conventional attachment procedures. Because the mass-spring system, composed of equipment and mounting, can vibrate relative to its attachment point, its peak displacement and acceleration may differ appreciably from that of the supporting structure. For design purposes, it is desirable to have a graph of maximum responses at an attachment point, for a wide range of mount stiffness-equipment weight ratios. This graph is called a response spectrum.

A spectrum requires that the reaction, delivered to the supporting structure through the mounting, does not alter the timewise movement of the support point. Thus, the weight of the equipment must be small compared to the supporting member, usually less than 10 percent.

4-6.2 Definition of the Response Spectrum

The single-degree-of-freedom system considered consists of a rigid mass, m , connected to the point of attachment by both a weightless spring and a dashpot (Figure 4-4).

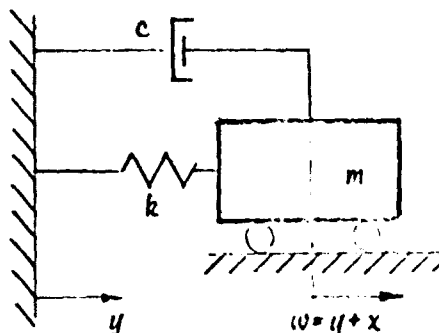


Figure 4-4 SIMPLE ELASTIC SYSTEM

The spring and dashpot exert restraining forces proportional, respectively, to the relative displacement and relative velocity of the mass and attachment. The displacement of the attachment is denoted y and the spring deformation by x .

The equation of motion for the system (Figure 4-4) may be written,

$$m\ddot{w} + c\dot{x} + kx = 0 \quad (4-38)$$

Noting that $\ddot{w} = \ddot{y} + \ddot{x}$, Equation 4-38 is rewritten,

$$m\ddot{x} + c\dot{x} + kx = -m\ddot{y} \quad (4-39)$$

Or, rewriting in terms of the damping ratio,

$$m\ddot{x} + 2\lambda m\dot{x} + kx = -m\ddot{y} \quad (4-40)$$

For a specific excitation, $m\ddot{y}$, of a simple system with a particular percentage of critical damping, λ , the maximum spring displacement, x , is a function only of the circular frequency of vibration of the system, ω .

A plot of the maximum simple system response, whether relative displacement x , absolute displacement w , acceleration \ddot{w} , or spring force kx , against the circular frequency of vibration ω , or the natural frequency of vibration f , is a response spectrum. The most useful spectrum is that of relative displacement, x . In the following, the spectral value of displacement relative to the point of attachment will be designated as U .

Maximum values of spectral pseudo-velocity, V , and pseudo-acceleration, A , may be conveniently defined as,

$$V = \omega U = 2\pi f U \quad (4-41a)$$

$$A = \omega^2 U = 4\pi^2 f^2 U \quad (4-41b)$$

These quantities are alternate measures of the maximum spring deformation U . If one is known, the other two are calculated easily. When the deformation spectrum is plotted on a logarithmic scale as shown in Figure 4-17, all three quantities are represented. (See Page 4-36)

Figure 4-17 shows the response spectra for one of the joints in the sample structure. The time-dependent acceleration of this joint is calculated by the procedure outlined in Section 4-4. This acceleration becomes the forcing function, \ddot{y} , of Equation 4-40. The calculated response spectrum is simply the maximum spring displacement x of the simple elastic system of Figure 4-4. The general characteristics of the spectra are as follows:

1. The spectra show marked peaks at a frequency of 20 cps, corresponding to the predominant box-structure frequency of response.
2. Peak values decrease as the damping increases.
3. For low frequencies, the maximum spectral displacements (equipment rattle-space) approach the peak attachment point displacement.

4-7 Sample Dynamic Analysis

4-7.1 Orientation of the Structure and Loading

In order to analyze a structure in the most efficient manner with respect to computer time it is necessary to orient the structure in such a way that the number of plates in the x direction (see Figure 2-1) is equal to or less than the y plates and, the number of y plates is equal to or less than the z plates. The joint coordinates are Cartesian and follow the right-hand rule.

When the structure has been oriented to satisfy the mechanics of solution, it then becomes necessary to orient the blast pressures and ground motion to be compatible with the concept of the problem. There are six possible cases of orientation of the loading which are numbered in accordance with Figure 4-5. The Figure depicts the six cases, each of which is a combination of joint coordinates and load coordinates. All permissible conditions can be satisfied with one of the six cases. In the case of a model not oriented in its natural position for mathematical reasons, there may be more than one way in which it can be turned but at least one way will be satisfied by one of the cases of Figure 4-5.

4-7.2 Numbering Sequence

Each plate of the model is divided into four rectangular elements. The division should be visualized as being accomplished by cutting planes entirely through the model. Wherever three planes (plates or cutting planes) intersect there is a joint. Where all three planes are cutting planes, the joint is a dummy joint. Each joint is given a number by the computer. These numbers are in sequence without regard to whether the joint is actual or dummy.

The joints are numbered in x, y, z sequence. (Figure 2-1). The computer starts on the xy plane with the smallest value of z . The numbering is row-wise sequenced downward and continuing through the z planes in ascending order.

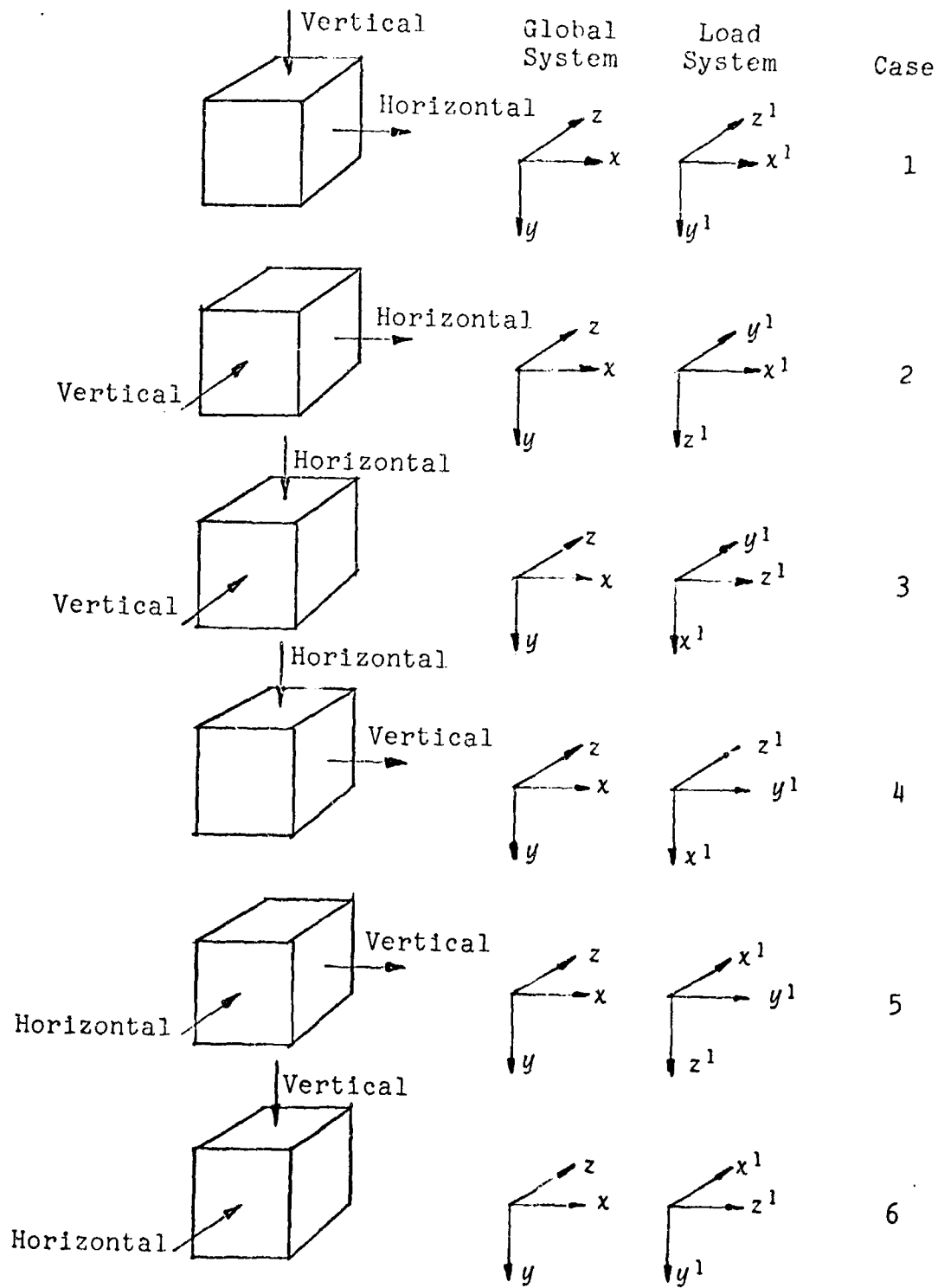


Figure 4-5
SIX CASES OF LOAD ORIENTATION

The elements are numbered in a manner similar to the joints. In each plane they are numbered left to right, top to bottom. The numbering starts with the elements in the xy plane, starting at the smallest value of z , and working to the largest value of z . It then continues in the yz plane starting with the smallest value of x and working through to the largest value of x . Finally, it takes the zx planes from the lowest to the highest value of y . No differentiation is made between the real and dummy elements. The exploded box (Figure 4-6) demonstrates the numbering sequence.

The order of recognition of the plates, e.g., for inputting the plate thicknesses, is the same as for the elements, however, the dummy plates which are introduced in the analysis are ignored.

4-7.3 Listing of the Data on the Input Forms

This Sub-section should be read in conjunction with input sheets 1 and 2 (Figures 4-9 and 4-10).

Job identification is an alphameric heading occupying not more than 72 spaces.

In the second line n_x, n_y and n_z are fixed point digital entries equal to the number of cross walls in the x, y and z directions respectively. If a calculation of response spectra is required, a digit is placed under the heading "Response Spectra." If this is left blank, no spectra will be calculated and input sheet No. 2 will not be required. The Case Number refers to the orientation of the structure and loads as described in sub-section 4-7.1 and Figure 4-5.

The following three lines are for the lengths of the plates in the x, y and z directions. In the following lines, the thicknesses of the plates are entered in sequence as described in Sub-section 4-7.2.

In line 9 are entered the modulus of elasticity and density of the material of the structure, and the density and thickness of the soil layer.

The next two lines contain the data required to define the loads due to the blast and ground motion, which are explained in Appendix A.

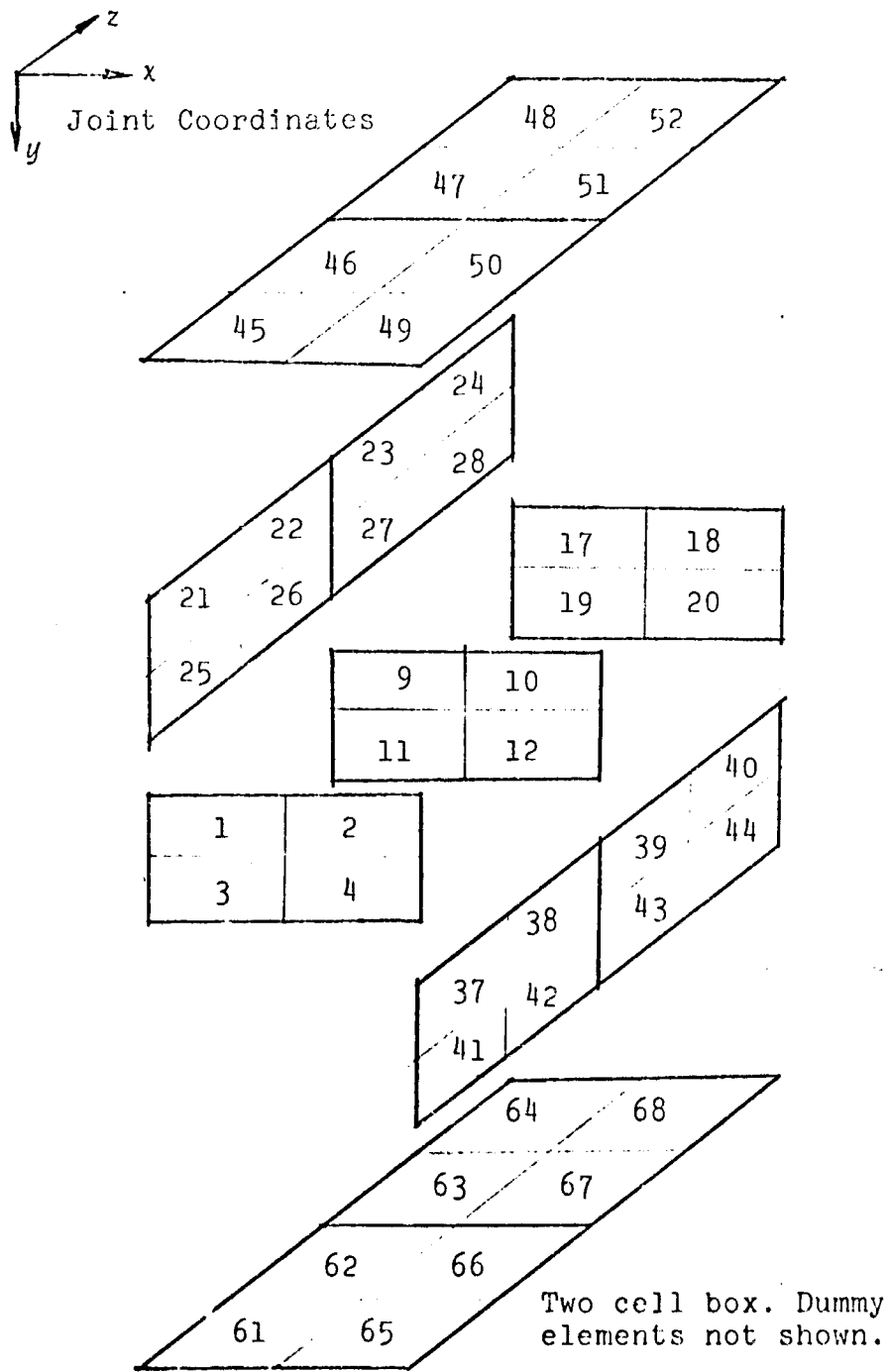


Figure 4-6

NUMBERING OF ELEMENTS

In line 12 are entered the viscous damping factors and the numerical integration controls, i.e., the time interval Δt and the number of time intervals.

The next four lines are used to identify the joints, if any, at which time dependent print out of the displacements, velocities and accelerations are required, and also which coordinate direction these responses are required. The coordinates are indicated numerically, i.e., $x = 1$, $y = 2$, $z = 3$. Because of the large amount of printed data that this computer program is capable of producing, it was decided to limit the time dependent print to three nodal points per run.

If response spectra are required, input sheet No. 2 must be used. Spectral velocities can be obtained for any twenty nodal point translational displacements. Four different damping factors may be used. The frequencies at which the spectral velocities are required are listed row-wise in sequence to a maximum of twenty-five.

4-7.4 Sample Analysis

The modeling of a structure, numbering of elements, reorientation of loading coordinates and entry of data onto the input forms is demonstrated in the sample analysis. The structure is shown in its natural position in Figure 4-7 and reoriented with reoriented loading in Figure 4-8. The numbering of the elements is identical with the sample of Figure 4-6. The data input forms are shown in Figures 4-9 and 4-10. A printing of the input is shown in Figure 4-11. A sample page from the output of load deflection history for two points is shown in Figure 4-12. Figures 4-13, 4-14 and 4-15 show the maximum displacements, velocities and accelerations. After each of these listings, the time at which these maxima occurred is also printed. Figure 4-16 shows the maximum positive stresses in the elements in local coordinates. The complete printout lists the moments M_x , M_y and M_{xy} , the forces Q_x and Q_y and the stresses σ_x , σ_y and τ_{xy} . This listing is followed by a listing of the times at which these maxima occurred, a listing of the maximum negative stresses and the times at which the maximum negative stresses occurred. Figure 4-17 shows response spectra for the midpoint of the base slab in the vertical direction.

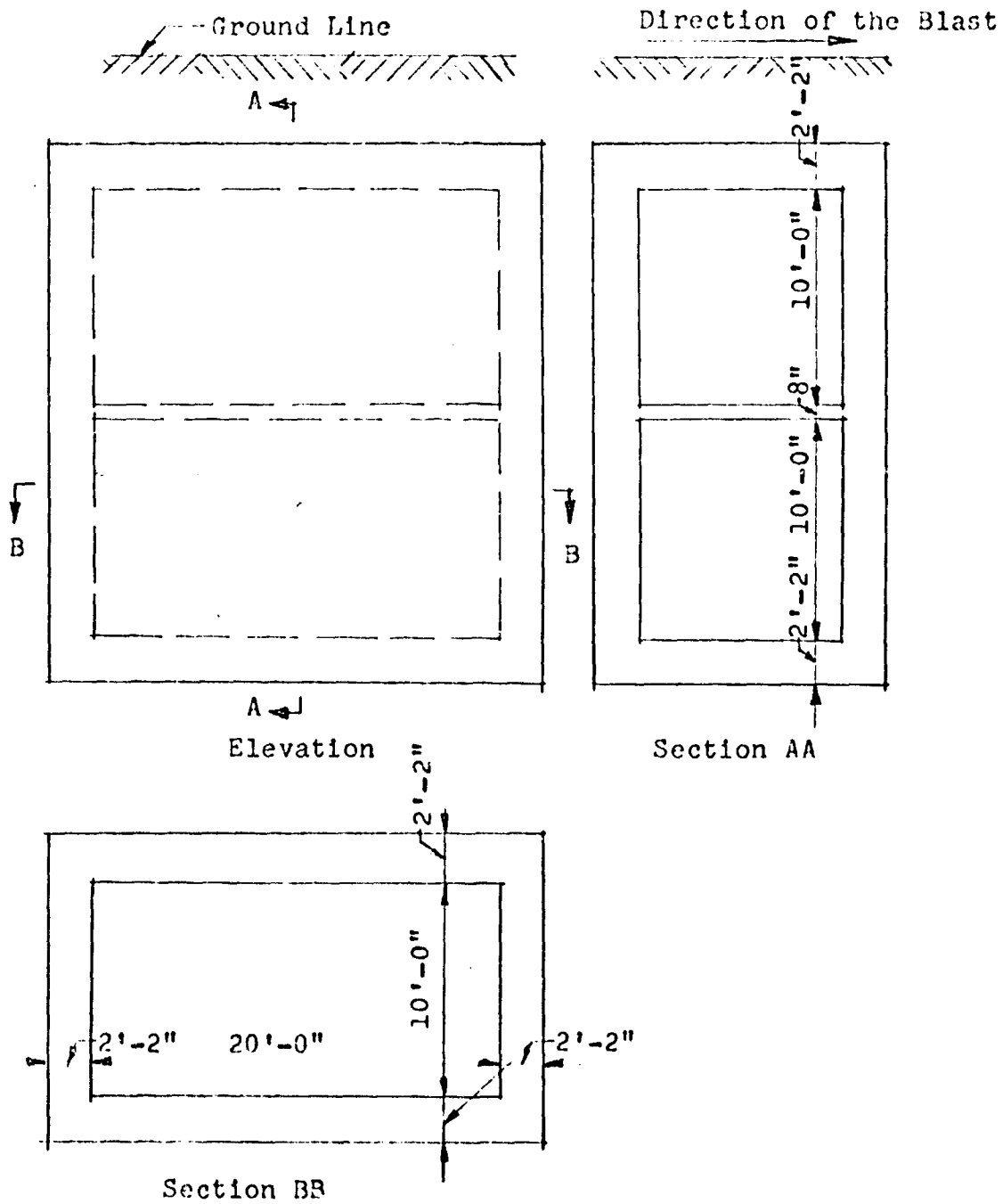


Figure 4-7
 SAMPLE STRUCTURE

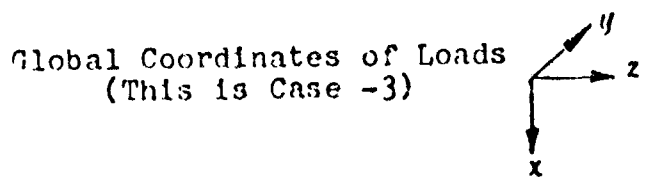
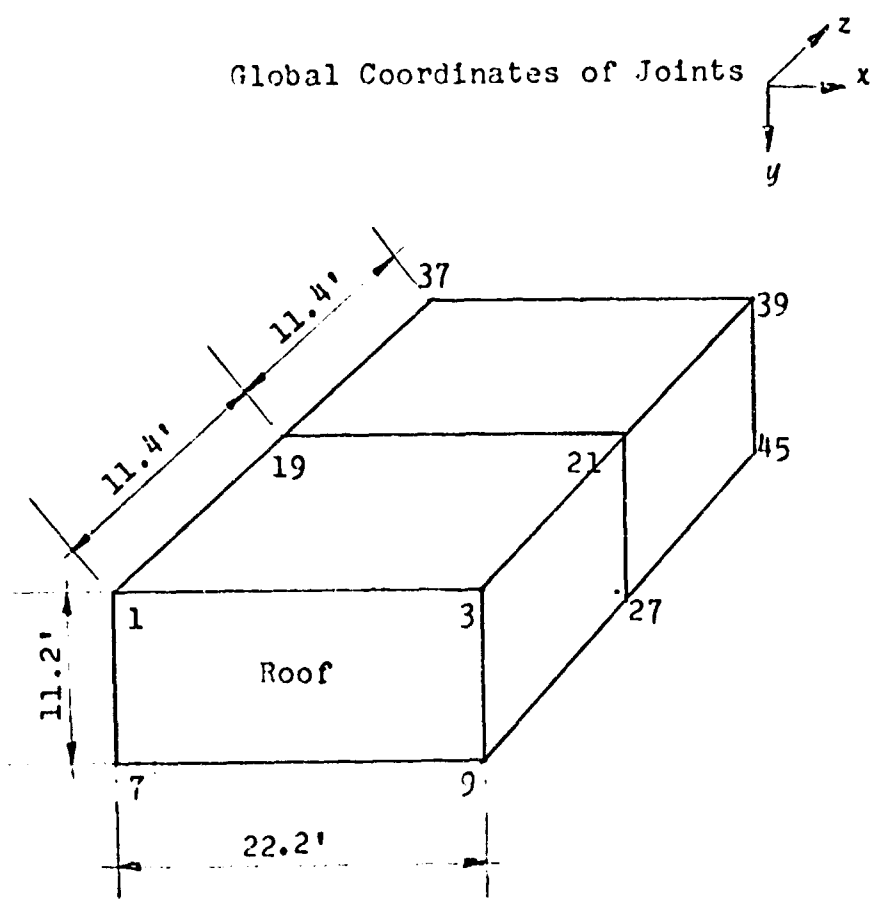


Figure 4-8
RE-ORIENTED LOADS

Input by <u>RA</u>		Underground Box Structures		Dynamic Linear Analysis		Input Sheet #1	
Date <u>12/12/66</u>		Program <u>Caps-1-UB1</u>		Job Identification			
Sample <u>2-Story, 2 Room Underground Box Structure</u>							
Number of Coordinates <u>x, y, z</u>		Res. Spect. Case No.					
<u>2</u>	<u>2</u>	<u>3</u>	<u>1</u>				
Length of Plates (ft)							
<u>22.2</u>				x-Axis			
<u>11.2</u>				y-Axis			
<u>11.4</u>				z-Axis			
Thickness of Plates in Sequence (ft)							
<u>2.17</u>	<u>.67</u>	<u>2.17</u>	<u>2.17</u>	<u>2.17</u>	<u>2.17</u>	<u>2.17</u>	<u>2.17</u>
<u>2.17</u>	<u>2.17</u>	<u>2.17</u>	<u>2.17</u>				
E (ksf)		Mt. (lb/cf)		S.G. Soil		K _o	
<u>43200.</u>	<u>150.</u>	<u>1.6</u>	<u>.3</u>				
W (mt)		ΔP _s (psi)		u (fps)		D _p (sec)	
<u>20.</u>	<u>50.</u>	<u>2300.</u>	<u>2.65</u>	<u>1.37</u>	<u>5.4</u>	<u>3.66</u>	<u>α</u>
R (ft)		ΔR (ft)		c _p (fps)		V _L * (fps)	
<u>12500.</u>	<u>0.</u>	<u>8000.</u>	<u>6000.</u>	<u>.83</u>	<u>0.025</u>	<u>4.0</u>	<u>ρ</u>
α ₀		α ₁		Δt		Number of Δt	
<u>90.</u>	<u>.00003</u>	<u>.0005</u>	<u>100</u>	Note: [C] = α ₀ [M] + α ₁ [K]			
Number of points for time dependent print							
<u>3</u>	<u>17</u>	Point number and coordinate		For x coordinate		enter	
<u>53</u>	<u>192</u>	<u>"</u>	<u>y</u>	<u>"</u>	<u>z</u>	<u>"</u>	<u>1</u>
<u>192</u>	<u>292</u>	<u>"</u>	<u>"</u>	<u>"</u>	<u>"</u>	<u>"</u>	<u>2</u>
		<u>"</u>	<u>"</u>	<u>"</u>	<u>"</u>	<u>"</u>	<u>3</u>

Figure 4-9

LINEAR PROGRAM - INPUT SHEET #1

Underground Box Structures Dynamic Linear Analysis			
Input by <u>RA</u>		Input Sheet #2	
Date <u>12/12/66</u>		Program <u>Cans-1-UB1</u>	
No. Freqs.	No. Damps.	No. Joints	
10	2	3	
233	Joint Number and Coordinate		
192	For x coordinate enter 1		
292	" y	"	" 2
	" z	"	" 3
Damping Factors			
.02	.20		
Frequencies in Cycles Per Second			
1.	2.	4.	10.
20.	40.	100.	200.
400.	1000.		

Figure 4-10

LINEAR PROGRAM - INPUT SHEET #2

DYNAMIC ANALYSIS OF BOX STRUCTURES

SAMPLE 2-3100Y, 2-3100Z (TYPE 1) BOX STRUCTURE

12-19-66

NO. OF JOINTS

X DIRECTION = 2
 Y DIRECTION = 2
 Z DIRECTION = 3

MODULES OF ELASTICITY

STRUCTURE = 432000.00 KSE
 SOIL = 165356.46 KSE
 RO = 150.00 LAYERS/FT.
 KO = 0.30
 CASE NO. 3

LENGTHS OF PLATES

X DIRECTION = 22.25
 Y DIRECTION = 11.25
 Z DIRECTION = 11.40 11.45

PLATE THICKNESSES

2.17	0.67	2.17	2.17	2.17
2.17	2.17	2.17	2.17	2.17
2.17				

BLAST AND GROUND MOTION CHARACTERISTICS

W(FT) = 20.00
 PS0(PST) = 50.00
 ALPHA = 1.37
 BETA = 3.40
 A = 0.66
 DP*(SEC) = 0.65
 U(FPS) = 100.00
 R(FT) = 1250.00
 DELX(FT) = 0.00
 VL(FPS) = 200.00
 VL*(FPS) = 600.00
 T/12 = 0.03
 SP.GRAV. = 1.00
 P FACTOR = 4.00
 PHASING = 0.025000

TIME INCREMENT = 0.0005

101 TIME INCREMENTS

DAMPING FACTORS

ALPHA = 0.000000000 BETA = 0.000500

Figure 4-11

PRINTING OF INPUT

LOAD-DEFLECTION HISTORY

LOAD IN KIPS, DEFLECTION IN FT., TIME IN SECONDS

25-3

25-2

TIME	LOAD	DEFLECTION	LOAD	DEFLECTION
0.00050	0.0000+000	-4.1596-018	1.1746-006	7.4355-015
0.00100	0.0000+000	-1.5243-016	2.9336-005	2.3756-013
0.00150	0.0000+000	-2.0633-015	2.0504-004	2.5047-012
0.00200	0.0000+000	-1.6045-014	3.2395-004	1.4643-011
0.00250	0.0000+000	-3.6005-014	2.4342-003	5.0213-011
0.00300	0.0000+000	-3.5191-013	5.9740-003	1.8728-010
0.00350	0.0000+000	-1.1735-012	1.2593-002	4.0697-010
0.00400	0.0000+000	-3.3342-012	2.4039-002	1.1524-009
0.00450	0.0000+000	-2.2055-011	4.2515-002	1.4655-009
0.00500	0.0000+000	-1.6387-010	7.0765-002	-2.3047-009
0.00550	0.0000+000	-7.6112-010	1.1212-001	-1.5355-008
0.00600	0.0000+000	-2.2793-009	1.7053-001	-3.6219-008
0.00650	0.0000+000	-5.2732-009	2.5060-001	-6.7844-008
0.00700	0.0000+000	-1.0737-008	3.5762-001	-1.2210-007
0.00750	0.0000+000	-2.1340-008	4.9756-001	-2.0097-007
0.00800	0.0000+000	-4.2039-008	6.7713-001	-3.2741-007
0.00850	0.0000+000	-7.8391-008	9.0378-001	-4.7943-007
0.00900	0.0000+000	-1.3572-007	1.1851+000	-6.7329-007
0.00950	0.0000+000	-2.2232-007	1.5311+000	-0.1569-007
0.01000	0.0000+000	-3.5181-007	1.9510+000	-1.1994-006
0.01050	0.0000+000	-5.3911-007	2.4552+000	-1.5289-006
0.01100	0.0000+000	-7.9704-007	3.0549+000	-1.9271-006
0.01150	0.0000+000	-1.1404-006	3.7619+000	-2.4162-006
0.01200	0.0000+000	-1.5888-006	4.5391+000	-2.9882-006
0.01250	0.0000+000	-2.1622-006	5.5497+000	-3.5414-006
0.01300	0.0000+000	-2.9731-006	6.6580+000	-4.3594-006
0.01350	0.0000+000	-3.7583-006	7.9286+000	-5.1283-006
0.01400	0.0000+000	-4.8350-006	9.3771+000	-5.9247-006
0.01450	0.0000+000	-6.1425-006	1.1020+001	-6.7385-006
0.01500	0.0000+000	-7.7074-006	1.2073+001	-7.5596-006

Figure 4-12

LOAD-DEFLECTION HISTORY

MAXIMUM DISPLACEMENTS

JOINT	DELTA (X)	DELTA (Y)	DELTA (Z)	PHI (X)	PHI (Y)	PHI (Z)
1	1.0594-004	8.1933-004	-1.0609-004	-5.5588-004	-5.7237-005	2.3891-004
2	2.2440-015	1.1255-003	3.7441-004	-2.0764-004	-2.0813-013	-3.5017-013
3	-1.0694-004	8.1907-004	-1.0609-004	-5.5584-004	5.7237-005	-2.3891-004
4	4.0583-005	7.1678-004	-1.0291-004	1.0430-003	-2.9444-004	8.8857-005
5	3.1157-013	7.7713-004	1.5704-003	3.2067-004	9.6895-014	-2.2173-013
6	-4.0583-005	7.1678-004	-1.0291-004	1.0430-003	2.9444-004	-8.8857-005
7	3.5952-005	5.2140-004	-1.3260-004	-4.4245-004	-6.3239-005	4.7345-005
8	4.9799-013	4.7336-004	2.9941-004	-2.3430-004	1.0130-013	-1.4288-013
9	-5.5952-005	6.2146-004	-1.3260-004	-4.4245-004	6.3239-005	-4.7345-005
10	1.0216-004	1.1122-003	-1.2837-004	1.3044-003	-2.6928-005	9.8473-004
11	1.3064-013	2.2254-003	-1.2693-004	-2.2746-004	-4.5591-013	-4.4461-013
12	-1.0216-004	1.1122-003	-1.2837-004	1.3044-003	2.6928-005	-9.8473-004
13	-3.0847-004	7.0936-004	-1.5461-004	-2.6906-003	5.9669-005	-2.1810-004
14	0.0000+000	0.0000+000	0.0000+000	0.0000+000	0.0000+000	0.0000+000
15	3.0987-004	7.0936-004	-1.5461-004	-2.6906-003	-5.9669-005	2.1810-004
16	-1.2243-005	5.1962-004	-1.4249-004	1.3287-003	-2.6753-005	-7.6834-005
17	3.1625-013	2.0236-005	-1.3908-004	2.8010-004	1.7439-013	-6.1386-014
18	1.2243-005	5.1962-004	-1.4249-004	1.3287-003	-2.6753-005	7.6834-005
19	1.0557-004	1.0927-003	-2.1277-004	-1.7748-003	-3.1660-005	5.8520-004
20	-7.1437-014	2.0148-003	-1.7307-004	1.6607-003	4.0027-013	-2.7938-013
21	-1.8057-004	1.0927-003	-2.1277-004	-1.7748-003	-3.1660-005	-5.8520-004
22	-2.2271-004	0.1215-004	-2.3043-004	3.5483-003	-2.8296-005	4.6798-005
23	9.9151-014	1.0105-003	-7.7870-005	-5.5806-005	-9.2011-014	-1.2229-013
24	2.2271-004	0.1215-004	-2.3043-004	3.5483-003	2.8296-005	-4.6798-005
25	-3.2209-005	5.5943-004	-2.2392-004	-1.7738-003	-2.3090-005	-3.9993-005
26	5.9734-013	7.9817-005	-1.7860-004	-2.0848-005	1.5740-013	-9.1164-014
27	3.2209-005	5.5943-004	-2.2392-004	-1.7738-003	2.3090-005	3.9993-005

Figure 4-13

MAXIMUM DISPLACEMENTS

MAXIMUM VELOCITIES

JOINT	DELTA (V)	DELTA (Y)	DELTA (Z)	PHI (V)	PHI (Y)	PHI (Z)
1	9.3542-003	7.3516-002	2.7237-002	4.1401-001	-2.1096-002	1.8034-002
2	1.0292-011	9.4996-002	6.0095-002	-1.6977-001	-1.4030-010	-3.6422-011
3	-9.3842-003	7.3516-002	2.7237-002	4.1401-001	2.1096-002	-1.8034-002
4	9.3525-003	6.5027-002	4.4043-002	-1.1161+000	-4.0230-002	8.0201-003
5	3.2777-011	7.1726-002	2.3893-001	-3.0295-001	3.5442-011	-3.7753-011
6	-9.3526-003	6.5027-002	4.4043-002	-1.1161+000	4.0230-002	-8.0201-003
7	7.5663-003	6.3135-002	3.4247-002	4.2021-001	-2.1261-002	-1.3317-002
8	3.7767-011	5.5450-002	7.4706-002	-1.3169-001	5.5895-011	-3.0444-011
9	-7.5663-003	6.3135-002	3.4247-002	4.2021-001	2.1261-002	1.3317-002
10	1.7040-002	9.6954-002	1.8674-002	-1.2974+000	-7.6906-003	6.9268-002
11	1.3520-011	1.9702-001	2.5236-002	-2.1903-001	3.0682-010	-5.4887-011
12	-1.7040-002	9.6954-002	1.8674-002	-1.2974+000	7.6906-003	-6.9268-002
13	-2.5704-002	7.1773-002	-1.6894-002	2.5878+000	1.1542-002	-1.6183-002
14	0.0000+000	0.0000+000	0.0000+000	0.0000+000	0.0000+000	0.0000+000
15	2.5704-002	7.1773-002	-1.6894-002	2.5878+000	-1.1542-002	1.6183-002
16	-1.9936-003	4.9246-002	1.9738-002	-1.2466+000	-7.7316-003	-4.6173-002
17	1.8439-011	7.3513-003	3.4461-002	-2.2348-001	-1.0870-010	2.1774-011
18	1.9936-003	4.9246-002	1.9738-002	-1.2466+000	7.7316-003	4.6173-002
19	1.5335-002	9.7415-002	2.2224-002	1.6159+000	-3.7767-003	4.1148-002
20	-2.3994-011	1.7301-001	2.3522-002	2.5671-002	-3.0210-010	-3.0812-011
21	-1.6336-002	9.7415-002	2.2224-002	1.6158+000	3.7767-003	-4.1148-002
22	-2.5691-002	7.4775-002	1.8772-002	-3.2345+000	-4.0789-003	4.4264-003
23	-3.3088-011	9.3643-002	-4.3643-003	-5.0716-002	-5.3876-012	-2.6745-011
24	2.5691-002	7.4775-002	1.8772-002	-3.2345+000	4.0789-003	-4.4264-003
25	1.9853-003	5.8146-002	-1.9168-002	1.6128+000	-3.5313-003	-1.7764-002
26	1.6927-011	2.6556-002	-2.0502-002	1.9516-002	1.2808-010	1.6012-011
27	-1.9853-003	5.8146-002	-1.9168-002	1.6128+000	3.5313-003	1.7764-002

Figure 4-14

MAXIMUM VELOCITIES

MAXIMUM ACCELERATIONS

JOINT	DELTA (X)	DELTA (Y)	DELTA (Z)	PHI (X)	PHI (Y)	PHI (Z)
1	4.3560+000	9.5139+001	-2.3073+002	2.2139+004	-1.0254+002	-1.0478+002
2	-3.3170+000	6.3317+001	-2.1656+002	-4.3495+003	-9.8419+006	1.0979+006
3	-4.3560+000	9.5139+001	-2.3073+002	2.2139+004	1.0254+002	1.0478+002
4	2.7656+000	7.6556+000	-2.3760+001	-5.3657+004	-6.4129+001	-2.7702+001
5	4.8427+000	8.5615+000	7.2379+001	-1.2196+004	5.1163+008	-2.0895+006
6	-2.7656+000	7.6556+000	-2.3760+001	-5.3657+004	6.4129+001	2.7702+001
7	3.9768+000	9.7794+001	2.5316+002	2.1233+004	9.2908+001	-9.6885+001
8	3.2495+000	7.0190+001	2.4135+002	-5.2393+003	3.5140+006	1.1174+006
9	-3.9768+000	9.7794+001	2.5316+002	2.1233+004	-9.2908+001	9.6885+001
10	2.2747+000	7.3541+001	1.4284+001	-6.4996+004	1.7086+001	9.5575+001
11	2.2703+000	4.7474+001	1.9854+001	-9.2675+003	2.1039+005	-1.6023+007
12	-2.2747+000	7.3541+001	1.4284+001	-6.4996+004	-1.7086+001	-9.5575+001
13	-1.9769+000	6.4740+000	9.5700+000	1.3148+005	1.2203+001	-1.2876+002
14	9.9000+000	0.0000+000	0.0000+000	0.0000+000	0.0000+000	0.0000+000
15	1.9769+000	6.4740+000	9.5700+000	1.3148+005	-1.2203+001	1.2876+002
16	2.9669+000	-7.6659+001	1.6145+001	-6.4713+004	-1.3039+001	-9.6753+001
17	1.6167+000	-4.1859+001	2.3311+001	-9.4141+003	-7.8040+006	5.8182+008
18	-2.9669+000	-7.6659+001	1.6145+001	-6.4713+004	1.3039+001	9.6753+001
19	3.9803+000	1.1673+002	1.6298+001	8.6598+004	-1.5033+001	6.9439+001
20	-2.3160+000	1.9739+002	1.5054+001	2.2345+002	-2.0384+005	8.5693+008
21	-3.5803+000	1.1673+002	1.6298+001	8.6598+004	1.5033+001	-6.9439+001
22	-2.2671+000	1.0733+001	4.5310+000	-1.7349+005	-6.0059+000	-2.1795+001
23	1.9812+000	1.4265+001	1.3917+000	-2.6600+003	1.0669+008	2.2892+007
24	2.2671+000	1.0733+001	4.5310+000	-1.7349+005	6.0059+000	2.1795+001
25	2.2860+000	1.1921+002	1.8469+001	8.6527+004	1.4480+001	-8.5410+001
26	-2.4301+000	1.0379+002	1.4787+001	-4.3664+002	4.1276+006	-4.3446+008
27	-2.2860+000	1.1921+002	1.8469+001	8.6527+004	-1.4480+001	8.5410+001

Figure 4-15

MAXIMUM ACCELERATIONS

MAXIMUM POSITIVE STRESSES IN LOCAL COORDINATES

ELEMENT	TYPE	JOINT	MOMENT-X	MOMENT-Y	MOMENT-XY	
a	1	1	4	3.2992+001	2.2573+002	1.4654+001
b	1	1	5	0.0000+000	4.0441+000	7.9660-002
c	1	1	1	1.9187+000	1.4742+001	4.2252+001
d	1	1	2	1.4010+001	3.2483+001	1.5945+001
e	2	1	5	0.0000+000	4.0441+000	5.2989+001
f	2	1	6	3.2092+001	2.2573+002	2.6682+001
g	2	1	2	1.4010+001	3.2483+001	5.5521+000
h	2	1	3	1.9187+000	1.4742+001	0.0000+000
i	3	1	7	3.4448+000	2.6622+001	7.7450+000
j	3	1	8	2.0115+001	1.1213+002	3.2989+001
k	3	1	4	1.6526-001	2.1871-001	0.0000+000
l	3	1	5	0.0000+000	0.0000+000	1.2300+001
m	4	1	8	2.0115+001	1.1213+002	3.0910-002
n	4	1	9	3.4448+000	2.6622+001	2.3076+001
o	4	1	5	0.0000+000	0.0000+000	3.1430+001
p	4	1	6	1.6526-001	2.1871-001	5.6674+001

	QX	QY	SIGMA-X	SIGMA-Y	TAU-XY
a	0.0000+000	4.6125+000	6.4523-002	0.0000+000	4.7210+000
b	0.0000+000	2.8666+001	0.0000+000	0.0000+000	4.9322-002
c	5.9934+000	4.6125+000	2.6969-002	0.0000+000	6.9292-001
d	5.9934+000	2.8666+001	2.6704-003	0.0000+000	0.0000+000
e	1.9474+001	2.8666+001	0.0000+000	0.0000+000	9.7866-001
f	1.9474+001	4.6125+000	6.4523-002	0.0000+000	1.8280-003
g	1.1378-002	2.8666+001	2.6704-003	0.0000+000	5.0067+000
h	1.1378-002	4.6125+000	2.6969-002	0.0000+000	6.5755-001
i	7.6713+000	0.0000+000	0.0000+000	0.0000+000	1.0735+000
j	7.6713+000	0.0000+000	0.0000+000	0.0000+000	2.3935+000
k	7.2901+000	0.0000+000	6.7959-002	0.0000+000	1.4277-001
l	7.2901+000	0.0000+000	0.0000+000	0.0000+000	4.9322-002
m	2.9172-002	0.0000+000	0.0000+000	0.0000+000	0.0000+000
n	2.9172-002	0.0000+000	0.0000+000	0.0000+000	4.8765-006
o	5.9292+000	0.0000+000	0.0000+000	0.0000+000	9.7866-001
p	5.9292+000	0.0000+000	6.7959-002	0.0000+000	2.8678+000

Figure 4-16

MAXIMUM POSITIVE STRESSES

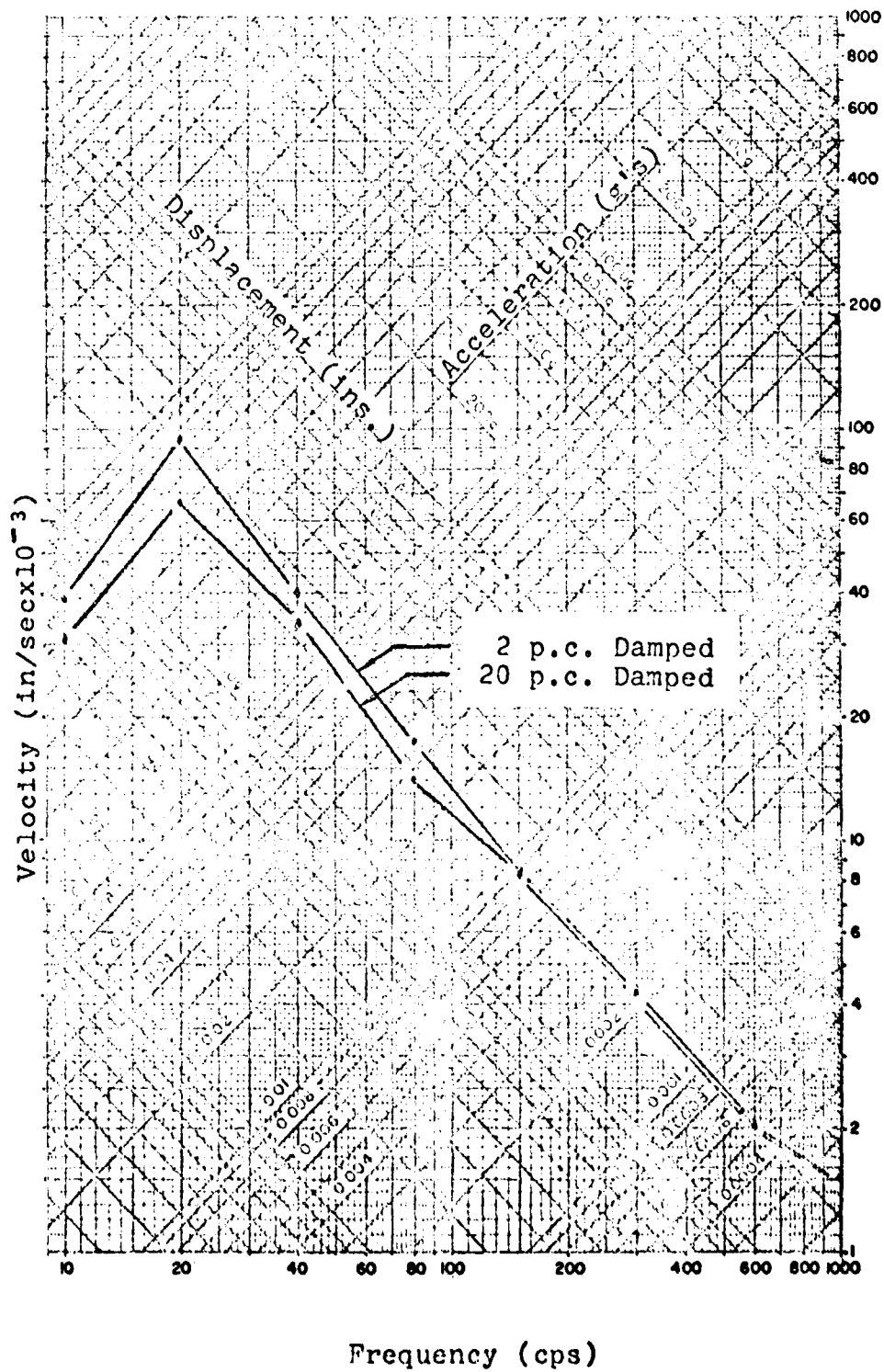


Figure 4-17
 RESPONSE SPECTRA FOR JOINT 41 (z Direction)

Section 5

DYNAMIC RESPONSE ANALYSIS - NON-LINEAR

5-1 General Procedure

The non-linear dynamic analysis is carried out by a step-by-step procedure in which the structure is assumed to respond linearly during each short time interval. The elastic properties may be changed, however, from one interval to the next; thus, the non-linear response is obtained as a sequence of linear responses of successively differing systems.

The analysis procedure involves the repeated application of the following steps for each successive time interval:

- First: the stiffness matrix appropriate to the time interval is evaluated, based on the forces existing in the plate elements at the beginning of the time interval.
- Second: changes in displacements of the elastic structure are computed, assuming the accelerations to vary linearly during the interval.
- Third: these incremental displacements are added to the deformation state existing at the beginning of the interval, to obtain total element deformations.
- Finally: based on these element deformations, plate forces are computed from which the stiffness matrix appropriate to the next time interval may be determined.

5-2 Failure Criterion

5-2.1 Method of Failure

There is no well established theory of failure of plates under the combined effect of bending and inplane forces. Therefore, in this study an assumption was made that the plates would fail in bending first, and once having failed, a plate could not recover its bending stiffness. Also, a plate is assumed to continue to

contribute elastically to the overall stiffness of the structure through its inplane stiffness after losing its bending stiffness.

Each element can lose its bending stiffness independent of any other element. The whole structure is considered to have failed when the application of load is such that a sufficient number of elements have failed, so that the stiffness of the structure becomes singular.

The stiffness matrix will become singular when all the elements coinciding at a node point will not provide additional flexural constraint thereby permitting infinite displacements at that node.

5-2.2 Failure Assumption

Figure 5-1 shows the Johansen's yield line theory¹¹ applied to a uniformly loaded rectangular plate clamped on all four edges.

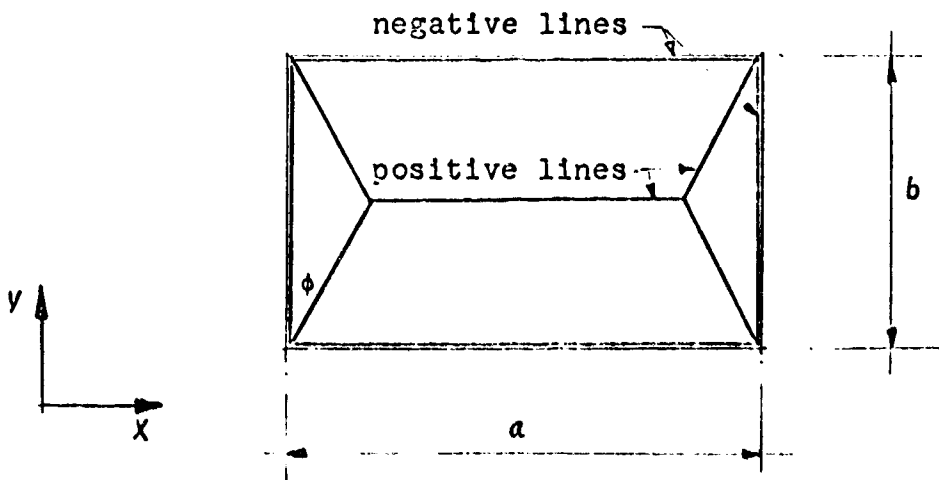


Figure 5-1

Based upon yield line theory, a kinematically compatible system of forces gives an upper bound to the solution whereas using any statically admissible system will give a lower bound. Investigations have shown that the difference between the two methods of solution is small, and that the yield line theory gives conservative answers. (See Section 6)

The angle ϕ is determined so that a minimum value of load p is obtained which will cause the plate to reach its yield capacity M_p .

Assuming the moment capacity is the same for positive and negative moments in both the X and Y directions it can be said,

(1) External Work

$$\begin{aligned} W_e &= p \frac{b^2}{6} \tan \phi + p \frac{b^2}{6} \tan \phi + 2p \frac{b}{2} (a - b \tan \phi) \frac{1}{2} \\ &= p \frac{b^2}{3} \tan \phi + p \frac{b}{2} (a - b \tan \phi) \end{aligned} \quad (5-1)$$

(2) Internal Work

$$\begin{aligned} W_i &= M_p \left[2b \frac{2}{b \tan \phi} + 2a \frac{2}{b} + 2a \frac{2}{b} + 2b \frac{2}{b \tan \phi} \right] \\ &= 8M_p \left[\frac{1}{\tan \phi} + \frac{a}{b} \right] \end{aligned} \quad (5-2)$$

Equating W_e and W_i and taking the derivative gives

$$p \frac{b^2}{3} \cos^2 \phi + p \frac{b^2}{3} \tan \phi - p \frac{b^2}{2} \cos^2 \phi - p \frac{b^2}{2} \tan \phi + \frac{8M_p}{\sin^2 \phi} = 0$$

Since $\dot{p} = 0$

$$p = \frac{48M_p}{b^2 \tan \phi^2} \quad (5-3)$$

Hence from Equations 5-2 and 5-3 substituting for p ;

$$4s'_p \left[\frac{1}{3} \tan \phi + \frac{a}{2b} \tan^2 \phi - \frac{1}{2} \tan \phi \right] - s'_p \left[\frac{1}{\tan \phi} + \frac{a}{b} \right] = 0$$

$$\text{or } \tan \phi = \frac{b}{a} + \sqrt{\frac{b^2}{a^2} + 3} \quad (5-4)$$

5-2.3 Failure Condition

Since the finite elements are equilibrated to nodal points at the four corners, it is necessary to make some assumption as to the development of the yield moment. The method elected was to average the moments in the ϕ direction at all four corners and compare the average to moment capacity of the element.

Using Mohr's circle, the moment at a point which makes an angle ϕ with the Y axis is,

$$M_\phi = M_y \cos^2 \phi - M_x \sin^2 \phi + M_{xy} \sin 2\phi \quad (5-5)$$

and the failure condition is,

$$M_p < \frac{1}{4} (M_\phi^i + M_\phi^j + M_\phi^k + M_\phi^l) \quad (5-6)$$

5-3 Sample Non-Linear Analysis

A single cell box structure was defined as shown in Figure 5-2.

The structure was 40 feet square by 20 feet deep with walls 0.3 feet thick. Different moment capacities were assigned to each plate so that the effect of successive failures could be demonstrated.

Figure 5-3 shows the input form and Figure 5-4 shows a printing of the input.

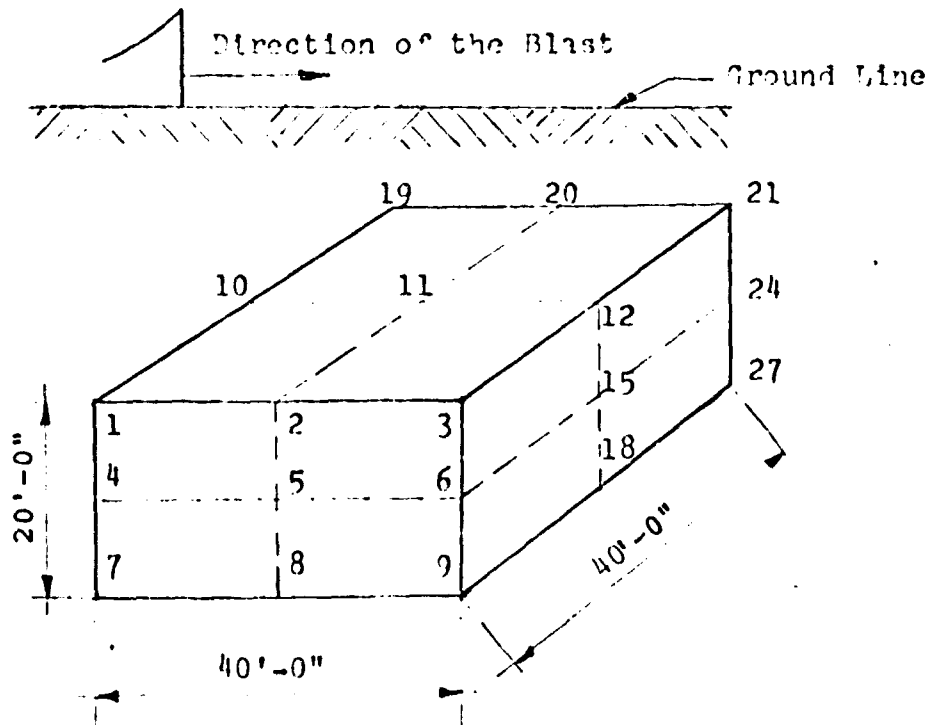


Figure 5-2

SAMPLE UNDERGROUND STRUCTURE

Figures 5-5, 5-6, and 5-7 are selected sheets from the output, Figure 5-5 shows the Load Deflection History. After each increment of time the moments in each plate are compared to the assumed average moment capacity of each plate. When any plate has failed, the plate number is printed on the output. The process continues until a sufficient number of plates have failed to produce an unstable structure, at which point the computer halts any further analysis and prints out maximum displacements (Figure 5-6), velocities and accelerations. The maximum positive moments and maximum negative moments (Figure 5-7) are also printed out. The times at which these maxima occur are also printed.

Innut By		IRS		Program		Cans-1-UB2	
Date		10/12/66					
Underground Box Structures Non-Linear Analysis				Job Identification			
Sample Problem---Single Box Dynamic Non-Linear Response				10/12/66			
x-AXIS	2	u-AXIS	2	z-AXIS	2	Number of Coordinates	
Length of Plates (ft)							
40.						x-AXIS	
20.						y-AXIS	
40.						z-AXIS	
Thickness of Plates in Sequence (ft)							
.3	.3	.3	.3	.3	.3		
Average Moment Capacity of Plates in Sequence (k-ft/ft)							
20.	20.	15.	15.	15.	100.	500.	
E (ksf) wt. (lb/cf) s.g. soil K _o							
432000.	150.	2.69	.33				
w (ft)	Δp_e (psi)	u (fms)	p_n^* (sec)	a	b	a	a
20.	15.	15000.	.08	1.36	8.40	0.67	
p (ft)	Δp (ft)	v_l (fms)	v_l^* (fms)	tmax/t ₂	Phase Time	n	
12500.	8300.	17000.	11700.	0.83	0.	4.	
a ₀	a ₁	Δt	Number of Δt	Note: [C] = a ₀ [M]+a ₁ [K]			
100.	.000025	.0005	40				

Figure 5-3

NON-LINEAR PROGRAM - INPUT

DYNAMIC NON-LINEAR ANALYSIS OF BOX STRUCTURES

SAMPLE PROBLEM ... SINGLE BOX DYNAMIC NON-LINEAR RESPONSE ... 10/12/66

NO. OF JOINTS

X DIRECTION = 2
 Y DIRECTION = 2
 Z DIRECTION = 2

MODULUS OF ELASTICITY
 STRUCTURE = 432000.00 KSF
 SOIL = 1255444.72 KSF
 RO = 150.00 LB/CU.FT.
 KO = 0.33

LENGTHS OF PLATES

X DIRECTION = 40.00
 Y DIRECTION = 20.00
 Z DIRECTION = 40.00

PLATE THICKNESSES

0.30 0.30 0.30 0.30 0.30 0.30

MOMENT CAPACITY (K*FT/FT)

20.00 20.00 15.00 15.00 100.00 500.00

BLAST AND GROUND MOTION CHARACTERISTICS

W(MT) = 20.00
 PSO(PSI) = 15.00
 ALPHA = 1.36
 BETA = 8.40
 A = 0.67
 DP+(SEC) = 0.08
 U(FPS) = 15000.00
 R(FT) = 12500.00
 DELR(FT) = 8300.00
 VL(FPS) = 17000.00
 VL*(FPS) = 11700.00
 TM/T2 = 0.83
 SP.GRAV. = 2.69
 P FACTOR = 4.00
 PHASING = -0.000000

40 TIME INCREMENTS

TIME INCREMENT = 0.0005

DAMPING FACTORS

ALPHA = 100.000000 BETA = 0.000025

Figure 5-4
 PRINTING OF INPUT

LOAD-DEFLECTION HISTORY

LOAD IN KIPS, DEFLECTION IN FT, TIME IN SEC

TIME	5-2		11-Y		13-X	
	LOAD	DEFLECTION	LOAD	DEFLECTION	LOAD	DEFLECTION
0.00050	5.3	0.000000	155.9	0.000011	71.1	0.000001
NEW FAILED PLATES** NONE						
0.00100	21.4	0.000000	311.7	0.000090	140.6	0.000005
NEW FAILED PLATES** NONE						
0.00150	47.4	0.000002	463.6	0.000301	136.6	0.000014
NEW FAILED PLATES** NONE						
0.00200	72.6	0.000005	607.9	0.000703	132.8	0.000022
NEW FAILED PLATES** NONE						
0.00250	97.1	0.000009	752.7	0.001352	129.1	0.000024
NEW FAILED PLATES** NONE						
0.00300	120.1	0.000013	786.1	0.002290	125.6	0.000019
NEW FAILED PLATES** NONE						
0.00350	130.3	0.000016	764.6	0.003522	122.2	0.000011
NEW FAILED PLATES** NONE						
0.00400	128.1	0.000018	743.8	0.005031	119.0	0.000006
NEW FAILED PLATES** NONE						
0.00450	124.6	0.000018	723.9	0.006793	115.8	0.000007
NEW FAILED PLATES**						
0.00500	121.2	0.000017 ¹⁵	704.7 ¹⁶	0.008790	112.8	0.000015
NEW FAILED PLATES**						
0.00550	118.0	0.000018 ³	686.3 ¹¹	0.011003	109.9	0.000019
NEW FAILED PLATES**						
0.00600	114.9	0.000017 ⁴	668.6 ¹²	0.013415 ²³	107.2 ²⁴	0.000017
NEW FAILED PLATES** NONE						
0.00650	112.0	0.000012	651.6	0.016012	104.5	0.000009
NEW FAILED PLATES** NONE						
0.00700	109.1	0.000005	635.1	0.018779	101.9	-0.000000
NEW FAILED PLATES**						

13 14 21 22

FAILED PLATES PRODUCE SINGULAR STIFFNESS MATRIX.

STRUCTURE BECOMES UNSTABLE

Figure 5-5

LOAD-DEFLECTION HISTORY

MAXIMUM DISPLACEMENTS

JOINT	DELTA (X)	DELTA (Y)	DELTA (Z)	PHI (X)	PHI (Y)	PHI (Z)
1	3.9989-005	2.3270-003	4.3995-005	-4.4806-002	-7.5120-005	3.7148-002
2	-1.0161-004	4.9065-003	2.0010-005	-2.5152-002	7.7058-005	-5.5585-003
3	-3.0253-005	2.1862-003	2.6632-005	-2.8353-002	1.1436-004	-3.6318-002
4	2.2417-005	1.8382-003	-1.7579-005	-5.1351-002	1.2553-003	4.3465-002
5	1.0965-004	2.6433-003	1.7946-005	8.9651-003	1.9427-003	-5.2663-003
6	1.8897-005	1.7523-003	1.5160-005	-3.2826-002	8.5432-004	-4.0922-002
7	2.2835-005	7.8180-004	-3.3043-005	-7.6180-002	6.6123-005	-6.6826-002
8	1.3781-004	6.9367-004	-1.6815-005	-4.8057-001	8.1539-005	-7.0026-003
9	1.4363-005	6.1806-004	-2.4952-005	-5.0411-002	1.4087-004	-5.9959-002
10	2.5241-005	5.1244-003	3.0387-013	-2.9178-011	-1.4438-013	-2.9384-002
11	1.4266-005	1.8779-002	4.5073-015	-2.9494-012	-1.1235-013	-6.2510-003
12	-2.6172-005	4.6875-003	5.3167-014	-3.5327-012	-8.8594-014	-2.0659-002
13	2.4060-005	2.6818-003	-7.1104-013	-3.5853-011	-1.8209-013	-9.5879-003
14	0.0000-000	0.0000-000	0.0000-000	0.0000-000	0.0000-000	0.0000-000
15	-2.3018-005	2.6042-003	-2.2995-014	-6.2282-012	-1.1210-013	3.1696-003
16	3.7608-005	7.7924-004	-3.5201-013	-5.5585-011	7.6219-014	6.7784-001
17	-1.9839-005	6.8991-004	-2.2849-015	-5.1151-011	4.0334-014	-2.2095-001
18	-1.2830-005	6.0808-004	-1.6691-014	-1.2866-011	-5.8631-014	-2.8555-001
19	3.9989-005	2.3270-003	-4.3995-005	4.4806-002	7.5120-005	3.7148-002
20	-1.0161-004	4.9065-003	-2.0010-005	2.5152-002	-7.7058-005	-5.5585-003
21	-3.0253-005	2.1862-003	-2.6632-005	2.8353-002	-1.1436-004	-3.6318-002
22	2.2417-005	1.8382-003	1.7579-005	5.1351-002	-1.2553-003	4.3465-002
23	1.0965-004	2.6433-003	-1.7946-005	-8.9651-003	1.9427-003	-5.2663-003
24	1.8897-005	1.7523-003	-1.5160-005	3.2826-002	-8.5432-004	-4.0922-002
25	2.2835-005	7.8180-004	3.3043-005	-7.6180-002	6.6123-005	-6.6826-002
26	1.3781-004	6.9367-004	1.6815-005	-4.8057-001	-8.1539-005	-7.0026-003
27	1.4363-005	6.1806-004	2.4952-005	5.0411-002	-1.4087-004	-5.9959-002

Figure 5-6

MAXIMUM DISPLACEMENTS

MAXIMUM NEGATIVE STRESSES IN LOCAL COORDINATES

ELEMENT #	TYPE #	JOINT #	MOMENT-X	MOMENT-Y	MOMENT-XY
1	1	4	-5.5221+000	-2.9776+001	-2.7428-002
1	1	5	-8.5711-001	-2.2518+000	-8.4298-003
1	1	1	0.0000+000	0.0000+000	-3.2826-001
1	1	2	0.0000+000	0.0000+000	-3.4805-001
2	1	5	-1.0471-001	-2.1077+000	-3.7118+000
2	1	6	-4.1761+000	-1.9107+001	-3.5308+000
2	1	2	0.0000+000	0.0000+000	-5.8600-001
2	1	3	-3.3463-003	-1.7338-004	-4.0493-001
3	1	7	-3.9758+000	-1.9922+001	-4.8388+000
3	1	8	-8.0417+000	-4.0164+001	-4.7730+000
3	1	4	0.0000+000	0.0000+000	0.0000+000
3	1	5	-4.6388-002	0.0000+000	0.0000+000
4	1	8	-1.2862+001	-6.4319+001	0.0000+000
4	1	9	-2.2483+000	-1.1246+001	-4.7270-007
4	1	5	0.0000+000	0.0000+000	-8.3182-001
4	1	6	-6.2172-002	-9.5414-004	-9.8023-001
5	1	13	0.0000+000	0.0000+000	0.0000+000
5	1	14	0.0000+000	0.0000+000	0.0000+000
5	1	10	0.0000+000	0.0000+000	0.0000+000
5	1	11	0.0000+000	0.0000+000	0.0000+000
6	1	14	0.0000+000	0.0000+000	0.0000+000
6	1	15	0.0000+000	0.0000+000	0.0000+000
6	1	11	0.0000+000	0.0000+000	0.0000+000
6	1	12	0.0000+000	0.0000+000	0.0000+000
7	1	16	0.0000+000	0.0000+000	0.0000+000
7	1	17	0.0000+000	0.0000+000	0.0000+000
7	1	13	0.0000+000	0.0000+000	0.0000+000
7	1	14	0.0000+000	0.0000+000	0.0000+000
8	1	17	0.0000+000	0.0000+000	0.0000+000
8	1	18	0.0000+000	0.0000+000	0.0000+000
8	1	14	0.0000+000	0.0000+000	0.0000+000
8	1	15	0.0000+000	0.0000+000	0.0000+000
9	1	22	-2.5286-002	0.0000+000	-4.6697+000
9	1	23	0.0000+000	0.0000+000	-4.5583+000
9	1	19	-5.6850+000	-2.8536+001	-1.3760+000
9	1	20	-1.6973+000	-8.3749+000	-1.2646+000
10	1	23	-1.8730-001	0.0000+000	-7.9570-004
10	1	24	0.0000+000	0.0000+000	-2.3633-002
10	1	20	-1.6542+000	-8.3662+000	-5.3776-001
10	1	21	-3.6424+000	-1.8131+001	-6.7632-001

Figure 5-7

MAXIMUM NEGATIVE STRESSES

Section 6

SYNOPTIC REVIEW OF SELECTED LITERATURE PERTAINING TO THE FAILURE MODES AND FAILURE LOADINGS OF TWO-WAY SLABS

6-1 Introduction

In the search for, and review of publications, emphasis was placed on reports of the results of load tests to failure and comparisons of test results with predictions calculated by analytical methods. The region of interest, in the load-deflection history of slabs, starts at the beginning of yield in the reinforcement and ends at collapse of the slabs. Slabs are assumed to have less than balanced reinforcement.

All of the tests, of which reports were examined, were made with static loads. Where the location of the test was reported, it is given in this review. Generally, locations are not reported but inasmuch as the tests were made in laboratories, it is assumed that they were facilities of the activity with which the author was connected.

In the listing of references, those publications which were considered to be significant contributors of knowledge in the region of interest are abstracted. Many other reports were examined and those addressed to objectives which bear to some lesser extent on the region of interest are listed but not abstracted.

6-2 Synoptic Review of Selected Literature

The pertinent phenomena reported in the region of interest are:

- 1) The yielding of the reinforcing steel.
- 2) The arching action of the slab.
- 3) The improvement of the plastic deformability of the concrete in the triaxially compressed zone.
- 4) The mobilization of tensile membrane forces in the suspended net of steel.

The excitation of interest in the post-yield history of overloaded slabs appears to have been triggered by Ocklestons^{1*} report of his load tests to destruction of

^{*}References designated by superscript in this Section 6 are found on pages 6-6 to 6-12.

some two-way slab floor panels in a reinforced concrete building in Johannesburg, South Africa, which was available because it was scheduled for demolition. Ockleston reported cracking patterns agreeing with the Johansen Yield Line Theory, but that he obtained failure loads over $2\frac{1}{2}$ times analytical predictions according to the theory. Approximately $2\frac{1}{2}$ years later (June 1958) he reported² his re-examination of his test results and his success, with a simple theory which he produced, in rationalizing the high failure loadings as resulting from the superposition of plastic hinge moments and the resisting moment produced by arching action of compressive axial force induced in the slab by large deflections associated with the functioning of plastic hinges.

A somewhat idealized version of arching action in a slab is depicted in Figure 6-1. It is assumed that the slab is under-reinforced, as is normally true, so that the concrete behaves elastically above the yield moment of the steel.

Relatively large deflection of the slab after the formation of plastic hinges imposes compressive strains for the simple reason that the diagonal distance, d , between compressive stress block centroids, is greater than the horizontal distance, $l/2$.

It is readily apparent that these compressive strains will not be imposed unless the structure surrounding the yielding slab is stiff enough to function as an effective abutment. It is also apparent that the limit of arching action is reached when the lever arm reaches zero and that, with small additional deflection, the lever arm becomes negative and the stored inplane strain energy performs work contributing to plastic hinge rotation. This produces additional deflection with rapidly diminishing load, transforming work already done into tensile membrane strain energy in the steel, which is already past its yield point. With sustained load, the rupture stress in the steel is likely to be reached, particularly with large depth span ratios and very stiff abutting structure. With impulse loads, the work of which is quickly transformed to kinetic energy, the kinetic energy remaining when the steel becomes the sole survivor may be within the capacity of the steel to accept it below the rupture stress. The worth of the suspended steel net depends considerably on the stress-strain properties of the steel above its yield point stress.

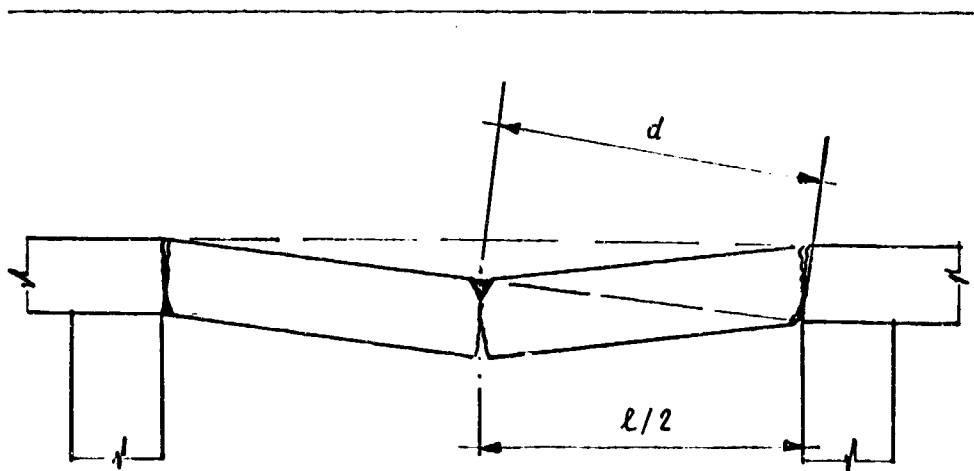


Figure 6-1

ARCHING ACTION IN A YIELDING SLAB

The characteristic load deflection curve is shown in Figure 6-2.

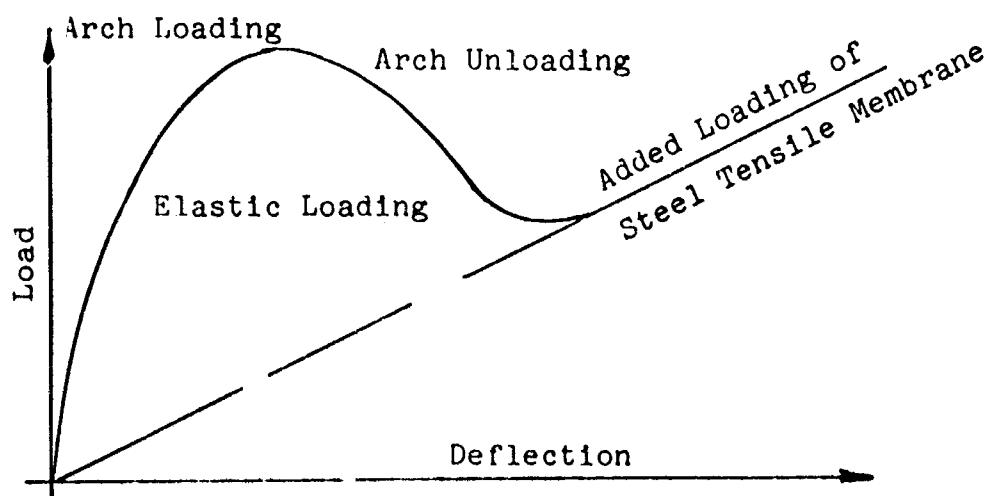


Figure 6-2

CHARACTERISTIC LOAD DEFLECTION CURVE OF REINFORCED SLAB WITH ARCHING ACTION MOBILIZED BY LATERAL BOUNDARY STIFFNESS

The foregoing synopsis of load-deflection history is a syllabus, to a large extent, of the findings from examination of References 1-12, inclusive. Tests reported by Park³ and by Christiansen⁴ manifested the existence of arching action and emphasized its dependence on lateral boundary stiffness. Christiansen's results with two quite widely differing cube strengths pointed up the sensitivity of arching action to the inplane stress-strain relation. Self⁵ reported tests with cold-rolled and hot-rolled steel which suggested the effect of strain hardening on the plastic hinge resisting moment. Gamble and Sozen⁷ reviewed the literature and studied the results of five scale model tests made at the University of Illinois by Seiss⁷, and advanced five reasons for the calculation of failure loads significantly less than test results. These are:

- 1) Incorrect determination of steel strength
- 2) Strain hardening of steel
- 3) Erroneous location of yield line
- 4) Arching Action
- 5) Effects of deformation of the structure

Undoubtedly, the increase in load capacity above the yield point in the steel is a superposition of strain hardening and arching effects. Hodge and Perrone⁶, Hillerborg⁸, Crawford¹⁰ and Kemp¹¹ report finding by means of theory that the yield line method gives an upper bound and that there is a lower bound that can be determined by finding a distribution of moments which satisfies the boundary conditions and the equilibrium equation⁹. Kemp found the lower bound to be only slightly less than the upper bound, but found the yield lines to be an infinite set of curves. These theoretical findings regarding the failure load are not borne out by the tests reported upon, in which test results were higher than calculated values. Gamble and Sozen⁷ found this to be true in the literature they reviewed and the results of scale model tests they studied. Relative to their advancement of incorrect determination of steel strength as one of the reasons for low calculated failure loads, the authors of the publications which have been examined, in which analytically predicted and experimental results were compared, did not report whether or not they had determined, by test, the yield point of the specific reinforcement earmarked for use in experimental loadings. The yield point stresses specified, according to steel grades, are the

producers' guaranteed minima, which are exceeded approximately 15 percent by the mean value.

Brotchic, Jacobson and Okubo¹² report the results of the comprehensive tests and investigation made at the Massachusetts Institute of Technology under contract with the U. S. Naval Civil Engineering Laboratory, Port Hueneme, California. This recent (August 1965) supported work in the field appears to have been a well integrated, comprehensive experimental investigation of the behavior of two way square slabs, supported around the four edges, with and without moment restraint. They were restrained against lateral displacement, but with strain gauge cells which permitted the restraining forces to be measured. The report presents straightforward analytical equations which, with a few exceptions, agree reasonably well with the results of the experiments. A feature of the report, not found in other literature examined, deals with the effect on concrete strength of the triaxial compression in the positive moment hinge area, comprised of axial forces in two directions and the vertical force of applied load. The authors conclude that, "The combination of increased load capacity and improved behavior produced by arching action is sufficiently large and sufficiently predictable, to warrant its serious consideration in design." They suggest its application to the roof and walls of reinforced protective structures of various kinds, eg. shelters, block houses, etc., particularly subterranean. They caution that, "tensile membrane action may be considered only in situations where excessive deflections are tolerable and reuse is not necessary: such as, protective slabs under debris loading."

Regarding the predictability of the increased load capacity produced by arching action, the authors did not address themselves to the problem of determining the lateral stiffness of the boundary of the loaded slab in an existing structure. Arching action is sensitive to lateral stiffness at the boundary and this parameter needs to be estimated rather closely. A structure may be designed with boundary lateral stiffness provided in such way that its effectiveness may be reliably verified by analytical methods, but such design may not be found in existing structures.

The capability of the tensile membrane to provide protection against catastrophic failure under destructive dynamic loading of buried structures is subject to certain

reservations which demand thorough consideration. Tensile membranes which are the surviving intact components of external horizontal slabs will be subjected to the sustained gravity load of earth overburden and residual kinetic forces. Cracked external walls with relatively large deflections will be axially loaded with the gravity reaction of earth overburden. If the concrete is not too badly crushed, this force will provide some resistance against the lateral forces. If the concrete toward the outside face is ineffective in compression, the line of force may be so far toward the inside face that the gravity reaction will contribute to collapse of the walls. The tensile membrane has no capability to resist collapse from such cause. The lateral force will be comprised of residual kinetic force and lateral pressure of disturbed soil. The tensile membrane has capacity within its strength limitation to resist these forces, provided the vertical force does not cause collapse.

6-3 Selected References with Abstracts of More Pertinent Publications

1. Ockleston, A. J., *Load Tests on a Three Story Reinforced Concrete Building in Johannesburg*, The Structural Engineer (London) October 1955, P.304.

Full scale static loading tests to failure were run on two 16ft. by 13ft. 6in. reinforced concrete slab panels which were part of a beam and slab floor system 27ft. wide by over 100ft. long. Slabs were bounded by transverse main beams spaced 16ft. apart and secondary longitudinal beams spaced 13ft. 6in. apart. Cracking pattern agreed with Johansen Yield Line Theory but failure loads were over 2½ times the analytical predictions.

2. Ockleston, A. J., *Arching Action in Reinforced Concrete Slabs*, The Structural Engineer (London) June 1958, P.197.

Ockleston re-examined the results of his earlier tests (ref. 1) and succeeded, with a simple theory he produced, in rationalizing the high failure loads as resulting from the superposition of plastic hinge resistance and the resisting moments afforded by compressive membrane forces.

3. Park, R., *The Lateral Stiffness and Strength Required to Ensure Membrane Action at the Ultimate Load of a Reinforced Concrete Slab and Beam Floor*, Magazine of Concrete Research (London) Vol. 17, No. 50, March 1965, PP.29-35.

Sand-cement mortar models of a nine panel slab and beam floor were tested to failure under static uniform load on the interior panel. Tests were made at the University of Bristol. Panels were 12in. square and varied in depth from about 3/8in. to about 11/16in. Twenty slabs were tested, varying in ages from 9 to 14 days. High abutment stresses were manifested by diagonal cracks across a corner of the surround, consisting of the eight exterior panels. The ultimate loads of the interior panels of slabs with continuous tee reinforcement showed good agreement with theory which includes compressive membrane strains in the panel, and lateral edge displacements once the concrete had cracked, but did not reach the results of theory which ignored these strains and displacements. Results emphasize the importance of abutment stiffness in the mobilization of arching forces.

4. Christiansen, K. P., *The Effect of Membrane Stresses on the Ultimate Strength of Interior Panel in a Reinforced Concrete Slab*, The Structural Engineer (London) Vol. 41, No. 8, August 1963.

Christiansen, a Civil Engineer in Copenhagen, performed the reported work and wrote the paper while a lecturer at the University of Witwatersrand, Johannesburg, South Africa. The author presents his theory for evaluation of arching action in slabs and reports results of tests of 4 identical pairs of simply supported beams, with one of each pair axially restrained by a welded steel frame and the other, unrestrained; all beams were 6 inches wide and spans and depths were 60 x 3.5 inches, 60 x 3 inches and 72 x 3 inches. Load carried by arching in the axially restrained beams was 30 - 35% of the total in three cases with cube strengths from 4090 to 4975 psi, and 70% of the total in a 60 x 3.5 inch beam with cube strength of 5660 psi. Author concludes that although loads supported by arching can be predicted with some accuracy, more research is required to make arching action a reliable and useful part of design.

5. Self, W. M., *Ultimate Strength of Reinforced Concrete Flat Slabs*, Journal, Structural Division, ASCE Vol. 90, No. St4, August 1964, P.205. Three reinforced concrete slab models were tested. Slabs were 10 feet square by 2 inches thick, and supported by four interior columns producing an interior panel $5\frac{1}{2}$ feet square. Overhang balanced moments over columns, thus eliminating influence of column stiffness.

Yield line pattern conformed to predictions in accordance with Johansen theory. Ultimate strength of slab No. 1, reinforced with cold-rolled steel, was 9% above prediction; slab No. 2, reinforced with hot-rolled steel, reached an ultimate strength 17% above prediction. (Slab No. 3 failed in shear before flexural yield). The variation is indicative of strain hardening of steel. The slabs lacked surrounding confinement necessary to mobilize compressive membrane forces.

6. Hodge, P. G., Jr. and Perrone, N., *Yield Load of Slabs with Reinforced Cutouts*, Journal of Applied Mechanics, Vol. 24, March 1957, PP.85-92.

Presents a method of computing the upper and lower bounds on the capacity of a plane slab with a reinforced cutout to carry uniaxial tensile loads which are either uniform or applied by means of a perfectly rigid clamp. Results are applied to several examples and found to agree quite well with experimental values.

7. Gamble, W. L., Sozen, M. A., and, Sless, C. P., *Measured and Theoretical Bending Moments in Reinforced Concrete Floor Slabs*, University of Illinois Civil Engineering Studies, Structural Research Series No. 246, June 1962.

Test results of two-way slabs reported in the literature and results of five tests of differing $1/4$ -scale slab models, performed at the University of Illinois, were reviewed with the objective of developing a slab design procedure.

Slab strengths were calculated according to yield line theory, Moe's formula for shear strength, Elstner and Hognestad punching shear equations or the equation from ACI committee 326.

In nearly all of the tests reported in the literature, the specimens failed at loadings higher than calculated according to yield line theory.

Some reasons advanced for the low calculated values are:

1. Incorrect determination of steel strength.
2. Strain hardening of reinforcement.
3. Errors in establishing location of yield line.
4. Arching of compressive membrane forces.
5. Effects of deformation of the structure.

In most of the five University of Illinois tests, the flexural mode of failure was complicated by other distress (shear failure, beam-column distress, etc.). The test results indicated that if flexural failure had been allowed to occur, the failure load would have exceeded the results obtained by yield line analysis.

8. Hillerborg, A., *A Plastic Theory for the Design of Reinforced Concrete Slabs*, Preliminary Publication, International Association for Bridge and Structural Engineering, Sixth Congress, Stockholm, 1960.

Conclusion is reached that although the yield line theory will reveal the magnitude of a load great enough to cause failure through the formation of plastic hinges, the load is theoretically unsafe since other yield lines may form at a lower level.

The equilibrium theory states that if a distribution of moments can be found which satisfies the equilibrium equation and the boundary conditions, under the action of a given load, and these moments do not exceed the yield moments at any section of the slab, the slab is capable of carrying that load. This is a lower bound and the exact ultimate load is somewhere between the results of the yield line and equilibrium theories.

9. Hillerborg, A., *Theory of Equilibrium for Reinforced Concrete Slabs*, Department of Scientific and Industrial Research, Building Research Station, Library Communication No. 1082, Great Britain.

If, for a certain external load, $q(x,y)$, a moment distribution can be found which satisfies the equation,

$$\frac{\partial^2 m_x}{\partial x^2} + \frac{\partial^2 m_y}{\partial y^2} - 2 \frac{\partial^2 m_{xy}}{\partial x \partial y} = -q(x,y)$$

and the edge conditions, and if the slab can take up these moments at each point, $q(x,y)$ is a lower limiting value for the bearing capacity of the slab. The moments are not coupled and therefore, two may be selected arbitrarily and the remaining one solved.

A practical solution is advanced, involving the division of the slab into strips, in which the load in one strip is carried in one direction only.

10. Crawford, Robert E., *Limited Design of Reinforced Concrete Slabs*, Journal of the Engineering Mechanics Division, American Society of Civil Engineers, Vol. 90, No. EMS, October, 1964.

The yield line theory is considered in terms of limit analysis and is shown to give an upper bound on the collapse load. Similarly, the equilibrium theory is reviewed and shown to give a lower bound.

11. Kemp, K. O., *A Lower Bound Solution to the Collapse of an Orthotropically Reinforced Slab on Simple Supports*, Magazine of Concrete Research (London) July, 1962.

A lower bound solution to the collapse of a simply supported, rectangular slab, orthotropically reinforced and carrying a uniformly distributed load is developed. The lower bound collapse loads, calculated for a range of coefficients of orthotropy and ratio of width to length of slab, agree closely with the upper bound values derived from the yield line theory. The yield lines, however, are quite different; they are found to be an infinite set of curves in the lower bound solution. With the solution, the negative reinforcement required in the corners of the slab and the loads transmitted to the supporting edges were determined.

12. Brotchie, John F., Jacobson, Amnon and Okubo, Sadaji, *Effect of Membrane Action on Slab Behavior, Report*, Department of Civil Engineering, M.I.T., U.S. Naval Civil Engineering Laboratory, Port Hueneme, California, August, 1965.

Forty-five square slabs of plain and reinforced concrete were tested under uniform loading. All spans were 15" x 15". Thicknesses were 0.75", 1.5" and 3.0", resulting in span/depths ratios of 20, 10 and 5.

Lower reinforcement only was used, distributed uniformly and equally in each direction. Reinforcement ratios were 0%, 0.5%, 1%, 2% and 3%.

Five sets of boundary conditions were used:

1. Restrained at edges against axial elongation only, at approximate level of reinforcement, by 24 cells.
2. Same as 1, with added resistance to internal shear in the slab at the support.
3. Same as 1, but with level of restraining force raised to the middle of the edge surface of the slab.
4. Slab clamped at the supports by top plate and base plate and restrained at the edges by epoxy resin fill.
5. Simply supported on 0.75" diameter roller bearings.

The steel restraining frame was designed for essentially complete lateral and vertical rigidity. Twelve of the 24 restraining cells, uniformly distributed along two adjacent edges, were wired with electrical resistance strain gauges for measuring the restraining force.

The effect of arching was found to be significant in slabs with span/depth ratios of 20; equivalent in load capacity to approximately 2% of conventional reinforcement. The effect of arching is greater for thick slabs and, for span/depth ratios of 5, is equivalent

to over 3% of conventional reinforcement. External restraint, mobilizing arching action, increases stiffness and reduces cracking. When maximum arching - supported load is reached, however, load capacity drops while deflection increases, allowing sudden failure if the slab is lightly reinforced and the applied loading is sustained.

The magnitude and distribution of the restraining force indicates that essentially the full capacity of the concrete in compression is utilized, when the slab is restrained.

For thin slabs, essentially full edge restraint is necessary to mobilize the full increase in load capacity. For thicker slabs, additional edge displacement may be tolerated, without significantly reducing the load capacity.

The effect of direct normal stress due to the uniform load, in combination with two-way inplane stresses, is to produce a triaxially compressed zone. In the case of very thick slabs, that is, span/depth ratios of 5, the effect is apparently significant; the plastic deformability of the concrete in the compressive zone is notably increased.

Tensile membrane action is significant only at deflections which are too large for use in resisting service loads. The tensile membrane action may have some appeal, however, to provide protection against collapse in the case of a single catastrophic loading, particularly in view of the energy absorption which precedes in this range.

Simple theoretical expressions are presented which were found to predict, with some exceptions, the ranges of behavior described.

Section 7

7-1 REFERENCES

1. Lin, T. Y. and Associates, *Computer Analysis of Protective Structures For Protection From Nuclear Blast*, Office of Civil Defense, Contract No. OCD-PS-65-7, June 1965
2. *Principles and Practices For Design of Hardened Structures*, Air Force Design Manual, Report Number AFSWC-TDR-62-138, December, 1962.
3. *Design of Structures to Resist Nuclear Weapons Effects*, ASCE Manual of Engineering Practice, No. 42, 1961.
4. Norris, C. H., et al, *Structural Design for Dynamic Loads*, McGraw-Hill Book Company, 1959.
5. White, M., *Design and Review of Structures For Protection From Nuclear Blast*, Protective Structures Division, Office of Civil Defense, PM-100-4, 1963.
6. Clough, R. W., *The Finite Element Method in Structural Mechanics, Stress Analysis*, Edited by O.C. Zienkiewicz and G. S. Holister, John Wiley and Sons, Ltd., London, 1965.
7. Adini, A. and Clough, R. W., *Analysis of Plate Bending By The Finite Element Method*, Report submitted to the National Science Foundation Grant G7337, 1960.
8. Stanford Research Institute, *Nuclear Geoplosics, Part IV*, D.A.S.A.-1285, May, 1964.
9. Stanford Research Institute, *Nuclear Geoplosics, Part V*, D.A.S.A.-1285, May, 1964.
10. Berg, G. V., *The Analysis of Structural Response To Earthquake Forces*, University of Michigan Industry Program of the College of Engineering, Report No. IP-291.

11. Johansen, K. W., *Yield Line Theory*, Cement and Concrete Association, 1962.
12. Archer, J. S., *Consistent Mass Matrix for Distributed Mass Systems*, Journal of the Structural Division, ASCE, August 1963.
13. Clough, R. W., and Tocher, J. L., *Finite Element Stiffness Matrices for Analysis of Plate Bending*, Proceedings of the Conference on Matrix Methods in Structural Mechanics, October 1965, AFFDL-TR-66-80, Air Force Flight Dynamics Laboratory, Wright Patterson AFB.
14. Wiehle, C. K., *Soil-Structure Interaction Under Dynamic Load, Part I, Analysis and Correlation*, DA-49-146-XZ-288, URS Corporation for the Defense Atomic Support Agency, November 1965.
15. Brode, H. L., *A Review of Nuclear Explosion Phenomena Pertinent to Protective Construction*, The Rand Corporation, R-425-PR, May 1964.
16. Stanford Research Institute, *Behavior of Equipment Platform Under Blast Loading*, Prepared for the Ralph M. Parsons Company, February 1963.

Appendix A

COMPUTER SUBROUTINE FOR CALCULATING LOADS ON AN UNDERGROUND BOX

The formulation of the load subroutine contained in the computer program is described in this appendix. Pressures felt by a shallow buried box are calculated using the engineering approach of Reference 2 (Chapter 4). Soil-structure interaction has not been considered, *per se*. The loading formulation assumes that the overpressure of interest are less than 100 psi. Also megaton yield weapons are assumed.

A-1 Airblast Characteristics

This section is a brief statement of the airblast characteristics, as recorded by Brode in *A Review of Nuclear Explosion Phenomena Pertinent to Protective Construction*¹⁵. This reference should be consulted for a complete review of the physical phenomena pertinent to protective construction.

Figure A-1 shows the shock arrival time t_s and the shock radius R_s for the overpressures resulting from the detonation of a 20 MT bomb. These values depend upon the energy of the explosion and may be scaled by the cube root of the yield ratio in megatons for yields other than 20 MT. This figure also illustrates the shock velocity as a function of the peak overpressure which is independent of weapon yield.

The time history of the overpressure is described quite well at all pressure levels under 100 psi by the sum of two decreasing exponential functions of time:

$$\Delta P = \Delta P_s (ae^{-a\tau} + be^{-B\tau})(1-\tau) \quad (A-1)$$

where τ is the time after shock arrival measured in units of positive phase duration. To force this curve to go to zero overpressure at the end of the positive phase, a linear factor has been included that becomes zero at a time equal to the duration of the positive phase ($\tau=1$ when $t-t_s = D_p$).

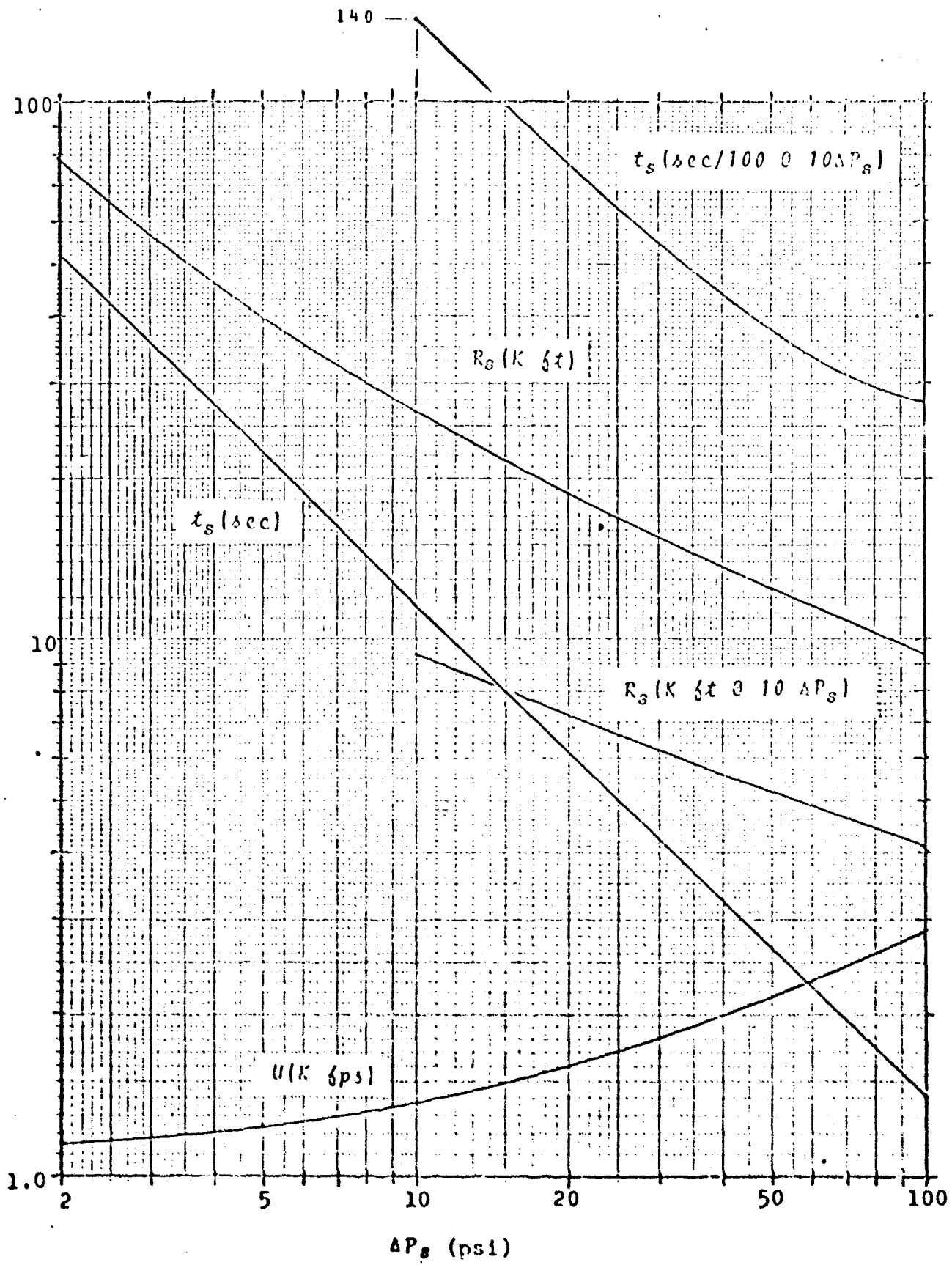


Figure A-1 SHOCK RADIUS (R_s), ARRIVAL TIME (t_s) AND SHOCK SPEED (u) VERSUS PEAK OVERPRESSURE (ΔP_s) FOR A 20WT SURFACE BURST. (Ref. 15)

Figure A-2 gives the values of all shock parameters and coefficients necessary to obtain the pressure-time curve for a given peak overpressure.

Curves showing the pressure time relations based on this analytical expression are given in Figure A-3.

A-2 General Characteristics of the Soil Pressure Wave

The alteration in free-field form of the vertical pressure wave as it progresses into the soil is illustrated in Figure A-4. The surface soil pressure has a very rapid rise, an exponential decay, and a duration time, D_p , similar to that of the airblast pressure wave. At greater depths a reduced soil pressure peak and a somewhat lengthened duration are present. Also, a lengthened rise time to peak soil pressure takes place. The impulse -- total area under the curve -- is nearly constant.

The attenuation of stress with depth is generally attributed to two causes, energy absorption by the soil and by three dimensional dispersion of the energy. Information regarding energy absorption is not available in a form useful for calculating loads. Three-dimensional or spatial attenuation can be approximated by the following expression proposed by Newmark²:

$$p_{vm} = \alpha_y \Delta P_s \quad (A-2)$$

$$\alpha_y = \frac{1}{1 + \frac{y}{L_w}} \quad (A-3)$$

$$L_w = \frac{2300 W^{1/3}}{(\Delta P_s)^{1/2}} \text{ ft.} \quad (A-4)$$

where

ΔP_s = peak overpressure at the surface, psi

p_{vm} = maximum vertical soil stress at depth y (ft), psi

α_y = geometric attenuation factor

W = yield in megatons

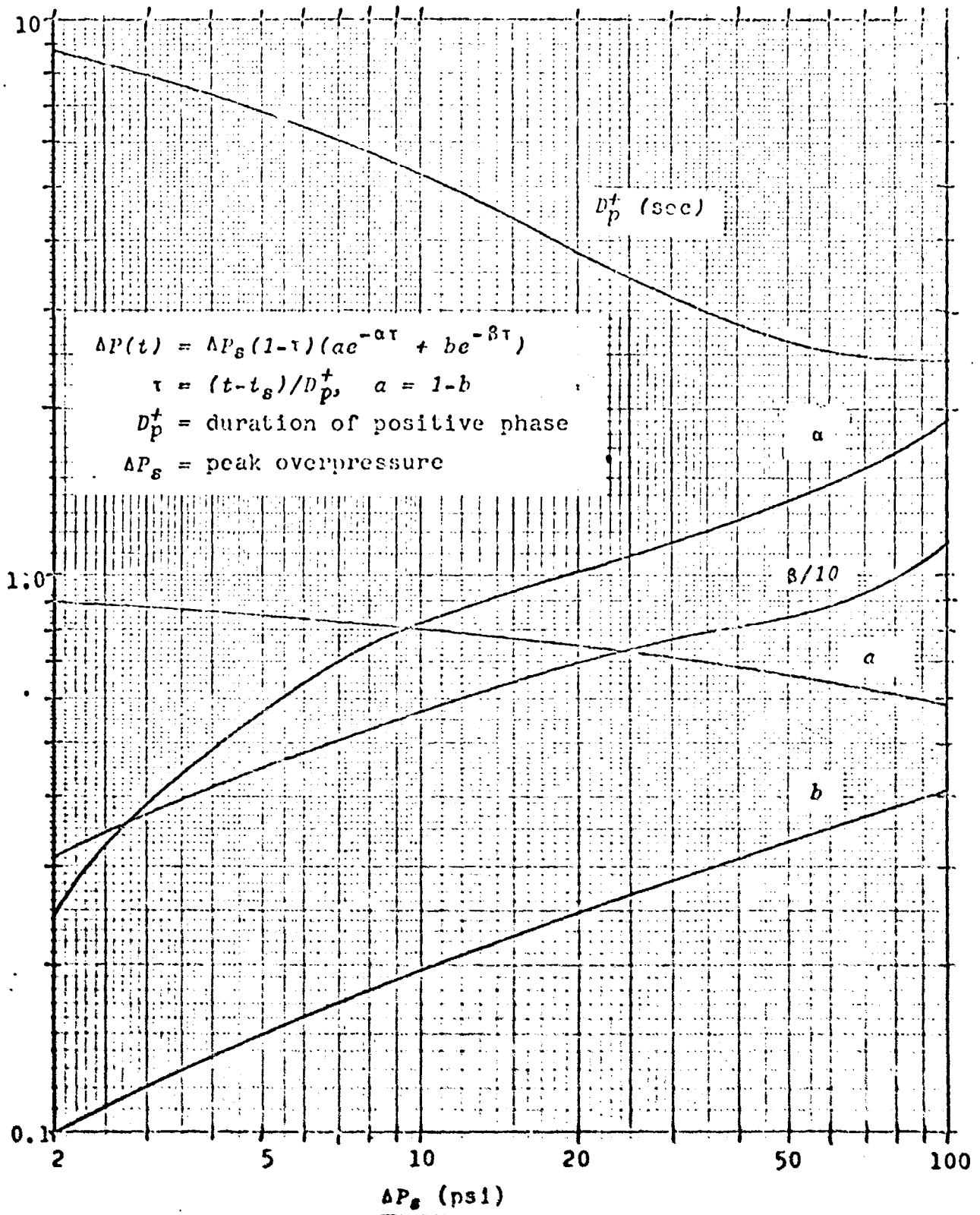


Figure A-2 ANALYTIC FORM FOR OVERPRESSURE VERSUS TIME
 IN TERMS OF PEAK OVERPRESSURE FOR A 20KT SURFACE BURST
 (Ref. 15)

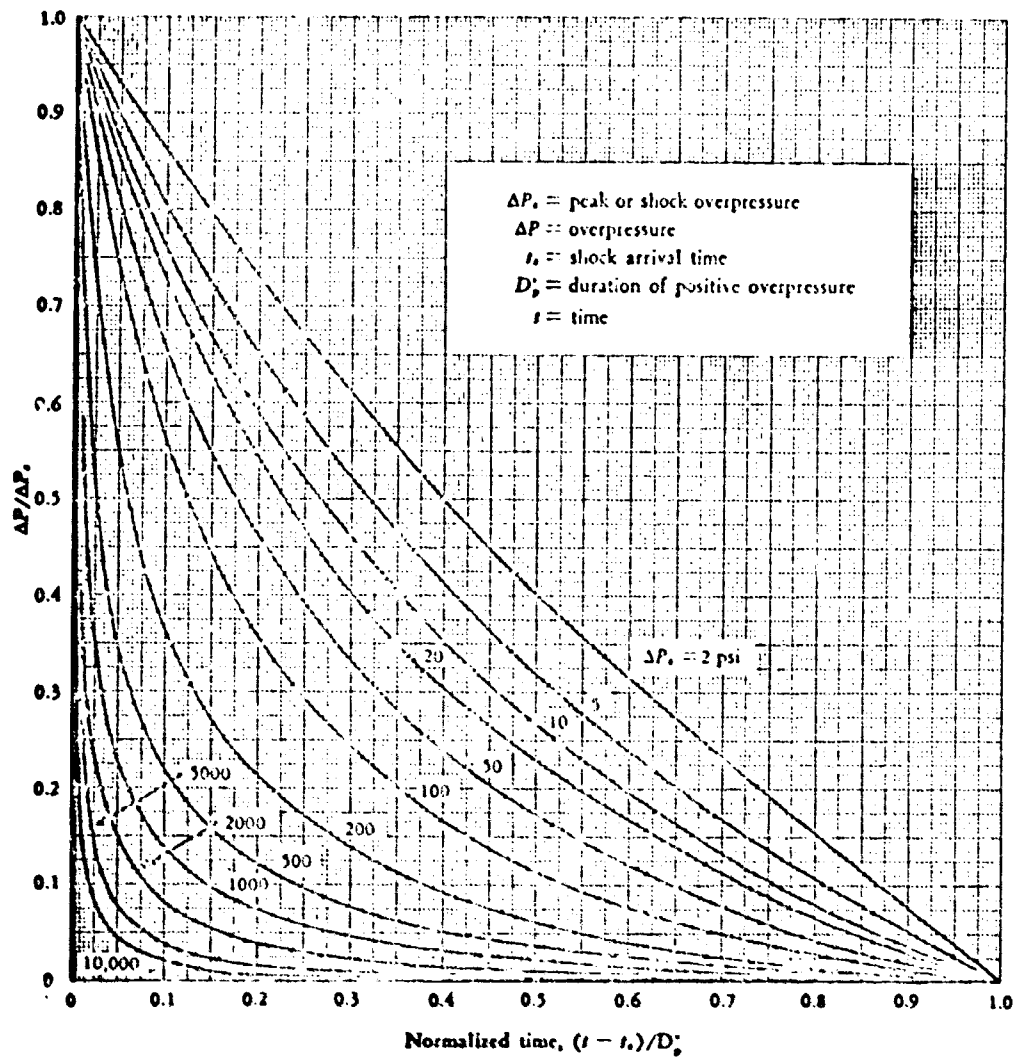
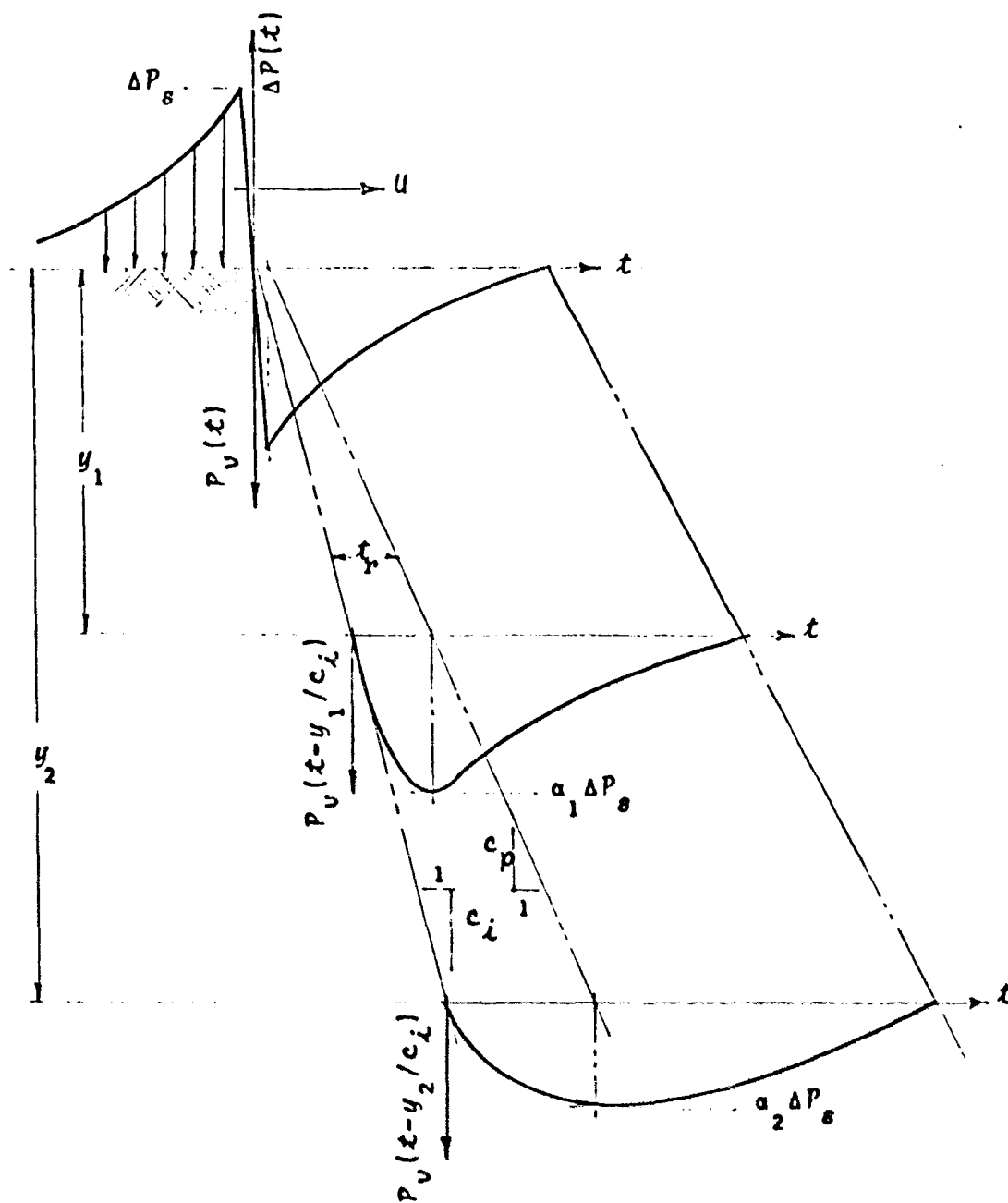


Figure A-3 FORM FACTORS FOR
 OVERPRESSURES FROM NUCLEAR EXPLOSIONS
 (Ref. 15)



α = Depth Attenuation Factor (Equation A-3)
 t_r = Time to Maximum Pressure (Equations A-5, A-6)

Figure A-4
 VERTICAL SOIL PRESSURE WAVE

The above approximation does not permit soil stress higher than the peak overpressure, a condition that can truly apply only when the airblast velocity is low compared to the seismic velocity.¹⁵

At the 100 psi range of a 20 MT surface burst, the geometric attenuation factor (Equation A-3) for 100 feet of depth is 0.86. For lower overpressures, higher yields or less depth, the attenuation factor approaches 1.0.

Referring again to Figure A-4, it is obvious that t_r , the time required for the vertical soil pressure to reach its peak value, can never be less than the airblast rise time. Figure 2-2.3 of Reference 3 gives an indication of the magnitude of this airblast rise time, as it varies with overpressure. However, the value of rise time is not well defined.

Reference 2 expresses the rise time in soil as;

$$t_r = t_{rab} + \frac{y}{c_p} - \frac{y}{c_i} \quad (A-5)$$

where

t_{rab} = airblast rise time

y = depth of interest

c_p = seismic velocity consistent with the loading modulus of the soil

c_i = seismic velocity consistent with the initial tangent modulus of the soil.

When the values of c_p and c_i are not well defined, an approximate evaluation of the rise time must be made. In view of the many uncertainties regarding airblast rise time and soil properties, Reference 2 suggests an approximation; that the rise time be taken as one-half the time required for the peak stress to reach the depth of interest.

$$t_r = \frac{1}{2} \frac{y}{c_p} \quad (A-6)$$

This expression (Equation A-6) has been used within the computer program.

Horizontal stress in the soil, p_h , is taken as some constant times the vertical soil stress.

$$p_h = K p_v \quad (A-7)$$

The value of the constant K , depends upon the soil properties, the degree of saturation, the stress level, and the condition of lateral restraint at the depth of interest.

A-3 Loads on the Box

Each finite element of the box-structure's exterior roof and walls is assigned a load-time history. Figure A-5 shows a roof element, a side wall element, and a front wall element. This figure gives each dimension used in calculating the idealized pressures on the box. Table A-1 lists the formulas used in calculating the form of the pressure on each finite element, expressed as an average uniform pressure over the element.

A-3.1 Roof Pressure

The vertical pressure on a roof element initiates with the arrival of the shock front at the leading edge and builds up to a maximum as the shock front reaches the trailing edge. The average pressure is assumed to increase linearly from zero to its maximum value during the time required for the shock front to travel across the element (see Table A-1).

Since the box roof is divided into a number of finite elements for analysis purposes, the average pressure is considered element-by-element in the direction of the shock travel.

Arching of the soil above the roof is not considered. Also, spatial attenuation of the peak pressure with depth of cover is not considered.

A-3.2 Wall Pressure

The horizontal pressures in the soil are calculated empirically by multiplying the vertical pressures by the coefficient of earth pressure at rest, K_0 . The analyst chooses the value of K_0 believed appropriate for the added increment of airblast induced horizontal stress. Suggested values are given in Table A-2.

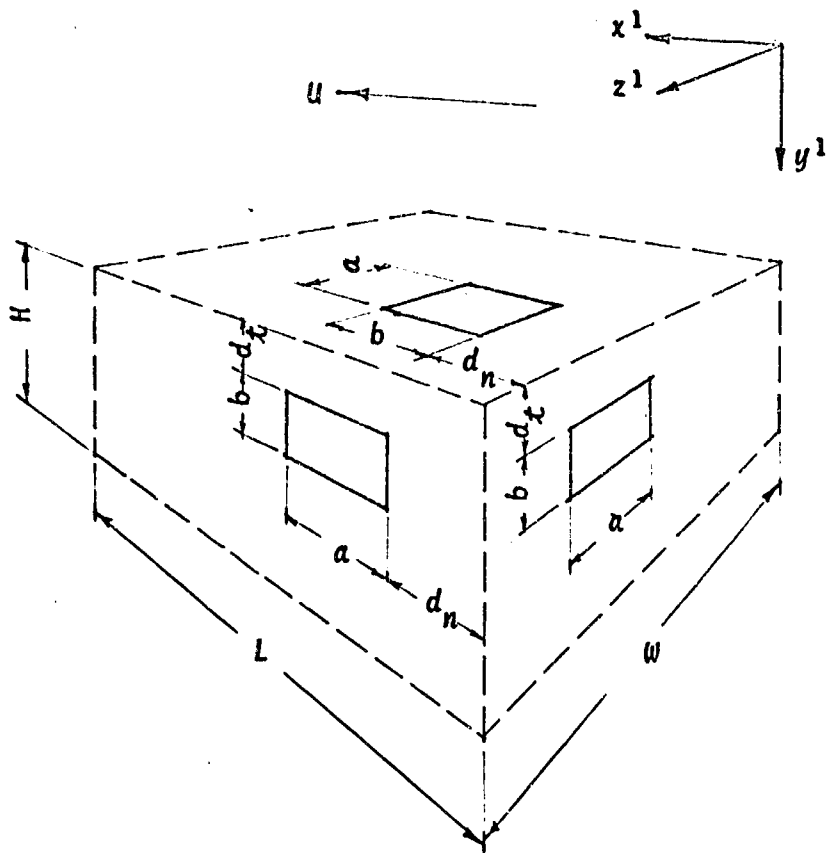
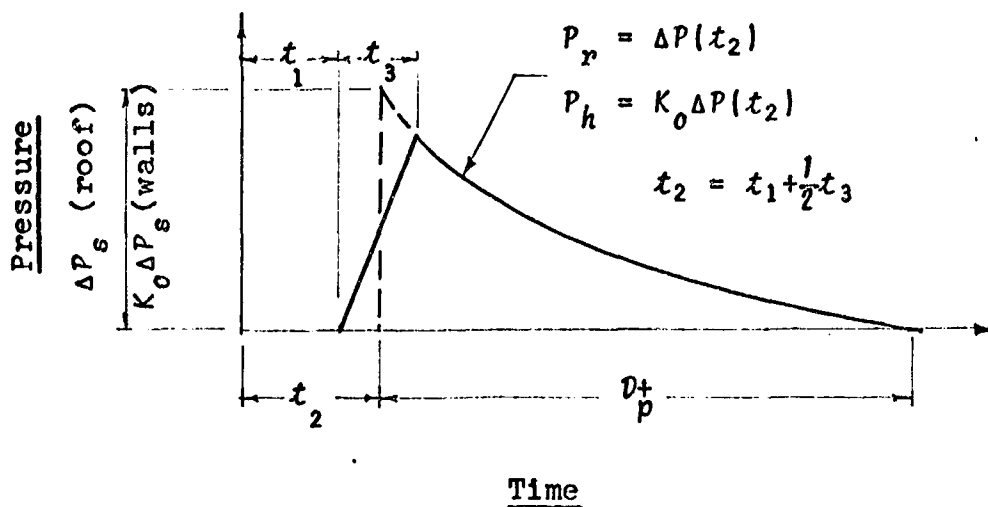


Figure A-5

LOCATION OF FINITE ELEMENTS
FOR LOAD CALCULATIONS



Location of Element*	Time in Seconds	
	t_1	t_3
Roof	d_n/u	b/u
Wall:		
Front	d_t/c_p	$t_r^{**} + (b/c_p)$
Rear	$(l/u) + (d_t/c_p)$	$t_r + (l/c_p)$
Side	$(d_n/u) (d_t/c_p)$	$t_r + (b/c_p)$

$$** t_r = \frac{1}{2} \frac{d_t + b/2}{c_p}$$

* See Figure A-5 for definitions of box dimensions

TABLE A-1
AVERAGE PRESSURE ON AN ELEMENT

No spatial attenuation of the peak horizontal soil pressure has been included in the programmed calculations. Very little spatial attenuation is predicted by Equation A-3 for depths less than 100-ft., located within the 100 psi range of megaton weapons. The coefficients of lateral earth pressure at rest (Table A-2) are too crude to be modified further by a depth attenuation factor.

The horizontal pressure on a wall element is assumed to initiate with the arrival of a vertical compression wave at the top edge, which is induced by the shock front as it arrives directly overhead. The average pressure is assumed to increase linearly from zero at initial arrival to a maximum value of $K_0 \Delta P_s$ during the time required for the soil pressure pulse to travel across the element plus the rise time calculated from Equation A-6. (See Table A-1.)

Since the box is divided into a number of finite elements, the average pressure is considered element-by-element with increasing depth and in the direction of shock travel.

A-3.3 Boundary Conditions

As the shock front passes over the box, the surrounding ground surface displaces vertically (Figure A-6). Overpressure loads are transmitted vertically through the box to the foundation material immediately below. A distributed elastic spring is used to represent the penetration compliance of the foundation. Thus, the vertical force system is one of overpressure forces driving the box into the foundation below. Frictional forces on the walls are ignored. The value of the foundation's penetration stiffness, K_v , is chosen by the analyst.

Horizontal pressures act concurrently with the vertical pressures. A horizontal soil spring value of stiffness, K_u , is chosen by the analyst. The program converts the average element pressures into displacements at the far end of this horizontal soil spring by dividing the pressures by the spring stiffness (see Figure A-7). The resulting time-dependent displacement is treated as the horizontal forcing function.

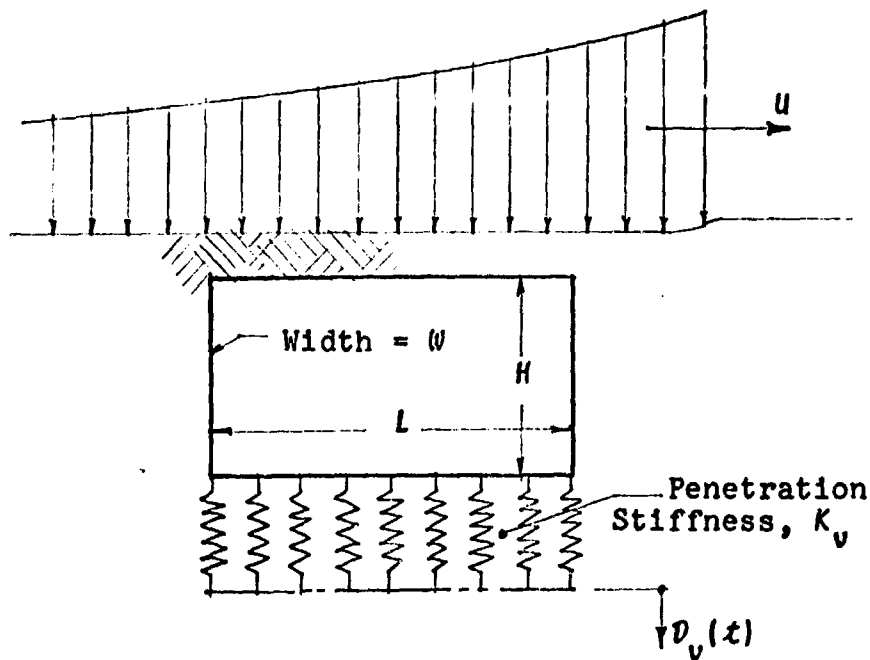


Figure A-6 BOUNDARY CONDITIONS,
VERTICAL RESPONSE.

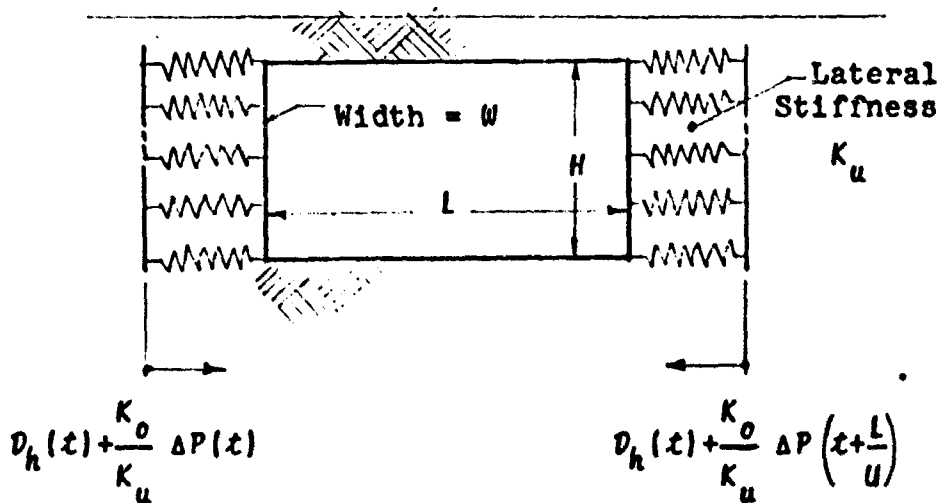


Figure A-7 BOUNDARY CONDITIONS,
HORIZONTAL RESPONSE

TABLE A-2

Ratio of Horizontal to Vertical Soil Pressures
(Reference 2)

Soil Description	K_0 , For Stresses Up to 1,000 psi		
	<u>Dynamic</u>	<u>Static</u>	
	<u>Undrained</u>	<u>Undrained</u>	<u>Drained</u>
Cohesionless Soils, Damp or Dry	1/4	1/3-dense 1/2-loose	1/3-dense 1/2-loose
Unsaturated Cohesive Soils of Very Stiff to Hard Consistency	1/3	1/2	1/2
Unsaturated Cohesive Soils of Medium to Stiff Consistency	1/2	1/2	1/2
Unsaturated Cohesive Soils of Soft Consistency	3/4	1/2 to 3/4	1/2 to 3/4
Saturated Soils of Very Soft to Hard Con- sistency and Cohesion- less Soils	1	1	1/2-stiff 3/4-soft
Saturated Soils of Hard Consistency. $q_u = 4$ tsf to 20 tsf.	3/4 to 1	1	1/2
Saturated Soils of Very Hard Consistency. $q_u = 20$ tsf.	3/4	1	1/2
Rock	Obtain from tests on rock cores and correlate with seismic data.		

A-3.4 Outrunning Ground Motions

Many structures, which are designed for overpressures less than 100 psi, will be in the region of outrunning ground motion. The phasing between outrunning ground motions and airblast arrival can be calculated by the procedure described in Reference 8 and need not be repeated here. The phasing time is part of the input data furnished by the analyst.

This section is a statement of ground motion prediction as given by Sauer.⁸ The equations used in the computer program to describe the amplitude of outrunning ground motion are presented. In addition, the particle velocity waveform is presented for both vertical and horizontal motion.

The vertical velocity waveform (Figure A-8) is completely identified by:

V_2 , the amplitude of the third velocity peak

t_2 , the period of the first three half waves

These variables are calculated from the following relationships:

$$V_2 = \frac{1}{s \cdot V_L^*} \left[4 \times 10^{11} \left(\frac{W^{1/3}}{R_g} \right)^2 - 75 \Delta P_g \right] \text{---(ft/sec)} \quad (\text{A-8})$$

$$t_2 (\text{msec}) = 100 + \Delta R / 4 \quad (\text{A-9})$$

where,

- ΔP_g = Peak overpressure (psi)
- R_g = Range from ground zero (ft.)
- ΔR = Distance from site to point of initial outrunning (ft.)
- s = In situ specific gravity
- V_L^* = Adjusted seismic velocity.
 - $V_L^* = \frac{3}{4} V_L$ for soils and incompetent rock;
 - $V_L^* = V_L$ for competent rock.
- V_L = Seismic velocity (ft/sec)
- W = Weapon yield (megatons).

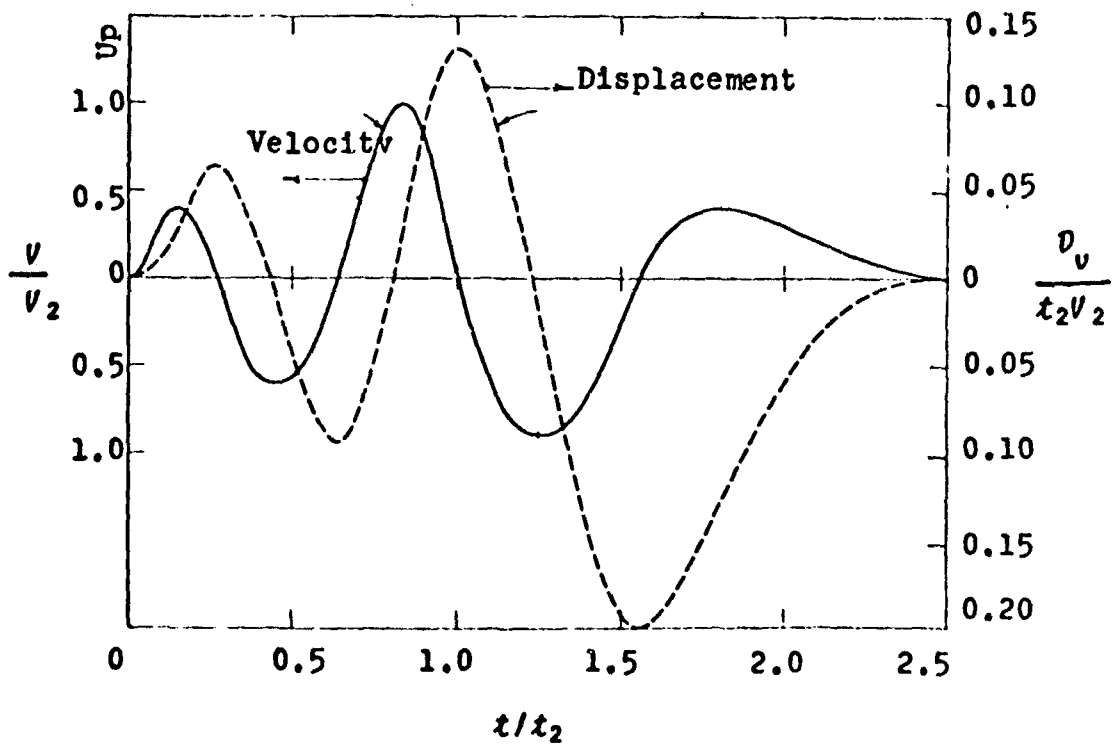


Figure A-8 NORMALIZED VERTICAL WAVEFORM
OUTRUNNING GROUND MOTION (Ref.8)

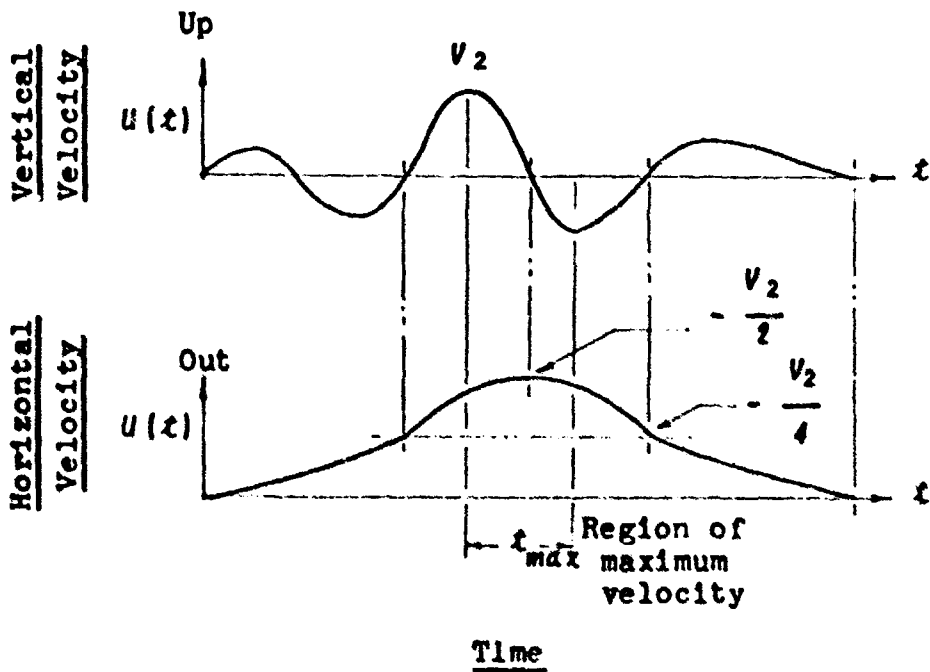


Figure A-9 RECOMMENDED PROCEDURE FOR
HORIZONTAL OUTRUNNING WAVEFORM (Ref. 16)

The displacement waveform of Figure A-8, $v_v(t)$, is stored in the program. This free-field displacement is applied through the foundation springs (Figure A-6) when the analyst enters the above data on the input forms. For computational purposes the equation

$$u(t) = -\frac{1}{2} \frac{\left(\frac{t}{2.5 t_2}\right)^p \left(1 - \frac{t}{2.5 t_2}\right)^m}{K \left(\frac{t_{max}}{2.5 t_2}\right)^p \left(1 - \frac{t_{max}}{2.5 t_2}\right)^m} \quad (A-10)$$

is adopted to represent the horizontal waveform shown in Figure A-9.

For $t = 0$ and $t = 2.5 t_2$, $u_2(t) = 0$.

$2.5 t_2$ is the duration of the wave, K fixes the amplitude, and m and p are constants responsible for the shape of the curve. Quantity m is related to p by

$$m = p \frac{\left(1 - \frac{t_{max}}{2.5 t_2}\right)}{\left(\frac{t_{max}}{2.5 t_2}\right)} \quad (A-11)$$

The program integrates Equation A-10, giving the free field horizontal soil displacements, $v_h(t)$. The wall loading used in the computer program assumes that the free-field displacements, $v_h(t)$, are applied through the effective soil springs (Figure A-7).

UNCLASSIFIED

Security Classification

DOCUMENT CONTROL DATA - R & D

(Security classification of title, body of abstract and indexing annotation must be entered when the overall report is classified)

1. ORIGINATING ACTIVITY (Corporate author)		2a. REPORT SECURITY CLASSIFICATION	
T. Y. Lin and Associates Consulting Engineers		Unclassified	
		2b. GROUP	
3. REPORT TITLE			
"A COMPUTER PROGRAM FOR THE DYNAMIC BLAST RESPONSE OF BOX-TYPE STRUCTURES"			
4. DESCRIPTIVE NOTES (Type of report and inclusive dates)			
Final - December 1966			
5. AUTHOR(S) (First name, middle initial, last name)			
Ian R. Stubbs Kalman L. Benuska			
6. REPORT DATE	7a. TOTAL NO. OF PAGES	7b. NO. OF REFS	
December 1966	122	16	
6a. CONTRACT OR GRANT NO	8a. ORIGINATOR'S REPORT NUMBER(S)		
OCD-PS-64-201			
b. PROJECT NO	9a. OTHER REPORT NO(S) (Any other numbers that may be assigned this report)		
OCD Work Unit 1157B			
c.			
d.			
10. DISTRIBUTION STATEMENT			
Distribution of this document is unlimited			
11. SUPPLEMENTARY NOTES		12. SPONSORING MILITARY ACTIVITY	
		Office of Civil Defense Office of the Secretary of the Army	
13. ABSTRACT			
<p>This report describes the development of two digital computer programs. Both programs analyze the response of a multi-cell rectangular box-structure to external dynamic loads. The programs use the principle of finite elements to represent the box-structure and solve the equations of equilibrium by means of a Gaussian elimination procedure. The first of the two programs considers the dynamic response of the box-structure with its material properties remaining linear. The output consists of displacements, moments and stresses. Also, response spectra may be generated at equipment attachment points within the structure. The second program calculates the dynamic response with the added provision that when moments in any plate exceed a predetermined yield value, that plate will not accept any increase in loads normal to its plane. However, it is assumed that the plate would still be able to carry the inplane diaphragm forces.</p> <p>A synoptic review of selected literature pertaining to the failure modes and failure loadings of two-way slabs is presented at the end of the report.</p>			

DD FORM 1473

UNCLASSIFIED

Security Classification

14 KEY WORDS	LINK A		LINK B		LINK C	
	ROLE	WT	ROLE	WT	ROLE	WT
computer programs response multi-cell rectangular box-structures dynamic finite elements Gaussian linear displacements moments stresses response spectra equipment plate yield diaphragm						